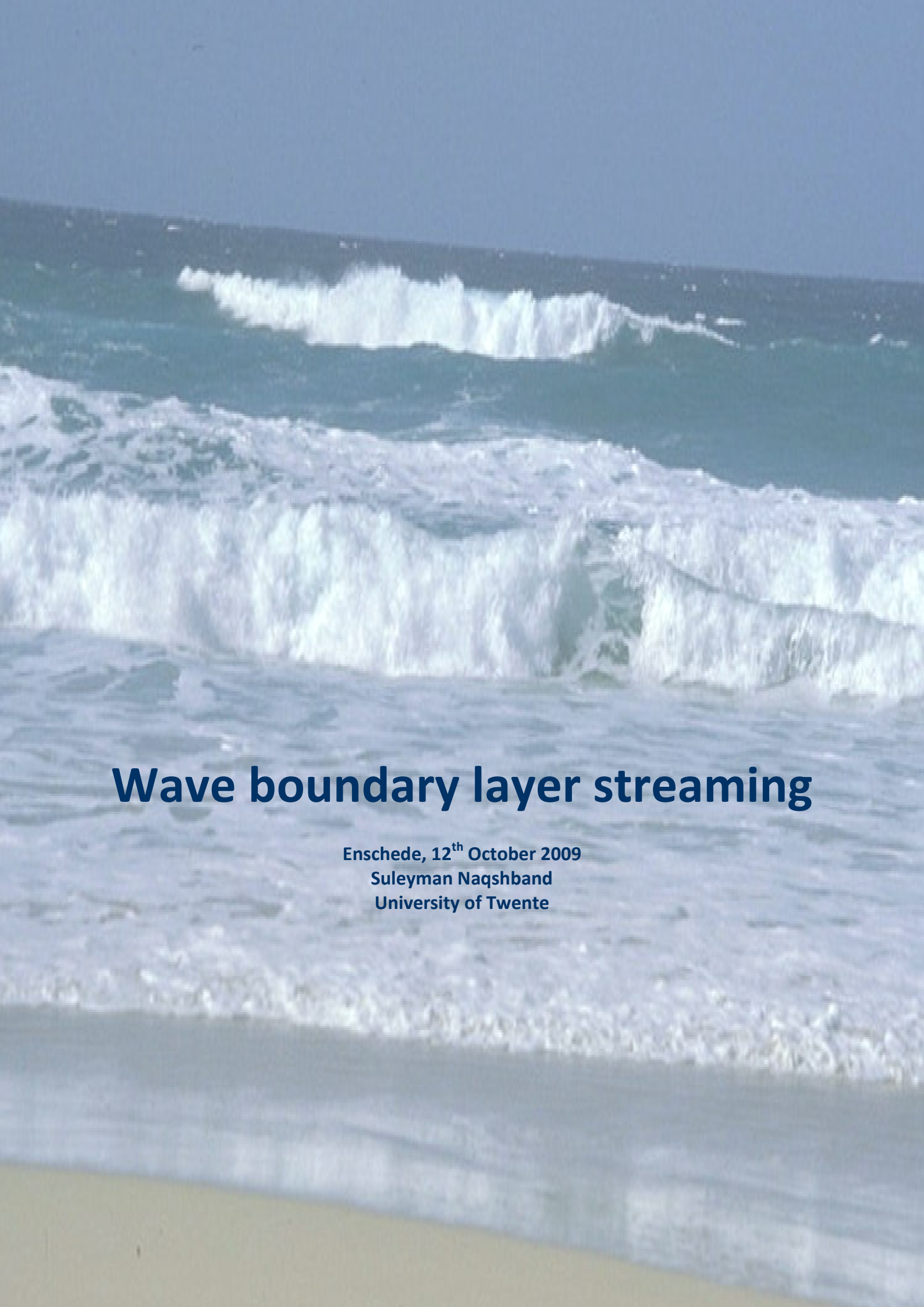

Wave boundary layer streaming

Enschede, 12th October 2009

Suleyman Naqshband
University of Twente

Wave boundary layer streaming – Analysis on wave boundary layer streaming and its effect on bed shear stress

Enschede, 12th October 2009

MSc. Project of Suleyman Naqshband

Graduation committee
Jan, S. Ribberink
Wouter, M. Kranenburg
Jolanthe, L.M. Schretlen

University of Twente
Enschede - The Netherlands

Contents

Abstract

Cross-shore morphological development of a sea bottom is mainly determined by sediment transport close to the seabed caused by the actions of waves and currents. In addition to pure fluctuations, waves can induce steady currents such as Eulerian boundary layer streaming or boundary layer drift. The presence of such additional near-bed currents can result in additional bottom sediment transport. The aim of this study is to get insight in underlying mechanisms of Eulerian streaming and their effects on bed shear stress that is determinative for sediment transport.

In this study three streaming models are compared under characteristic wave conditions in the North-Sea: a constant viscosity model (Longuet-Higgins, 1953), a time-dependent viscosity model (Davies and Villaret, 1999) and a 1-DV numerical POINT SAND model of Uittenbogaard [1999]. Furthermore, two analytical models for bed shear stress are verified with bed shear stress results from the POINT SAND model: the bed shear stress model of van Rijn [2007], and Nielsen and Callaghan [2003]. Van Rijn [2007] takes account for streaming by adding a positive streaming velocity, where Nielsen and Callaghan [2003] add the wave Reynolds stress to take account for streaming.

This study has shown that the streaming velocities, above flat beds, are positive as well near-bed as away from the bed. This is the result of the dominant, positive contribution to streaming of the wave Reynolds stress compared to the negative contribution of the wave component of mean turbulent Reynolds stress.

The study also showed that a better representation of the bed shear stress is given by the model of Nielsen and Callaghan [2003] compared to the model of van Rijn [2007]. Furthermore, the bed shear stress model of Nielsen and Callaghan [2003] is adjusted to represent the physical situation as is simulated with the PONIT SAND model. This adjustment has resulted in better agreement with the PSM compared to the original model.

Preface

After finishing the bachelor of Civil Engineering and Management on the University of Twente, I started the master course of Water Engineering and Management. This master course consists of several theoretical subjects and is finished with a thesis. This report is the result of this six-month thesis at the University of Twente, department of Water Engineering and Management. Here I did research on wave mechanisms that are determinative for sediment transport and thus the morphological development of a sea bottom.

Finishing this thesis would not be possible without the great contribution of my supervisors. Therefore, I would like to thank Jan, Wouter, and Jolanthe for their patience and effort that they have put in this work. Furthermore, I would like to thank my parents Hamidullah and Zarghona together with Ellaha and other family members for their love and support over the years.

Suleyman Naqshband
Enschede, 12th October 2009

Introduction

Cross-shore morphological development of a sea bottom is mainly determined by sediment transport close to the seabed caused by the actions of waves and currents. In addition to pure fluctuations, waves can induce steady currents which do not change their direction during a time long in comparison with a wave period [Mei et al., 2005]. Eulerian streaming is an example of such wave-induced currents that is also known as boundary layer drift. It is called Eulerian as the fluid motion is analyzed at a fixed point in contrast to Lagrangian point of view where the position of each water particle is studied.
Streaming has its origin in the existence of vertical velocities within the bottom boundary layer caused by non-uniformity of the flow beneath progressive waves. The horizontal and vertical velocities in a wave motion are not exactly 90 degrees out of phase, as they would be in a perfectly inviscid wave motion [Longuet-Higgins, 1953]. This gives rise to a non-zero time-averaged near-bed drift that is called streaming. This near-bed drift that is associated with the existence of vertical velocities is therefore only present under real waves and not in tunnels. However, streaming can also occur in oscillatory water tunnels in absence of vertical velocities as long as there is an asymmetry in the turbulence intensity in successive wave half cycles [Trowbridge and Madsen, 1984]. In this research the term streaming is used in both cases: for oscillating flow in tunnel and in presence of vertical velocities under surface waves.

Although Eulerian streaming is weak compared to the oscillatory component of velocity, it has a significant effect on the transport of sediments and pollutants in the sea [Marin, 2003]. The presence of such additional near-bed currents can result in additional bottom sediment transport but also in additional suspended sediment transport as the entire water column is affected. In order to understand the morphology of a sea bottom it is necessary to get good knowledge of the hydrodynamic processes involved, such as currents generated by waves. The aim of this study is to get insight in underlying mechanisms of Eulerian streaming and to include its effects in bed shear stress modelling that is determinative for sediment transport.

In this report, first of all, the research framework and methodology is discussed where the overall significance of this research and its goals are outlined. In chapter two the governing equations of this research are presented which is the starting point for the analysis of fluid motion. Chapter three gives an analysis on the different streaming models and their cross-shore behaviour. The bed shear stress models that take account for streaming are subsequently discussed in chapter 4. Here the effect of streaming on bed shear stress is made visible. Furthermore, it is examined to what extend these models take account for streaming and the bed shear stress models are (possibly) improved in chapter 5. Eventually, a discussion is posted in chapter 6 where the important outcomes of this research are listed (conclusions) in chapter 7.

1 Research framework and methodology

In this chapter the research framework is outlined. Here first of all the theoretical background of this research is discussed from which the problem definition and research objective is derived. To meet this objective a certain approach is necessary which is outlined next. Eventually, the (boundary) conditions and the focus of this research are discussed.

1.1 Theoretical background

Cross-shore morphological development is mainly determined by sediment transport close to the seabed caused by the actions of waves and currents. To model the sediment transport and thus get insight in the morphological behaviour of a sea bottom the hydrodynamic processes involved should be well understood. An example of such hydrodynamic processes is the existence of boundary layer streaming that is a wave-induced near-bed current. The presence of such a current can have significant effects on net sediment transport rates as shown by experimental and theoretical studies of Davies and Li [1997], and Dohmen-Janssen and Hanes [2002] (discussed further on). However, the magnitude and even the direction of the boundary layer streaming are still uncertain. Furthermore, its effects on sediment transport rates are often not well included in sediment transport models. Sediment transport models usually include the effects of streaming in the modelling of the bed shear stress which is determinative for sediment transport. Therefore good modelling of bed shear stress is of great importance.

Davies and Li [1997] have modelled sediment transport beneath symmetrical and asymmetrical (velocity-skewed) waves, and also wave-current flow above a plane bed. In absence of vertical velocities asymmetrical waves give rise to streaming due to turbulence asymmetry in successive wave half cycles. They have found that net sediment transport rates are highly sensitive to the presence of residual currents and that good agreement is found with Ribberink and Al Salem's [1992] laboratory data when residual currents are taken into account. Davies and Li [1997] therefore recommend careful modelling of residual currents.
Dohmen-Janssen and Hanes [2002] have conducted several experiments under sheet flow regime (plane bed) in the full-scale GWK wave flume in Hannover. They have found transport rates that may be up to 2.5 times greater than in "equivalent" oscillatory tunnels. Dohmen-Janssen and Hanes [2002] have concluded that this is (partly) caused by the presence of streaming under real waves.

Eulerian streaming was firstly explained by Longuet-Higgins [1953] as an onshore-directed current that has its origin in the existence of vertical velocities induced by waves (hereafter referred to as LH53). Here purely progressive waves were assumed beside constant viscosity, flat bed and laminar flow.

Davies and Villaret [1999] modelled streaming under turbulent flow and above rippled beds (hereafter referred to as DV99). Here viscosity is assumed to be time-dependent but constant over the depth. In addition to the drift associated with the vertical velocity field (LH53), wave asymmetry in successive wave half cycles will give rise to a near-bed drift component. The reason for this is the fact that asymmetrical waves cause shedding of vortices of unequal strength in successive wave half cycles as explained by O' Donoghue and Ribberink [2007]. For flat beds this drift component is in the offshore direction as demonstrated by Ribberink and Al Salem [1995] and therefore the drift associated with vertical velocity field is reduced. The magnitude and direction of this drift component depends on the value of bed roughness and degree of wave asymmetry. The Davies and Villaret model is applicable above rippled beds where the momentum transfer is dominated by vortex shedding in contrast to flat beds, where the momentum transfer is dominated by random turbulence. In this research the validity of the DV99 model is investigated above flat beds as well.
Uittenbogaard [1999] has developed a numerical, one-dimensional vertical, unsteady model that simulates the currents and waves as a function of time as well as a vertical co-ordinate. The model is called POINT SAND model (hereafter referred to as PSM) and takes good account for the hydrodynamic processes involved such as simulating the Stokes drift as shown by Uittenbogaard & Klopman [2001]. Furthermore, Bosboom and Klopman [2000] found good agreement between the flow field computed using PSM and the flow field from wave-current flume experiments of Klopman [1994]. The wave-induced streaming in the wave boundary layer, as occurs under propagating waves, is an integral part of the computed flow field. This shows the validity of the POINT SAND model for real wave processes and for this reason this numerical model is used as reference for the assessment of other (analytical) models in this research. Here the situation under real waves is simulated where streaming is associated with the presence of vertical velocities (LH53) as well as asymmetry in the turbulence intensity.

The three streaming models discussed above take account for different processes and mechanisms. Where the Longuet Higgins solution and the POINT SAND model are valid above flat beds the DV99 model is applicable above rough rippled beds. The degree of complexity increases from LH53 to DV99 and to PSM as more and more mechanisms are involved. To be able to assess the importance of these mechanisms, a comparison between these models is necessary.

For practical reasons a simple, analytical expression of bed shear stress is required where the effects of streaming are included. Two, generally used bed shear stress models that take streaming effects into account are derived by Nielsen [2006] and Van Rijn [2007]. However, the validity of both models is yet questionable and therefore the numerical POINT SAND model is used as reference in this study to validate these models.

1.2 Problem definition

The effects of different hydrodynamic processes on streaming are not well understood and therefore the magnitude and even the direction of the boundary layer streaming are still uncertain. These uncertainties can result in less reliable predictions of bed shear stresses and thus sediment transport rates.

1.3 Objective and questions

The overall objective of this research is to get insight in the underlying mechanisms of Eulerian streaming and to include its effects in bed shear stress modelling. This is done by comparing three different streaming models under characteristic wave conditions in the North-Sea: Longuet-Higgins [1953], Davies and Villaret [1999] and POINT SAND model by Uittenbogaard [1999]. Furthermore, the generally used analytical and practical bed shear stress models that take streaming effects into account are validated using the numerical POINT SAND model.

To achieve the research objective as formulated above the following central questions should be answered. These questions are further subdivided as can be seen below.

Central questions

1) How is the Eulerian streaming affected by different flow mechanisms?
2) How well do the existing analytical bed shear stress models take account for streaming? And in what way can the analytical model(s) be improved?

Sub-questions

1.1) What are the characteristic cross-shore wave conditions in the North-Sea and how can these conditions be translated in wave properties such as wave-asymmetry?
1.2) What are the differences between the three streaming models? And how do these models compare under the characteristic wave conditions from 1.1) and depth variations?
1.3) How can the Davies and Villaret [1999] model be adjusted to represent flat bed situations and how does this adjusted model compares to the original DV99 model, LH53 and the PSM?
2.1) Which generally used analytical and practical bed shear stress models take streaming effects into account? And what are the underlying assumptions of these models?
2.2) How do these bed shear stress models compare with the POINT SAND model considering same (wave) conditions?
2.3) How can the considered bed shear stress model(s) be possibly adjusted to achieve better agreement with the hydrodynamic results of the POINT SAND model?

1.4 Approach

To achieve the research objective formulated in paragraph 1.3, a certain research approach is necessary. This approach is outlined in a few steps below where each step corresponds to a certain sub-question.

- The first step is to choose characteristic wave conditions in the North-Sea and different cross-shore water depths for the analysis of the models. These data are then used to calculate wave properties such as wave-asymmetry (sub-question 1.1).
- The calculated wave properties and water depths are then used to compare the three streaming models (sub-question 1.2). This is done by plotting the vertical mean velocity distributions according to the three different models.
- Next the Davies and Villaret model [1999] is adjusted to represent flat bed situations. In order to do this, the eddy viscosity model of DV99 will be matched to that of the POINT SAND model. Subsequently, the results of the adjusted model are compared to the original DV99 model, the LH53 solution and the PSM (sub-question 1.3).
- Using literature two generally used bed shear stress models have been found (sub-question 2.1). These models are compared with the results of POINT SAND model to see to what extend agreement is found in the values of certain quantities such as time-averaged bed shear stress (sub-question 2.2).
- Finally, the analytical bed shear stress model that is the most promising one is adjusted to get even better agreement with the results of POINT SAND model (sub-question 2.3).

The research approach discussed above is visualised in the figure below.

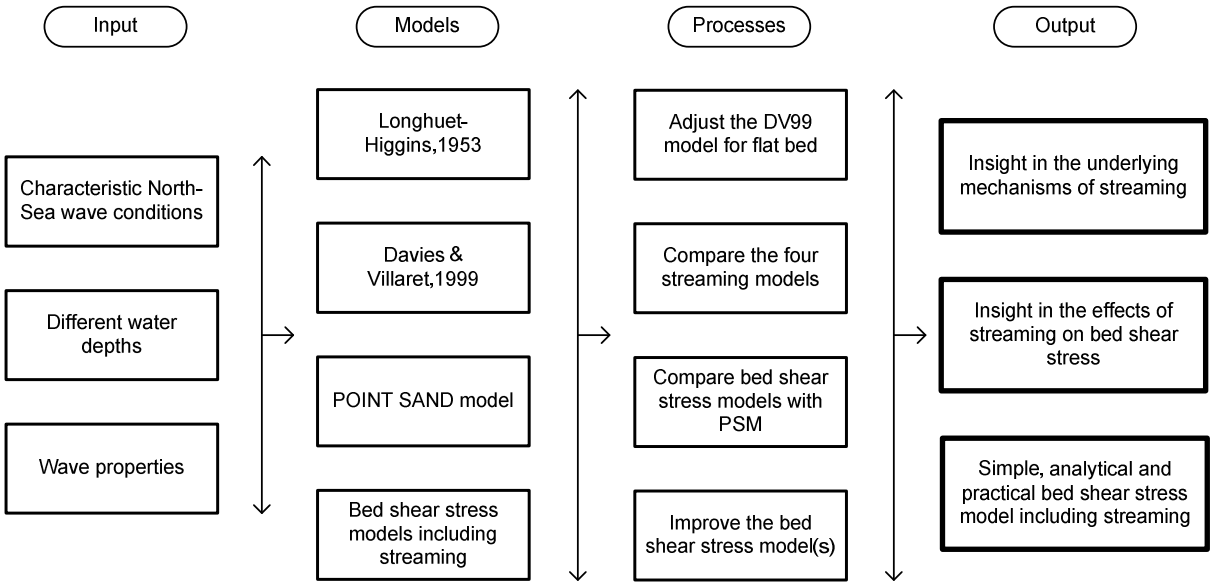

Figure 1: Research model

1.5 Focus and conditions

The focus of this research is mainly on the bottom boundary layer which is a small fraction of the water depth. In this region the viscous stresses are more important as close to the bottom there is a region of strong shear [Longuet-Higgins, 1953]. The behaviour of the streaming and the bed shear stress models are analyzed cross-shore outside the surf zone thus in the zone where shoaling occurs but the waves stay intact. In this zone the wave asymmetry *R* increases with decreasing water depths. The wave asymmetry in this case considers velocity-skewness with zero acceleration skewness and is calculated using (1.5.1), after Watanabe and Soto [2004]. Here u_{max} is the maximum onshore-directed velocity where u_{min} is the maximum offshore-directed velocity. Furthermore, the bed is assumed flat with roughness height k_s which is assumed equal to 2.5 times the d_{50}.

$$R = \frac{u_{max}}{u_{\max} - u_{\min}} \tag{1.5.1}$$

The conditions for the analysis on streaming and bed shear stress models are derived from the lecture notes of Hulscher et al., [2002]. Hulscher et al., [2002] give wave heights for a range of characteristic wave conditions in the North Sea as a function of cross-shore water depth. For the analysis in this research two wave conditions are chosen: moderate waves with a wave period of 5.7 seconds and storm waves with a wave period of 7.6 seconds. This is done in order to get insight in the behaviour of streaming under practical and actual circumstances. The probability of exceedance of a significant wave height at certain water depth is 50 % for moderate wave (wave 1) and 2.5 % for storm wave (wave 2). In order to get a good representation of the cross-shore behaviour of streaming, different water depths are chosen such that the waves are still intact.

Using these wave conditions several wave characteristics for both waves are calculated which are used as input for the streaming and bed shear stress models. Furthermore, using the numerical method of Rienecker and Fenton [1981] time-dependent horizontal near-bed orbital velocities are derived. This method uses the wave period and wave height to calculate the amplitudes of the first eight Fourier components. The time dependent orbital velocity is then given by (1.5.2) where U_i is the amplitude of the i^{th} Fourier component. Subsequently, this is translated to time-dependent surface elevation which is used as input for the POINT SAND model. Using Linear wave theory, the surface elevation *a* is given by (1.5.3).

$$u(t) = \sum_{i=1}^{8} U_i \cos\left(i * 2\pi t / T\right) \tag{1.5.2}$$

$$a(t) = \sum_{i=1}^{8} \frac{U_i * \sinh(kh)}{\omega} \cos\left(i * 2\pi t / T\right) \tag{1.5.3}$$

In Table 1 and Table 2 the wave characteristics are shown for different cross-shore water depths. From left to right *h* is the water depth, *H* the significant wave height, *kh* the wave number multiplied by water depth and U_1 is the maximum horizontal orbital velocity at the bed as given by the linear wave theory. For both waves the time-dependent orbital velocities are shown in Figure 2 and Figure 3, for different cross-shore water depths.

As the wave heights of wave 2 are larger than that of wave 1, wave 2 breaks on water depths larger than wave 1. Another noticeable aspect is the magnitude of the velocity skewness *R*. When *R* becomes too large the shape of the orbital velocities are no longer smooth. Therefore, in this research the analysis on different models are restricted to cross-shore water depths larger than 2 meters for wave 1 and larger than 5 meters for wave 2.

Wave 1	h [m]	H [m]	kh [-]	U_1 [m/s]	u_{max} [m/s]	u_{min}[m/s]	R [-]
	2	1.00	0.52	1.02	1.21	-0.47	0.72
	3	0.98	0.63	0.80	0.88	-0.58	0.60
$P(H_s>H)$ = 50 %	4	0.94	0.77	0.61	0.68	-0.54	0.56
T = 5.70 s	5	0.94	0.86	0.53	0.55	-0.48	0.53
L_0 = 50.7 m	6	0.93	0.98	0.45	0.45	-0.42	0.52
	7	0.93	1.09	0.39	0.40	-0.37	0.52
	8	0.93	1.19	0.34	0.34	-0.33	0.51

Table 1: Wave characteristics for wave 1

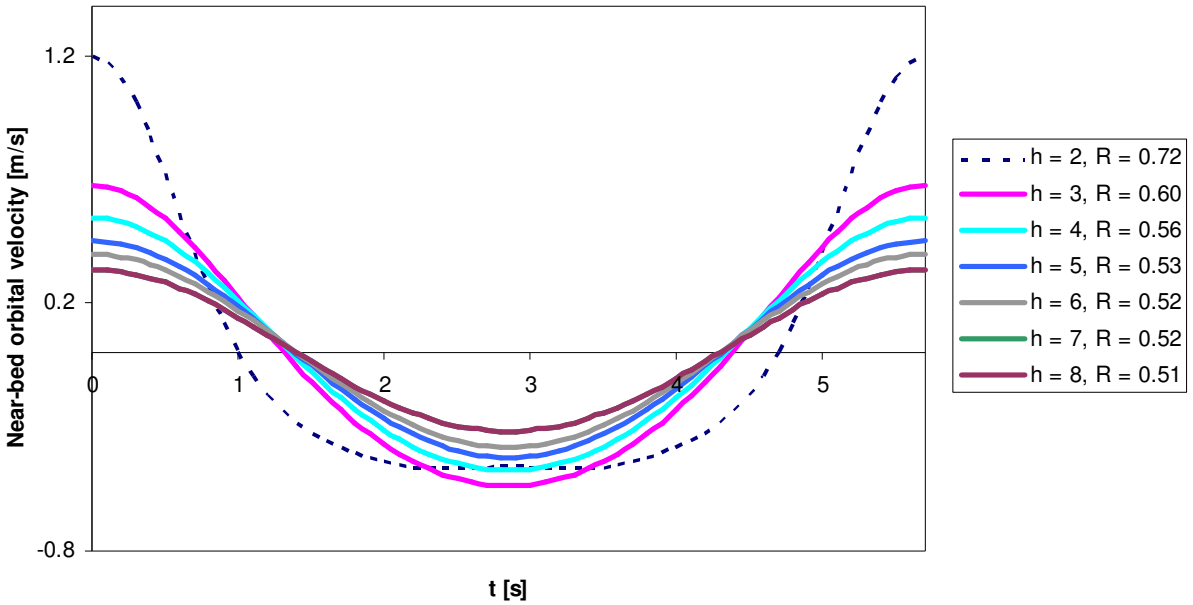

Figure 2: Horizontal orbital velocities for different water depths (wave 1)

Wave 2	h [m]	H [m]	kh [-]	U_1 [m/s]	u_{max} [m/s]	u_{min}[m/s]	R [-]
$P(H_s>H)$ = 2.5 % T = 7.60 s L_0 = 90.2 m	5	2.25	0.55	1.60	1.63	-0.71	0.70
	6	2.70	0.70	1.47	1.70	-0.97	0.64
	7	2.75	0.76	1.36	1.48	-1.01	0.59
	8	2.80	0.82	1.26	1.30	-1.01	0.56

Table 2: Wave characteristics for wave 1

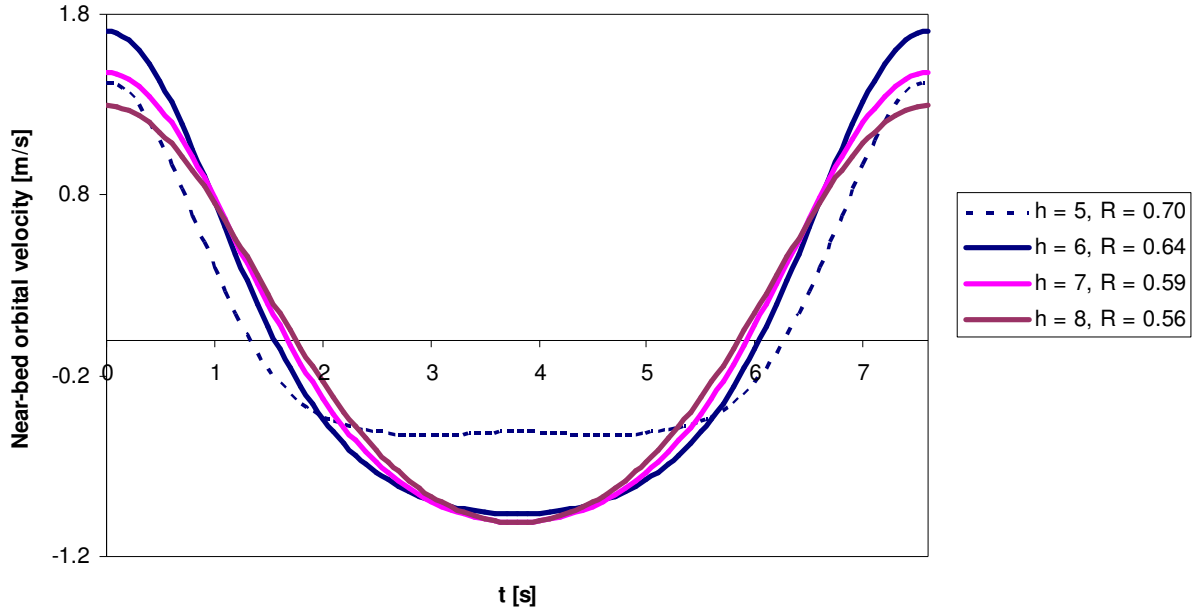

Figure 3: Horizontal orbital velocities for different water depths (wave 2)

From the figures above it can be seen that the wave asymmetry *R* increases with decreasing water depths: u_{max} and u_{min} increase with decreasing water depths. Furthermore, the duration of the offshore-directed velocities increase with decreasing water depths and therefore the duration of the onshore-directed velocities decrease with decreasing water depths, as the wave period *T* remains unchanged.

2 Governing equations

In this chapter first the basic flow equations are presented from which then the wave-averaged equations are derived using Reynolds decomposition. This leads to stresses which are of central interest with respect to modelling of mean velocity profiles as a function of the vertical. Furthermore, the time-dependent boundary layer equations are presented which form the basic of boundary layer models.

2.1 Equations of motion

As usual the starting point for the analysis of fluid motion is the Navier Stokes equations. Here only the equations for the horizontal and vertical components of the flow in the x-z plane are considered where *u* and *w* are the velocities in the *x* and *z* directions respectively, ρ is the fluid density, *P* is the pressure, *g* is the gravity constant and *v* is the kinematic viscosity. The continuity equation is given by (2.1.1) where the momentum equations in the x- and z-directions are given by (2.1.2) and (2.1.3), respectively.

$$\frac{\partial u}{\partial x}+\frac{\partial w}{\partial z}=0 \tag{2.1.1}$$

$$x: \quad \frac{\partial u}{\partial t}+\frac{\partial u^2}{\partial x}+\frac{\partial uw}{\partial z}=-\frac{1}{\rho}\frac{\partial P}{\partial x}+\frac{1}{\rho}\frac{\partial \tau_{xx}}{\partial x}+\frac{1}{\rho}\frac{\partial \tau_{zx}}{\partial z} \tag{2.1.2}$$

$$z: \quad \frac{\partial w}{\partial t}+\frac{\partial wu}{\partial x}+\frac{\partial w^2}{\partial z}=-g-\frac{1}{\rho}\frac{\partial P}{\partial z}+\frac{1}{\rho}\frac{\partial \tau_{xz}}{\partial x}+\frac{1}{\rho}\frac{\partial \tau_{zz}}{\partial z} \tag{2.1.3}$$

Using continuity and the expression for the viscous stress the momentum equations can also be written as follows.

$$x: \quad \frac{\partial u}{\partial t}+u\frac{\partial u}{\partial x}+w\frac{\partial u}{\partial z}=-\frac{1}{\rho}\frac{\partial P}{\partial x}+\nu\left(\frac{\partial^2 u}{\partial x^2}+\frac{\partial^2 u}{\partial z^2}\right) \tag{2.1.4}$$

$$z: \quad \frac{\partial w}{\partial t}+u\frac{\partial w}{\partial x}+w\frac{\partial w}{\partial z}=-g-\frac{1}{\rho}\frac{\partial P}{\partial z}+\nu\left(\frac{\partial^2 w}{\partial x^2}+\frac{\partial^2 w}{\partial z^2}\right) \tag{2.1.5}$$

2.2 Wave-averaged equations

In this section equations are derived for combined wave current flows. These equations are useful in identifying stresses or momentum transfer contributions from different flow components. To derive these equations Reynolds decomposition is used which considers flow that contains a periodic flow component $\tilde{u}$ as well as the familiar steady $\overline{u}$ and turbulent components u'. Inserting $(u,w)=(\overline{u}+\tilde{u}+u',\overline{w}+\tilde{w}+w')$ and $P=\overline{P}+\tilde{P}+P'$ into the continuity and momentum equations above and taking phase- (~) and time-averages (¯) gives the following equations. Here the continuity equation is given by (2.2.1) where the momentum equations in the x- and z-directions are given by (2.2.2) and (2.2.3), respectively. For a detailed overview of these derivations reference is made to Appendix A.

$$\frac{\partial \overline{u}}{\partial x}+\frac{\partial \overline{w}}{\partial z}=0 \tag{2.2.1}$$

$$x: \quad \frac{\partial \overline{u}^2}{\partial x}+\frac{\partial \overline{\tilde{u}^2}}{\partial x}+\frac{\partial \overline{u'^2}}{\partial x}+\frac{\partial \overline{uw}}{\partial z}+\frac{\partial \overline{\tilde{u}\tilde{w}}}{\partial z}+\frac{\partial \overline{u'w'}}{\partial z}=-\frac{1}{\rho}\frac{\partial \overline{P}}{\partial x}+\nu\left(\frac{\partial^2 \overline{u}}{\partial x^2}+\frac{\partial^2 \overline{u}}{\partial z^2}\right) \tag{2.2.2}$$

$$z: \quad \frac{\partial \overline{w}^2}{\partial z}+\frac{\partial \overline{\tilde{w}^2}}{\partial z}+\frac{\partial \overline{w'^2}}{\partial z}+\frac{\partial \overline{wu}}{\partial x}+\frac{\partial \overline{\tilde{w}\tilde{u}}}{\partial x}+\frac{\partial \overline{w'u'}}{\partial x}=-g-\frac{1}{\rho}\frac{\partial \overline{P}}{\partial z}+\nu\left(\frac{\partial^2 \overline{w}}{\partial x^2}+\frac{\partial^2 \overline{w}}{\partial z^2}\right) \tag{2.2.3}$$

Considering the momentum equation in the x-direction and assuming uniform wave conditions, the balance of forces in the horizontal direction is given by (2.2.4). Here, from left to right the terms are referred to as the wave Reynolds stress, mean turbulent Reynolds stress, mean pressure gradient which represents return flow in case of a closed boundary (coast), and mean viscous stress. Expression (2.2.4) is of central interest with respect to modelling of the horizontal mean velocity profile as a function of the vertical.

$$\frac{\partial \overline{\tilde{u}\tilde{w}}}{\partial z}+\frac{\partial \overline{u'w'}}{\partial z}=-\frac{1}{\rho}\frac{\partial \overline{P}}{\partial x}+\nu\left(\frac{\partial^2 \overline{u}}{\partial z^2}\right) \tag{2.2.4}$$

To derive an equation for the horizontal mean velocity distribution, Boussinesq hypothesis is applied to the mean turbulent Reynolds stress as shown in equation (2.2.5).

$$\rho\overline{u'w'}=-\rho\left[\overline{\upsilon_t}\frac{\partial \overline{u}}{\partial z}+\overline{\tilde{\upsilon}_t\frac{\partial \tilde{u}}{\partial z}}\right] \tag{2.2.5}$$

Substituting this into (2.2.4) and reorganising the terms gives the following equation:

$$\frac{\partial}{\partial z}\left[(\upsilon+\upsilon_t)\frac{\partial \overline{u}}{\partial z}\right]=-\frac{\partial}{\partial z}\left[\overline{\widetilde{\upsilon}_t\frac{\partial \widetilde{u}}{\partial z}}\right]+\frac{\partial \overline{\widetilde{u}\widetilde{w}}}{\partial z}+\frac{1}{\rho}\frac{\partial \overline{P}}{\partial x} \tag{2.2.6}$$

Vertical integration of (2.2.6), with boundary condition given in (2.2.7) results in equation (2.2.8) which shows the horizontal mean velocity distribution. The boundary condition is based on the assumption that there is no wind stress at the trough level which results to a zero wave-averaged shear stress at this level. The wave-averaged bed shear stress using $\overline{\widetilde{u}\widetilde{w}}=0$ at the bed $z=0$ is then given by equation (2.2.9) where τ_{surf} is the wave-averaged shear stress at the surface.

$$\frac{\partial \overline{u}}{\partial z}_{z=h}=0 \tag{2.2.7}$$

$$\overline{\upsilon_t}\frac{\partial \overline{u}}{\partial z}=-\left[\overline{\widetilde{\upsilon}_t\frac{\partial \widetilde{u}}{\partial z}}\right]+\left[\overline{\widetilde{u}\widetilde{w}}-\overline{\widetilde{u}\widetilde{w}}_{\delta}\right]+\frac{1}{\rho}\frac{\partial \overline{P}}{\partial x}[z-h] \tag{2.2.8}$$

$$\overline{\tau_b}=\overline{\tau_{surf}}-\rho\left(\overline{\widetilde{u}\widetilde{w}}\right)_{z=\delta}-\frac{\partial \overline{P}}{\partial x}h \tag{2.2.9}$$

The shape of the horizontal mean velocity profile as a function of the vertical is determined by the three terms on the right hand side of equation (2.2.8). From different studies it has been shown that the effect of the mean pressure gradient on the boundary layer streaming can be neglected (see below) and therefore in this study the focus is mainly on the behaviour of the other two terms: the first term on the right hand side of (2.2.8) is referred to as the wave component of mean turbulent Reynolds stress and the second term is referred to as the wave Reynolds stress.

Nielsen [1992] discussed the influence of currents on the wave boundary layer. From experimental data of Van Doorn [1981], and Myrhaug and Slaattelid [1989] he concluded that there is no evidence of change in the boundary layer structure for superimposed currents. Furthermore, Svendsen [2006] discussed the effect of return flow on the wave boundary layer inside and outside the surf zone. He concluded that inside the surf zone the (negative) velocities in the return flow are such high that the (positive) steady streaming can be neglected. However, outside the surf zone the steady streaming can not be neglected as the forcing due to return flow (negative velocities) are negligibly weak. Thus inside the surf zone, the influence of return flow on the boundary layer streaming is significant while outside the surf zone this effect is negligible. As mentioned in section 1.5 the focus in this study is on the region seaward of the surf zone.

The driving forces of streaming are thus the wave component of mean turbulent Reynolds stress that is associated with wave asymmetry and the wave Reynolds stress that originates from the existence of vertical velocities induced by progressive waves. The contribution of both terms to streaming velocities above flat beds is discussed next.

Under real waves the horizontal and vertical velocities in the boundary layer are not exactly 90 degrees out of phase, as they would be in a perfectly inviscid wave motion [Nielsen, 1992]. Averaged over a wave period, this results in a net vertical exchange of momentum (wave Reynolds stress) between the boundary layer and the flow field outside the boundary layer. As shown by Longuet-Higgins [1953] the net vertical momentum exchange is negative and thus the momentum transfer is downwards into the boundary layer. To balance this, there must be a backwards stress on the layer at the bottom. In other words a forwards gradient of mean velocity is needed to induce a momentum transfer at the bottom. The wave Reynolds stress thus results in a positive contribution to streaming velocities as is illustrated in Figure 4.

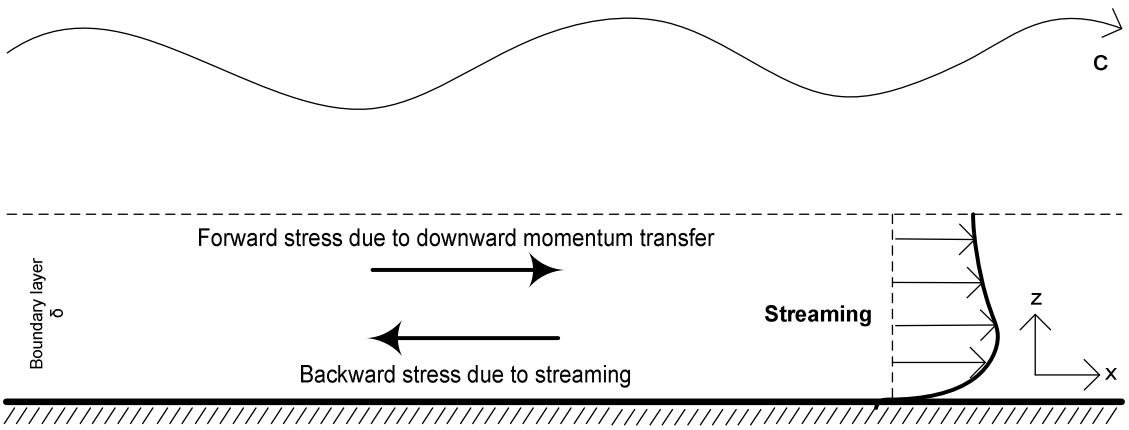

Figure 4: Positive streaming due to the wave Reynolds stress (vertical scale of δ is exaggerated, after Longuet-Higgins, 1958)

In contrast to the wave Reynolds stress, the wave component of mean turbulent Reynolds stress that is associated with wave asymmetry results in negative streaming velocities above flat beds (Davies and Villaret, 1999). This was demonstrated by the experiments of Ribberink and Al Salem [1995] which were conducted in an oscillatory water tunnel with asymmetrical waves. In the figure below the schematic behaviour of this term is illustrated for asymmetrical waves. Here different components of this term are distinguished. As discussed before asymmetrical waves give rise to turbulent intensity of unequal strength in successive wave half cycles. This is shown in the figure below where the wave-averaged turbulent intensity is zero.

Considering a wave period *T* the oscillating part of the wave component of mean turbulent Reynolds stress is positive under wave crest and, both positive and negative under wave trough. Averaging this over one wave period will result into a positive value for the wave component of mean turbulent Reynolds stress. From equation (2.2.8) it can be seen that eventually a positive value for the wave component of mean turbulent Reynolds stress will result into a negative contribution to streaming velocities. The magnitude of this negative contribution will increase with increasing wave asymmetry as the wave component of mean turbulent Reynolds stress will become more positive with increasing wave asymmetry. However, a sinusoidal wave will give rise to turbulent intensity of equal strength in successive wave half cycles. Therefore, the wave component of mean turbulent Reynolds stress gives no contribution to streaming for sinusoidal waves.

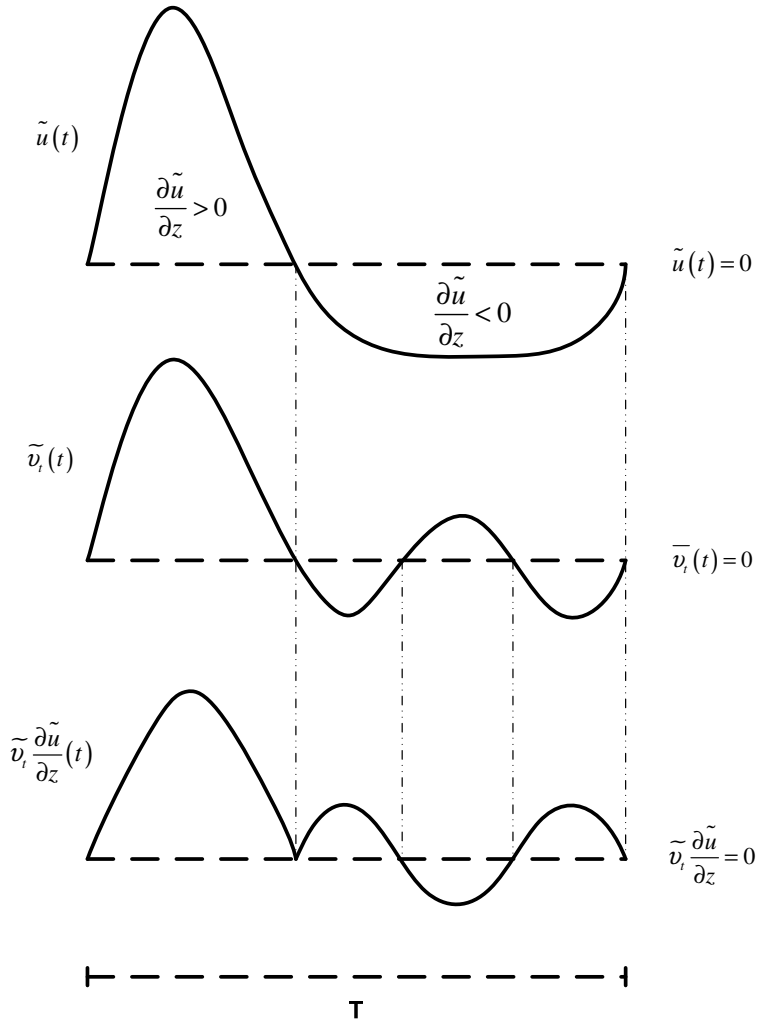

Figure 5: Schematic illustration of the behaviour of the wave component of mean turbulent Reynolds stress

Under real waves and above flat beds, the streaming profiles are thus determined by the negative contribution of the wave component of mean turbulent Reynolds stress and the positive contribution of the wave Reynolds stress. Trowbridge and Madsen [1984] found that the near-bed streaming velocities are positive for wave lengths smaller than 10 times the water depth (kh larger than 0.63). For increasing wave lengths the near-bed streaming is reduced and even reversed (opposite to the direction of wave propagation) for waves longer than about 10 times the water depth. In other words, for longer waves the mean turbulent Reynolds stress is more determinative for the streaming profiles than for shorter waves where the opposite is true for the wave Reynolds stress.

2.3 Boundary layer equations

In this section the time- and depth-dependant boundary layer equations are derived in contrast to section 2.2 where the flow equations are given as a function of the vertical *z* but time-averaged over the wave period. Furthermore, the first order solutions for the horizontal and vertical velocities in the boundary layer are shown.

The bottom boundary layer is defined as the layer inside which the flow is significantly influenced by the bed [Nielsen, 1992]. This layer develops in the presence of a solid wall (bottom) as the viscous fluid is forced to adhere to this wall. This results in large velocity gradients in the boundary layer and hence large stresses in the direction perpendicular to the bottom where at the bottom the velocity is zero. Thus, in the boundary layer the viscous stresses are important and therefore the potential theory is no longer valid in this layer.
In oscillatory flow such as waves, the boundary layer with high velocity shear perpendicular to the bottom is very thin which implies that the pressure variation perpendicular to the wall can be neglected [Svendsen, 2006]. Here, the boundary layer is considered under the assumption of a plane bed and laminar flow which makes it possible to simplify the 2-dimesional Navier-Stokes equations for the flow in the boundary layer. The resulting equations are given below which are known as the *boundary layer equations* [Svendsen, 2006]. Equation (2.2.10) is the simplified continuity equation where equations (2.2.11) and (2.2.12) are the simplified momentum equations in the x- and z-direction, respectively.

$$\frac{\partial u}{\partial x}+\frac{\partial w}{\partial z}=0 \tag{2.2.10}$$

$$x: \quad \frac{\partial u}{\partial t}+u\frac{\partial u}{\partial x}+w\frac{\partial u}{\partial z}=-\frac{1}{\rho}\frac{\partial P}{\partial x}+\nu\frac{\partial^2 u}{\partial z^2} \tag{2.2.11}$$

$$z: \quad \frac{\partial P}{\partial z}=0 \tag{2.2.12}$$

The boundary conditions for these equations are given by (2.2.13). The first boundary condition implies that the horizontal and vertical flow velocities are zero at the bottom. The second boundary condition is called the matching condition where δ is the boundary layer thickness [Svendsen, 2006]. This boundary condition implies that outside the boundary layer the flow velocity equals U_b which is the potential flow velocity at z=0.

$$\begin{aligned} &i) \quad u=0, \quad w=0 \qquad at \quad z=0 \\ &ii) \quad u\to U_b \qquad\qquad at \quad z/\delta\to\infty \end{aligned} \tag{2.2.13}$$

Considering the boundary layer equations and the boundary conditions, the first order solution for the horizontal and vertical flow velocities are given by equations (2.2.14) and (2.2.15), respectively [Svendsen, 2006]. Here β is the Stokes length given by $(2\nu/\omega)^{1/2}$ and θ=ωt-kx. These solutions are illustrated in the figures below. These figures show velocity profiles for 9 different phases over a wave period. Following these phases the oscillating flow behaviour is observed clearly. The horizontal flow velocities as shown in Figure 6, increase from zero at the bed towards the potential flow velocity U_b as follows from the boundary condition in (2.2.13).

$$u^{(1)}(\theta,z)=U_1\left[\cos\theta-e^{-\beta z}\cos(\theta-\beta z)\right] \tag{2.2.14}$$

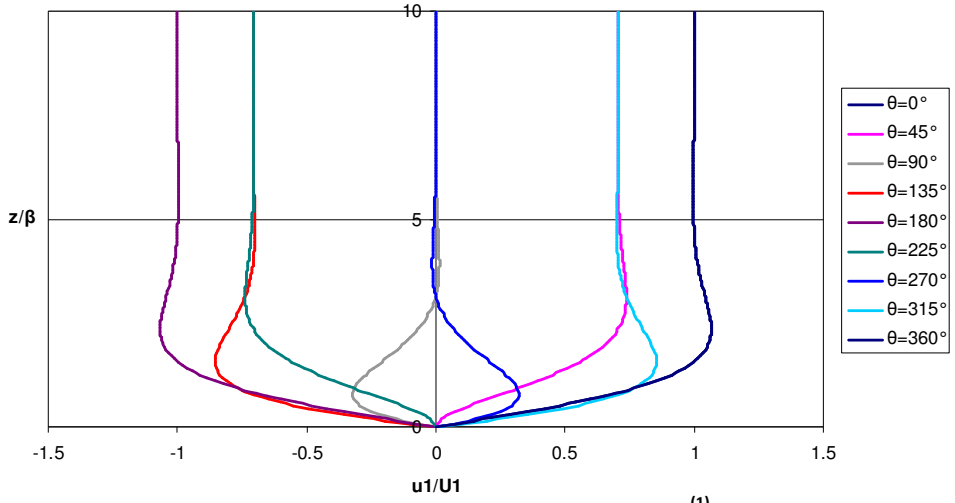

Figure 6: First order horizontal velocity profile $u^{(1)}(z,\theta)$

$$w^{(1)}(\theta,z)=-\frac{U_1 k}{\beta}\left\{\beta z\sin\theta+\frac{1}{\sqrt{2}}e^{-\beta z}\sin\left(\theta-\beta z-\frac{\pi}{4}\right)-\frac{1}{\sqrt{2}}\sin\left(\theta-\frac{\pi}{4}\right)\right\} \tag{2.2.15}$$

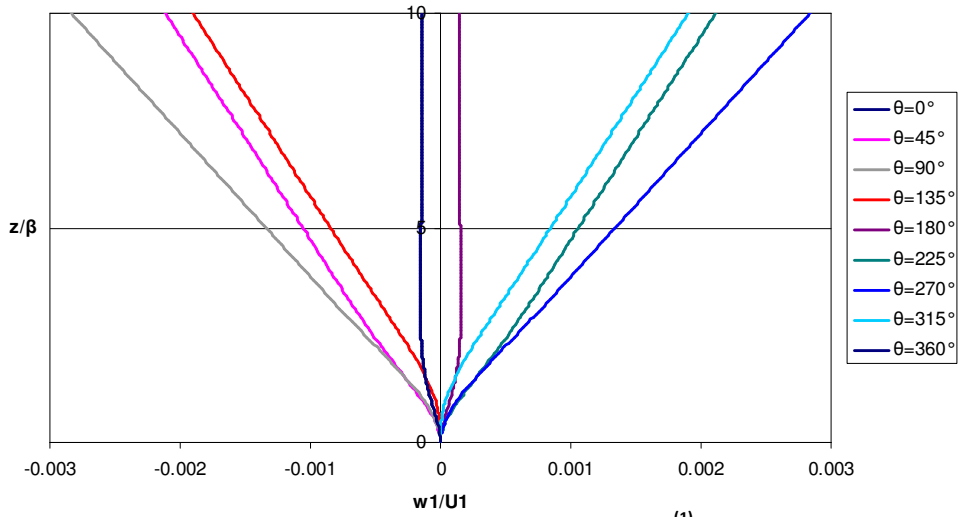

Figure 7: First order vertical velocity profile $w^{(1)}(z,\theta)$

The parameter δ=1/β is often considered as a measure of the boundary layer thickness but there is no well defined upper limit to the boundary layer. A more realistic measure of the boundary layer thickness is 2δ or 3δ as this is the height where it appears reasonable to say that $u^{(1)} \approx U_b$ [Svendsen, 2005]. In this research the boundary layer thickness is defined as twice the distance from the bed where the amplitude of the horizontal oscillating velocity $u^{(1)}$ has reached the maximum (see Figure 6). The reason for this is to make sure that the shear stress is negligible and thus the flow is not influenced by the bed.
The time-dependant wave Reynolds shear stress and the wave Reynolds shear stress is calculated from the product of $u^{(1)}w^{(1)}$ and is shown in the figure below for different phases over an entire wave period. Furthermore, the wave-averaged Reynolds stress is also shown in this figure. It can be seen that the wave Reynolds stress is zero at the bed and increases towards an asymptotic negative value. As a result there is a downward transfer of momentum into the boundary layer, as discussed in section 2.2 (see Figure 4) that gives positive streaming velocities. This positive steady streaming u_s was first derived by Longuet-Higgins [1953] and is shown in equation (2.2.16). In chapter 3 the behaviour of this solution is further analysed for different wave conditions.

$$u_s(z) = \frac{U_1^2}{4c}\left\{3 + e^{-2\beta z} - 2e^{-\beta z}\left[(\beta z - 1)\sin\beta z + (\beta z + 2)\cos\beta z\right]\right\} \qquad (2.2.16)$$

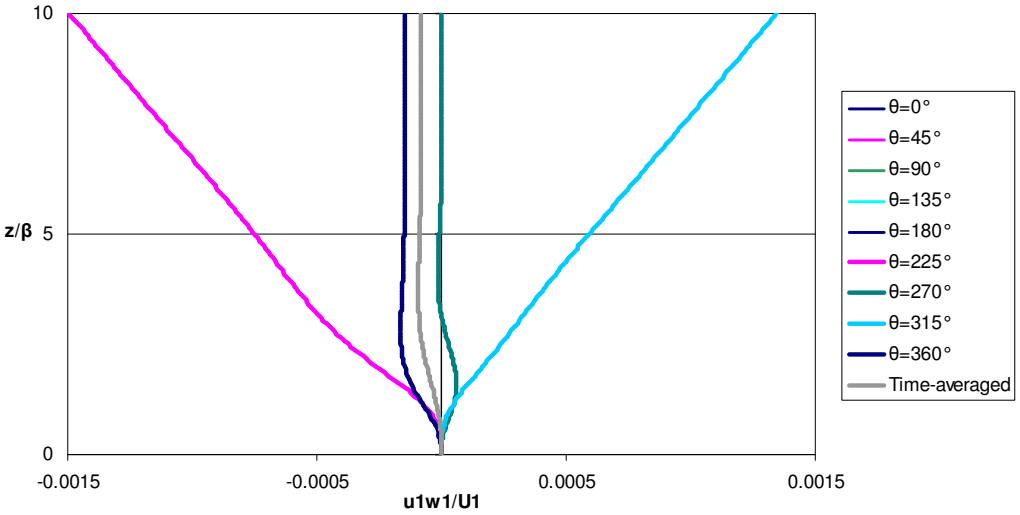

Figure 8: Time-dependant behaviour of the wave Reynolds shear stress

Summary of chapter 2

In this chapter the governing equations for the boundary layer are shown together with the wave-averaged equations. It is shown that the driving forces for streaming are the wave Reynolds stress that originates from the existence of vertical velocities and the wave component of mean turbulent Reynolds stress that is associated with wave asymmetry. Above flat beds the wave Reynolds stress has a positive contribution to streaming where the wave component of mean wave Reynolds stress has a negative contribution to streaming.

3 Analysis on streaming models

In this chapter, first of all, cross-shore streaming profiles are calculated according to different streaming models under (wave) conditions formulated in 1.5. In this way the cross-shore behaviour of streaming is analyzed (paragraph 3.1). Furthermore, the three streaming models as well as the adjusted model of DV99 are compared to examine how different mechanisms affect the streaming velocities and which of the three streaming models compare the best to the POINT SAND model (paragraph 3.2).

3.1 Cross-shore streaming profiles

In the following sections, first a short description is given of different streaming models and the underlying assumptions made in each model are discussed. Subsequently, cross-shore streaming profiles are calculated to analyze the cross-shore behaviour of streaming according to each model and finally, the results are discussed.

3.1.1 LH53 – constant viscosity

Here the Longuet-Higgins solution [1953] for streaming as shown in equation (3.1.1) is further analyzed for characteristic wave conditions (see Table 1 and Table 2). This solution is limited to the first order approximation of the boundary layer equations discussed in section 2.3. The LH53-solution is valid in case of purely progressive, monochromatic waves, and a flat bed. Furthermore, a constant viscosity v is required where the flow could be laminar or turbulent. The streaming profile is thus determined only by the presence of the wave Reynolds stress. In the figures below the Longuet-Higgins solution is shown for different cross-shore water depths. It should be noticed that not only the water depths are variable in these figures but also other wave parameters such as wave height *H* and wave propagation speed *c* (see wave conditions formulated in section 1.5).

$$u_s(z) = \frac{U_1^2}{4c}\left\{3 + e^{-2\beta z} - 2e^{-\beta z}\left[(\beta z - 1)\sin\beta z + (\beta z + 2)\cos\beta z\right]\right\} \tag{3.1.1}$$

$$U_1 = \frac{H\omega}{\sinh(kh)} \tag{3.1.2}$$

From the figures below it can be seen that the streaming velocities at all depths are positive. As mentioned before the reason for this is the assumption of monochromatic waves and thus the presence of only the wave Reynolds stress that gives a positive gradient of mean velocity (see section 2.2). Furthermore, the streaming velocities grow from zero at the bed towards an asymptotic positive value as the mean pressure gradient is neglected while deriving the Longuet-Higgins solution.

Both figures show increasing streaming velocities as the water depths decrease. This can be explained by the term $U_1^2/4c$ at the right hand side of (3.1.1) as this determines the magnitude of the streaming velocities while the other part inside brackets determines the shape of the streaming profiles. Approaching the coast, the near-bed peak orbital velocity U_1 given by (3.1.2) increases (wave height increases while kh decreases, see wave conditions in section 1.5). In contrast to this the wave propagation speed *c* decreases (the wave lengths decrease while the wave period remains constant). As a result, the value of the $U_1^2/4c$ term increases which gives higher streaming velocities while approaching the coast. Therefore, above flat beds and purely progressive, monochromatic waves an increasing wave height *H* results in higher streaming velocities for a certain wave period. In contrast to this streaming velocities increase with decreasing wave length *L* for a certain wave period.
The streaming velocities are higher for wave 2 than for wave 1, at same depths. The reason for this is the greater wave heights and wave periods for wave 2 which results in higher near-bed peak orbital velocities U_1 and lower wave propagation speed *c*.
Another remarkable aspect that can be noticed in both figures is that the streaming velocities are maximum at the same level *z* independent of the water depths. The reason for this is the fact that a constant viscosity *v* is assumed and therefore the thickness of the boundary layer δ, which is proportional to the square root of vT, remains unchanged approaching the coast. However, this level *z* is higher for wave 2 than that of wave 1 as can be seen from both figures. This is caused by the greater wave period *T* of wave 2 compared to that of wave 1 resulting in thicker boundary layer for wave 2.

Shortly summarized, for purely progressive, monochromatic waves and a time- and depth-independent viscosity above flat beds, the streaming velocities according to the solution of Longuet-Higgins [1953] are determined only by the presence of the wave Reynolds stress. Therefore the streaming velocities are positive at all depths and grow from zero at the bed towards an asymptotic value. Furthermore, the streaming velocities increase with decreasing water depths while the (vertical) shape of the profiles remains unchanged. Approaching the coast, the streaming velocities increase with increasing wave height *H* and decreasing wave length *L*.

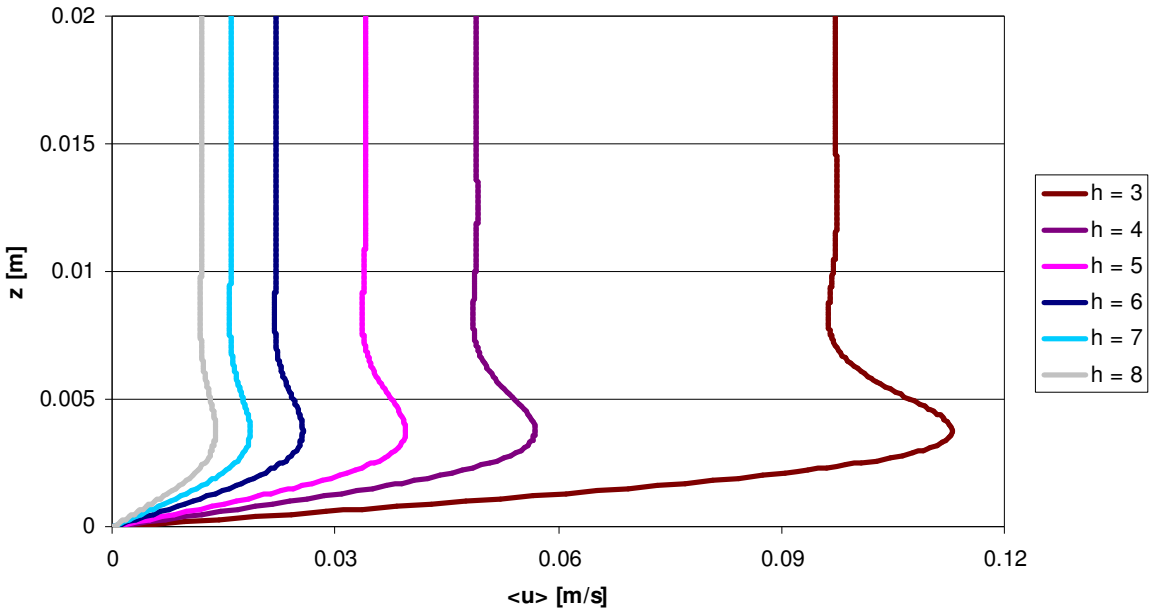

Figure 9: Cross-shore behaviour of LH – solution, for wave 1

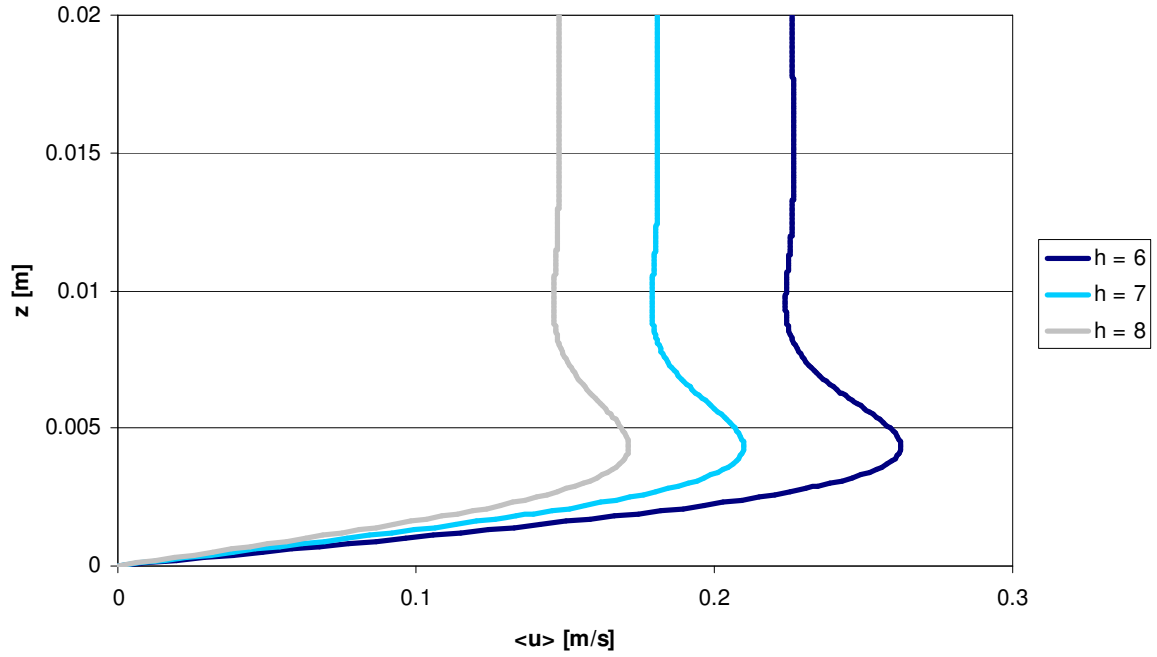

Figure 10: Cross-shore behaviour of LH – solution, for wave 2

3.1.2 DV99 [(a)] – time varying viscosity above rippled bed

In this section the Davies and Villaret solution [1999] for streaming is analyzed. Where Longuet-Higgins gives a solution to first order neglecting the convective terms in the boundary layer equations, Davies and Villaret [1999] give a solution to second order approximation of the boundary layer equations (see section 2.3). However, both models assume an open boundary thus neglecting the pressure gradient.

In contrast to the LH53 solution, the waves in DV99 solution are velocity-skewed and the bed is very rough consisting of ripples. Above such beds the momentum transfer is not dominated by random turbulence, but by the well-organized process of vortex shedding. In order to take account for this, a strongly time-varying eddy viscosity model has been formulated by Davies and Villaret [1999] and is discussed here as well. The streaming profile according to Davies and Villaret [1999] is thus determined by the presence of the wave Reynolds stress as well as the wave part of the mean turbulent Reynolds stress.

The time-dependent eddy viscosity model of Davies and Villaret [1999] is given by the following equation.

$$K = \frac{1}{2} K_0 \left[1 + \varepsilon_1 e^{i(\omega t - kx)} + \varepsilon_2 e^{2i(\omega t - kx)} \right] \tag{3.1.3}$$

The first term on the right hand side of this equation is the cycle-mean value of the eddy viscosity (K_0) that is calculated using equation (3.1.5) or (3.1.4), according to whether A_1/k_s is less than or greater than 2.5. A_1 is the near-bed velocity amplitude where k_s is the equivalent bed roughness. For rough rippled beds a value of 0.213 m is assumed for k_s (after the experiments of Mathisen and Madsen, 1996a,b).

$$\frac{K_0}{2} = 0.004 U_1 k_s \qquad \frac{A_1}{k_s} < 2.5 \tag{3.1.4}$$

$$\frac{K_0}{2} = 0.00253 U_1 \sqrt{A_1 k_s} \qquad \frac{A_1}{k_s} > 2.5 \tag{3.1.5}$$

The second term on the right hand side of equation (3.1.3) represents the time variation in the eddy viscosity, which occurs at the first harmonic frequency as a result of asymmetry in the free stream flow. The magnitude of this asymmetry is represented by the value of the complex coefficient ε_1 given by equation (3.1.6): the greater the asymmetry in the turbulence intensity the greater is the value of ε_1.

$$\varepsilon_1 = \left| \varepsilon_1 \right| \exp\left(i \phi_1 \right) \tag{3.1.6}$$

The third term on the right hand side of (3.1.3) represents symmetrical time variation in the eddy viscosity, which occurs as a result of eddy shedding from the bed in each wave half cycle. The magnitude of this variation (fluctuations from the cycle-mean value K_0) is represented by the value of the complex coefficient ε_2 given by (3.1.7): the greater the time variation in the eddy viscosity the greater is the value of ε_2.

$$\varepsilon_2 = |\varepsilon_2| \exp(i\phi_2) \tag{3.1.7}$$

The phase angels of the complex coefficients are given by ϕ_1 and ϕ_2. Here the value of ϕ_1 is governed by the eddy shedding process at the bed where the value of ϕ_2 is governed by the phase of eddy shedding at flow reversal. Considering rough rippled beds, Davies and Villaret [1999] give the following values for the complex coefficients and phase angles such that the peak value of *K* occurs at about the time of flow reversal following the passage of each wave crest: $I\varepsilon_1 I = I\varepsilon_2 I = 1.3$, $\phi_1 = -80^\circ$ and $\phi_2 = 200^\circ$. The different terms of the eddy viscosity model in (3.1.3) are visualised in Figure 11 where the resulting time-dependent eddy viscosity *K* is illustrated in Figure 12 together with the variation in the free stream velocity.

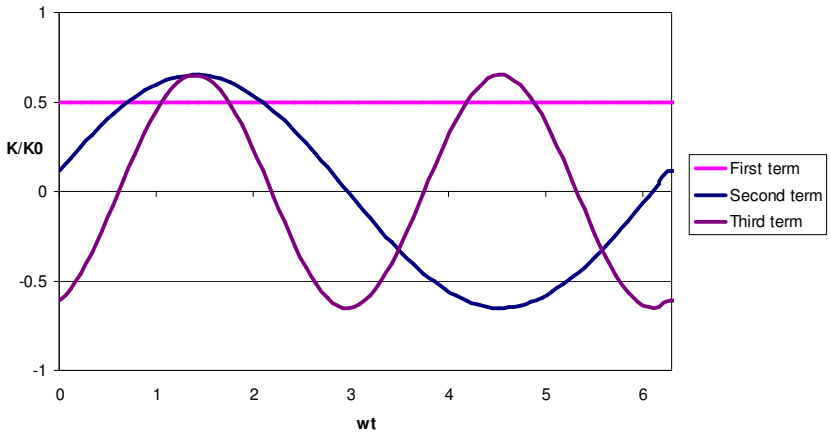

Figure 11: Contribution of different terms to the Eddy viscosity model

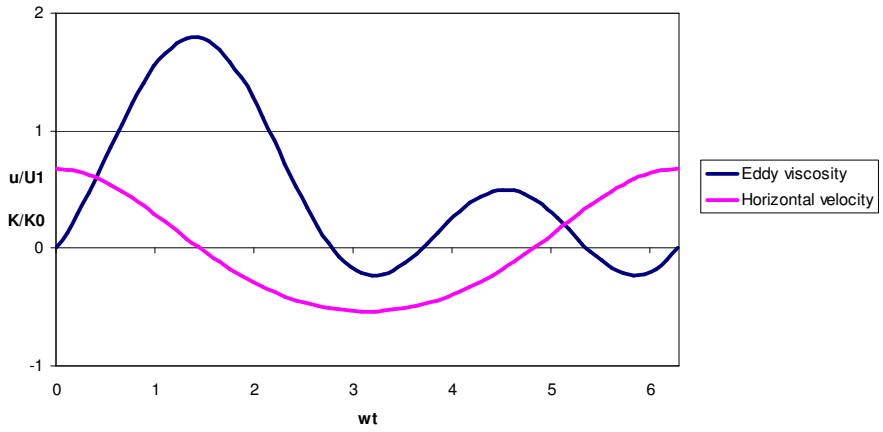

Figure 12: Time-dependent eddy viscosity model of DV99

The Davies and Villaret solution for streaming is given by (3.1.8) that consists of three terms.

$$\overline{U} = \overline{U^{(1)}} + \overline{U^{(2)}} + \overline{U^{(3)}} \tag{3.1.8}$$

The first term (3.1.9) arises from the wave Reynolds stress associated with the first order velocity field where $\bar{u}_s$ is the Longuet-Higgins solution as discussed in the previous section. Here ϕ_2 determines the shape of the $U^{(1)}$ profile where ε_2 determines its magnitude. The greater the time variation in the eddy viscosity, the smaller is the contribution of this term to the streaming velocities. In other words, the greater the value of ε_2 the smaller is the $U^{(1)}$ term.

$$\overline{U^{(1)}} = \overline{u_s}\left[1+\frac{1}{2}|\varepsilon_2|\cos\varphi_2\right] \tag{3.1.9}$$

The second term (3.1.10) is the contribution to the streaming velocity associated with asymmetry in the turbulent intensity and thus contribution of the wave part of the mean turbulent Reynolds stress. The shape of the profile of this term is determined by ϕ_1 where its magnitude is determined by ε_1. The greater the asymmetry in the turbulent intensity, the greater is the contribution of this term to the streaming velocities.

$$\overline{U^{(2)}} = U_1|\varepsilon_1|\left[\frac{1}{2}e^{-\beta z}\cos(\beta z+\varphi_1)-\frac{1}{2}\cos\varphi_1\right] \tag{3.1.10}$$

The third term (3.1.11) is the contribution to streaming associated with time variation in the eddy viscosity. The shape of the profile of this term is determined by ϕ_2 where its magnitude is determined by ε_2. The greater the time variation in the eddy viscosity, the greater is the contribution of this term to the streaming velocities. Furthermore, the effect of the wave asymmetry parameter *B* is to increase the contribution of this term to streaming.

$$\begin{aligned}\overline{U^{(3)}} = \frac{|\varepsilon_2|U_1^2}{4c}\Big\{&e^{-\beta z}\cos(\beta z+\varphi_2)+\beta z e^{-\beta z}\left[\cos(\beta z+\varphi_2)+\sin(\beta z+\varphi_2)\right]\\&-e^{-\sqrt{2}\beta z}\cos\left(\sqrt{2}\beta z+\varphi_2\right)\Big\}+\frac{|\varepsilon_2|}{2}BU_1\left[e^{-\sqrt{2}\beta z}\cos\left(\sqrt{2}\beta z+\varphi_2\right)-\cos\varphi_2\right]\end{aligned} \tag{3.1.11}$$

Here $\beta=(K_0/\omega)^{1/2}$ is the wave number that characterises the decay rate of the shear wave with height above the bed. Furthermore, U_1 is the near-bed horizontal velocity amplitude where *B* is the wave asymmetry parameter equal to the ratio between U_2 (near-bed horizontal velocity amplitude of Stokes second order solution) and U_1.

In the figures below the Davies and Villaret solution is shown for different cross-shore water depths, for wave 1 (Figure 13) and wave 2 (Figure 14). It should be noticed that not only the water depths are variable in these figures but also other wave parameters such as wave height *H* and wave propagation speed *c* (see wave conditions formulated in section 1.5). Both figures show streaming velocities that grow from zero at the bed towards an asymptotic positive or negative value depending on the water depth. Close to the bed, the streaming velocities are positive at all water depths as it is the case according to the LH53-solution. Away from the bed (at the edge of the boundary layer which is somewhere between 5 to 10 cm for wave 1), the streaming velocities can reverse direction and thus become negative for increasing water depths.
In contrast to the LH53-solution, the near-bed streaming velocities are maximum at different (higher) levels z while approaching the coast. The reason for this is the presence of a time-dependant eddy viscosity. Approaching the coast, the near-bed peak orbital velocity U_1 increases which leads to an increasing cycle-mean value of the eddy viscosity K_0 according to both (3.1.4) and (3.1.5). This increasing value of K_0 results in increasing thickness of the boundary layer as can be seen in both figures, while approaching the coast. The wave boundary layer thickness as defined by Davies and Villaret [1999] is $\delta = 5(K_0/\omega)^{1/2}$.
As shown in equation (3.1.8), the DV99-solution for streaming is composed of three terms. To understand the cross-shore behaviour of streaming profiles, the cross-shore behaviour of the individual terms ($U^{(1)}$, $U^{(2)}$ and $U^{(3)}$) should be analyzed. The cross-shore behaviour of these terms, for both waves, is shown in appendix B. From the figures in appendix B, it can be seen that the $U^{(2)}$ term gives the largest contribution to streaming velocities followed by $U^{(3)}$ and eventually by $U^{(1)}$. Therefore, it can be concluded that above rough rippled beds the streaming velocities are mostly determined by the contribution of the wave part of the mean turbulent Reynolds stress, where the contribution of the wave Reynolds stress is significantly smaller. This is caused by the strong, well-organized process of vortex shedding above rippled beds. This is also observed in the cross-shore streaming profiles for wave 1 as shown in Figure 13. From this figure it can be seen that the shape of the streaming profiles are greatly determined by the $U^{(2)}$ and $U^{(3)}$ term (especially for more offshore water depths): positive near-bed jet and negative outer flow.

Shortly summarized, for progressive, velocity-skewed waves and time-dependent eddy viscosity above rough rippled beds, the streaming velocities according to the solution of Davies and Villaret [1999] grow from zero at the bed towards an asymptotic negative or positive value. In contrast to flat rough beds where asymmetry in turbulence intensity gives rise to negative near-bed streaming velocities (see section 2.2), asymmetry in turbulence intensity above rippled beds leads to positive near-bed streaming velocities. This behaviour is clearly visible in streaming profiles of wave 1 and wave 2. Furthermore, it can be concluded that above rough rippled beds the streaming velocities are mostly determined by the contribution of the wave part of the mean turbulent Reynolds stress, where the contribution of the wave Reynolds stress is significantly smaller.

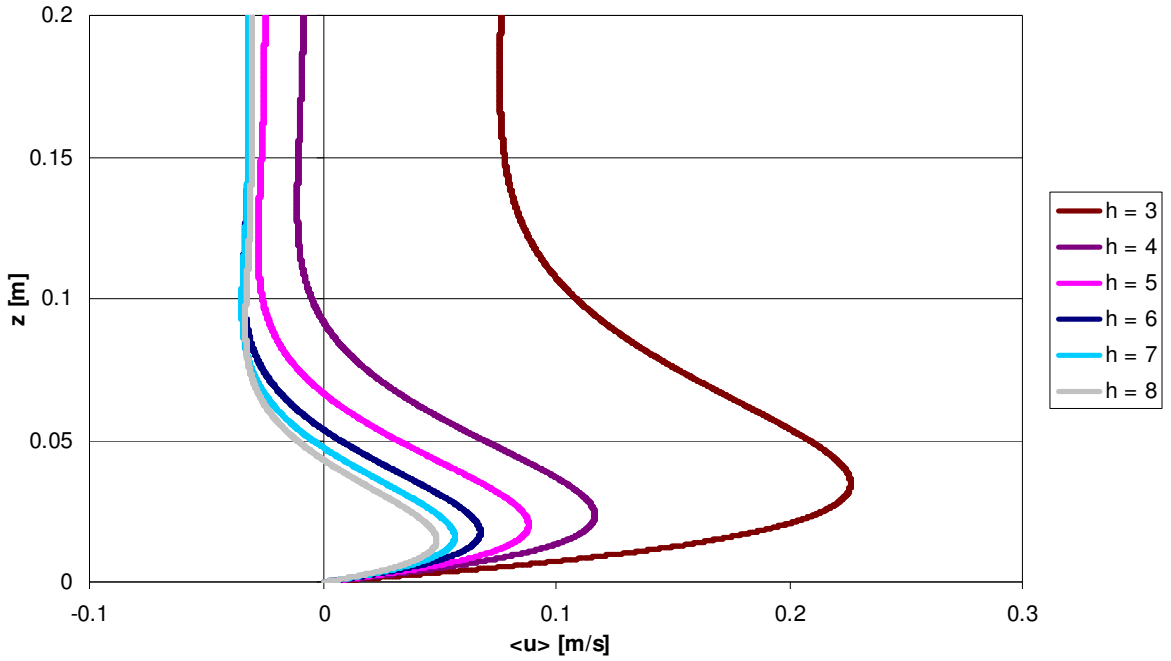

Figure 13: Cross-shore solution of DV99[(a)] above rippled beds, for wave 1

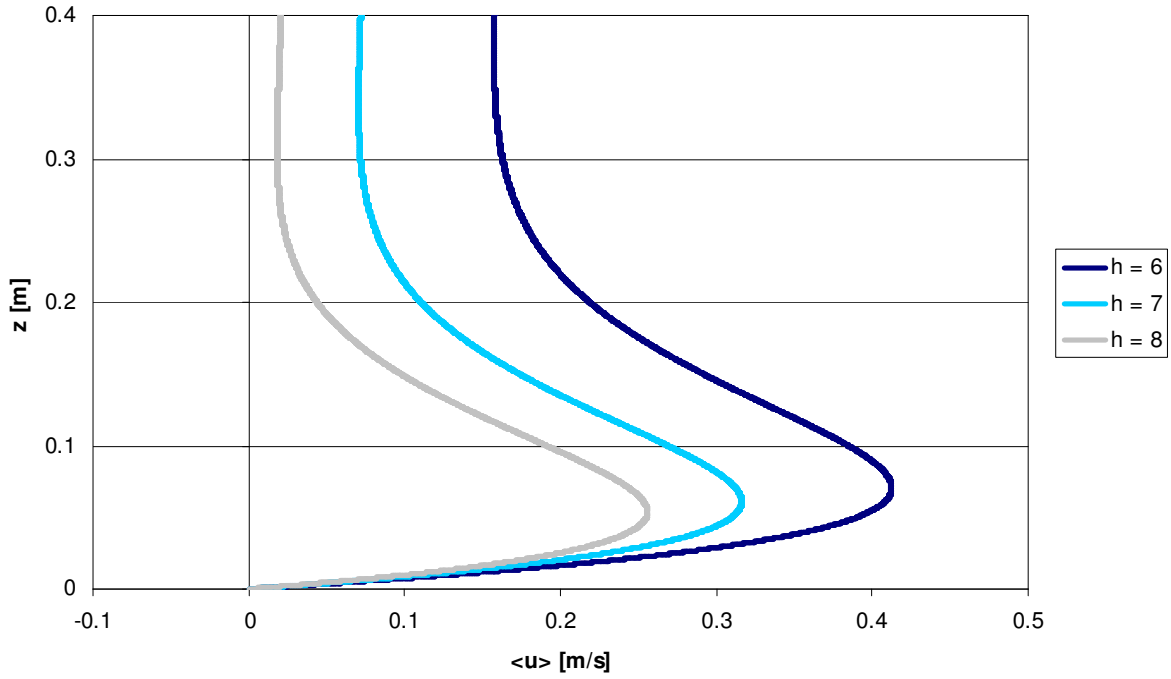

Figure 14: Cross-shore solution of DV99[(a)] above rippled beds, for wave 2

3.1.3 PSM – time and depth varying viscosity

In this section the POINT SAND model (PSM) by Uittenbogaard [1999] is discussed and is then used to calculate cross-shore streaming profiles for (wave) conditions formulated in section 1.5. In order to use the PSM, first a sensitivity analysis is done with respect to the run time of the model, used time steps and grid sizes.

PSM is a 1-DV (one-dimensional vertical), unsteady model that exists of two parts: a hydrodynamic part and a part for sediment transport. In this case the focus is on the hydrodynamic part of the model. In contrast to the LH53 and DV99 solutions, PSM gives a numerical solution to the set of flow equations formulated in section 2.1. In order to transform these equations to a 1-DV framework, which is attractive from a computational point of view, all horizontal derivatives are translated to time derivatives by assuming waves of permanent form propagating with celerity

$$\overline{C_w} = \left(C_{w,x}, C_{w,y} \right) \tag{3.1.12}$$

and thus

$$\frac{\partial}{\partial x} = -\frac{1}{C_{w,x}} \frac{\partial}{\partial t}; \frac{\partial}{\partial y} = -\frac{1}{C_{w,y}} \frac{\partial}{\partial t} \tag{3.1.13}$$

In contrast to the solutions of Longuet-Higgins [1953] and, Davies and Villaret [1999] the pressure gradient is not neglected in the PSM and therefore account is taken for the return flow that results from a closed boundary. As mentioned in section 1.5 the focus of this research is on the bottom boundary layer and therefore the effect of such superimposed currents on the boundary layer is not considered in this research.

The flow solved by the model is time-dependent during the wave cycle. Firstly, the model solves the horizontal and vertical orbital velocities. Then the net-effect of turbulent motions on the flow is determined where the turbulence fluxes are represented by a k-ε turbulence model. Finally, the mean velocity profiles and the mean flow rates are determined. The solution procedure is split into an *outer loop* for the mean-flow equations and into *inner loops* for each spectral component of the orbital motions. The time step used in the *inner loop* is a fraction of the shortest wave period, the time step of the *outer loop* usually equals the shortest wave period. Furthermore, a time-independent and non-equidistant grid is used where a grid size that increases exponentially from the bed-layer is preferred (Uittenbogaard, 2000) and also used in the model simulations (see PSM input file in Appendix C).

The POINT SAND model simulates the currents and waves as a function of time as well as a vertical co-ordinate *z*, while using turbulent closures (Uittenbogaard, 1999). The eddy viscosity ν_t is thus time- and depth dependent as shown in Figure 15, where ν_0 is the time- and depth-averaged eddy viscosity above flat beds. Here also the depth-averaged horizontal velocity is shown. As can be seen from this figure, there is a time-lag in the eddy viscosity which increases with increasing distance from the bed. The eddy viscosity close to the bed (z=3 mm) is in phase with the horizontal velocity: maximum eddy viscosity occurs at about the same time where the horizontal velocity is at its maximum value. Further away from the bed (outside the boundary layer) maximum eddy viscosity seems to occur at flow reversal.

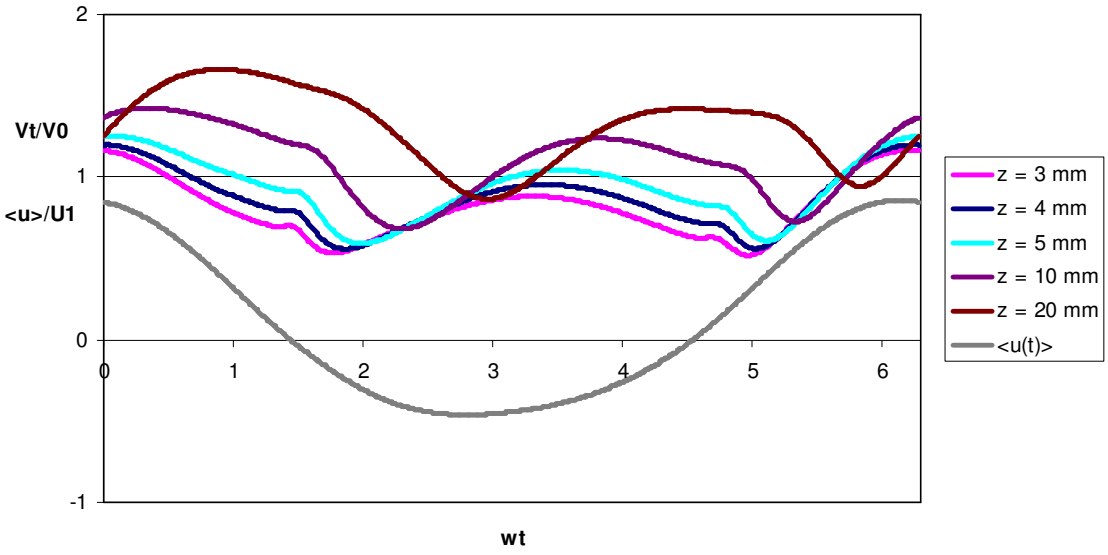

Figure 15: Time- and depth dependent eddy viscosity according to the PSM

The model is able to simulate different situations: in presence of only an oscillatory horizontal flow in a tunnel, in presence of both horizontal and vertical orbital velocities in free-surface wave channel or in the field with different wave and current directions. Furthermore, the PSM can only be used where the bed is flat and the waves are stationary and do not break. In this study the PSM is used to simulate free-surface wave channels.

In order to calculate cross-shore streaming profiles with the POINT SAND model, a sensitivity analysis is performed where the convergence and the stability of the model is examined (see appendix C). Here the effect of different time steps, grid sizes and model run time on the time-averaged horizontal velocity is considered. Furthermore, an example of an input file of the POINT SAND model is shown in appendix C. The combination of model run time, time step and grid size for which the time-averaged velocity is practically constant, is used for further calculations. From the figures in appendix C, it can be concluded that for a run time of about 2300 seconds, time step of T/600 (wave period divided by 600) and grid size of h/200 (water depth divided by 200) the model results are quite stable.

Using this combination of model characteristics, the cross-shore streaming profiles for (wave) conditions formulated in section 1.5 are calculated and discussed below. It should be noticed that not only the water depths are variable in these figures but also other wave parameters such as wave height *H* and wave propagation speed *c*.
The cross-shore behaviour of streaming profiles above flat beds is illustrated in Figure 16 (wave 1) and Figure 17 (wave 2). From these figures it can be seen that the streaming velocities are positive for both waves regardless of the cross-shore water depths. Therefore, above flat beds and the considered (wave) conditions, the positive contribution of the wave Reynolds stress to streaming velocities is more dominant than the negative contribution of the wave part of the mean turbulent Reynolds stress. This statement is investigated in more detail in the following section (see Figure 28).

For wave 1 (Figure 16), the streaming velocities increase as the water depths decrease thus as the coast is approached. In contrast to this, for wave 2 with a larger wave period and wave length, the streaming velocities decrease with decreasing water depths. However, the streaming velocities for wave 2 are larger than for wave 1, at same water depths. Apparently, the contribution of the wave part of the mean turbulent Reynolds stress to streaming velocities becomes more important with increasing wave period and wave length, while approaching the coast.
Furthermore, for both waves the near-bed streaming velocities are maximum at different levels z while approaching the coast. This is a reflection of the time- and depth-dependent eddy viscosity of the POINT SAND model. However, this level *z* is higher for wave 2 than that of wave 1 as can be seen from both figures. This is caused by the greater wave period of wave 2 compared to that of wave 1 resulting in thicker boundary layers for wave 2.

Shortly summarized, for progressive, velocity-skewed waves and time- and depth dependent eddy viscosity above flat beds, the streaming velocities according to the POINT SAND model are positive for both waves regardless of the cross-shore water depths. Therefore, the positive contribution of the wave Reynolds stress to streaming velocities is more dominant than the negative contribution of the wave part of the mean turbulent Reynolds stress.
The streaming velocities for wave 1 increase with decreasing water depths (approaching the coast). In contrast to this, the streaming velocities for wave 2 decrease with decreasing water depths. For waves with longer wave period and wave length, therefore the contribution of the wave part of the mean turbulent Reynolds stress to streaming velocities becomes more important while approaching the coast.

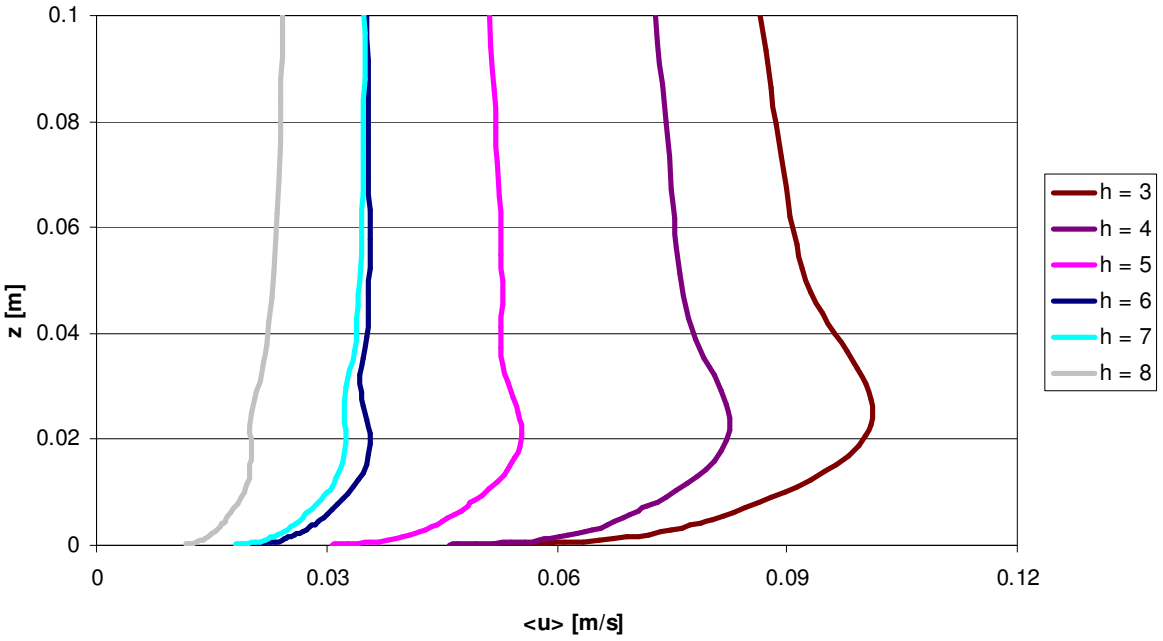

Figure 16: Cross-shore behaviour of the PSM, for wave 1

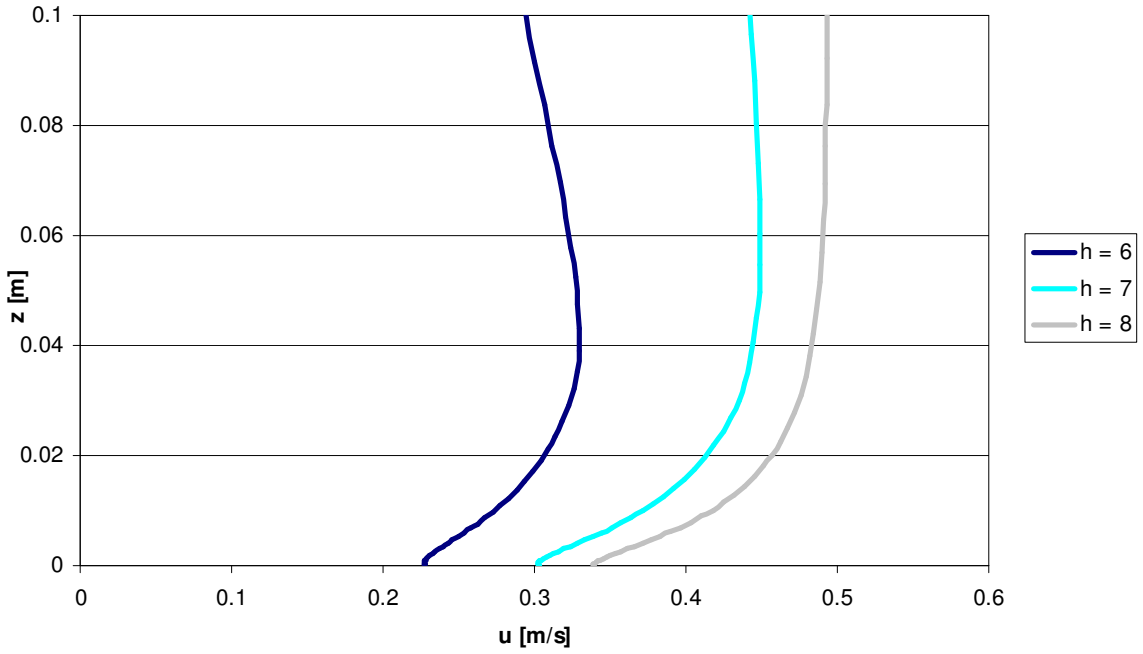

Figure 17: Cross-shore behaviour of the PSM, for wave 2

3.1.4 DV99 (b) – time varying viscosity above flat bed

In this section the Davies and Villaret solution [1999] is used to calculate streaming profiles above rough flat beds. In contrast to rough rippled beds, above flat beds the momentum transfer is dominated by random turbulence and not by vortex shedding. Therefore, to represent rough flat bed situations the values of parameters of the eddy viscosity model (ε_1, ε_2, ϕ_1 and ϕ_2) should be adjusted. This is done by using the time- and depth dependent eddy viscosity from the POINT SAND model that is discussed in the preceding section. The eddy viscosity model of Davies and Villaret [1999] is then matched to the eddy viscosity from PSM that results in adjusted values of the different parameters.

Where Davies and Villaret [1999] give time-dependent eddy viscosity profiles, the POINT SAND model gives eddy viscosity profiles which are depth- and time dependent as shown in Figure 15. In order to match these models, the eddy viscosity profile from PSM should be depth-averaged over the boundary layer thickness. Therefore, first of all the boundary layer thickness for the PSM should be determined. Here the boundary layer thickness δ is defined as twice the distance from the bed where the amplitude of the horizontal oscillating velocity has reached the maximum value. Using this definition, for each water depth the boundary layer thickness is determined as shown in Figure 53 of appendix D. The cross-shore eddy viscosity profiles, depth-averaged over the boundary layer thickness, are then shown in Figure 56 (wave 1) and Figure 57 (wave 2) of appendix E. The cross-shore averaged eddy viscosity profiles are also shown in these figures. These profiles are subsequently used to determine the values of different parameters in the eddy viscosity model of Davies and Villaret [1999].

In the figures below the eddy viscosity model of Davies and Villaret [1999] with the original values of the parameters are shown together with the cross-shore averaged profiles of eddy viscosity obtained from the POINT SAND model. For wave 1 it can be seen that the cross-shore averaged profile from the PSM shows almost no asymmetry in the turbulence intensity. Furthermore, the maximum viscosity occurs at about the time of flow reversal. However, for wave 2 that has a longer wave period and wave length, the cross-shore averaged profile from the PSM shows more asymmetry in turbulence intensity. The maximum viscosity for wave 2 occurs slightly after the time of flow reversal. Using these characteristics of the eddy viscosity profiles of both waves, the parameters of the DV99-model are adjusted in a way to obtain good agreement between viscosity profiles of PSM and DV99-model (see Figure 18 and Figure 19). The focus here is not on the absolute magnitude of the eddy viscosities but on their courses as the direction of the streaming velocities is determined not by the magnitude of the eddy viscosity but by its course. This results in the following values for the parameters of DV99-model:

- Wave 1: $I\varepsilon_1 I = 0.05$, $I\varepsilon_2 I = 0.45$, $\phi_1 = -240^\circ$ and $\phi_2 = -120^\circ$
- Wave 2: $I\varepsilon_1 I = 0.25$, $I\varepsilon_2 I = 0.80$, $\phi_1 = -250^\circ$ and $\phi_2 = -140^\circ$

For wave 2 the value of ε_1 is larger than for wave 1. This reflects the greater asymmetry in the turbulence intensity for wave 2 than for wave 1. Furthermore, the value of ε_2 is also larger for wave 2 than for wave 1. This reflects the more pronounced shape of the eddy viscosity profile of wave 2 (larger fluctuations from the cycle-mean value of eddy viscosity for wave 2 than for wave 1). As discussed above, for wave 1 the maximum viscosity occurs at about the time of flow reversal where for wave 2 this occurs at some time after flow reversal. This is reflected in the different values of ϕ_1 and ϕ_2 for both waves.

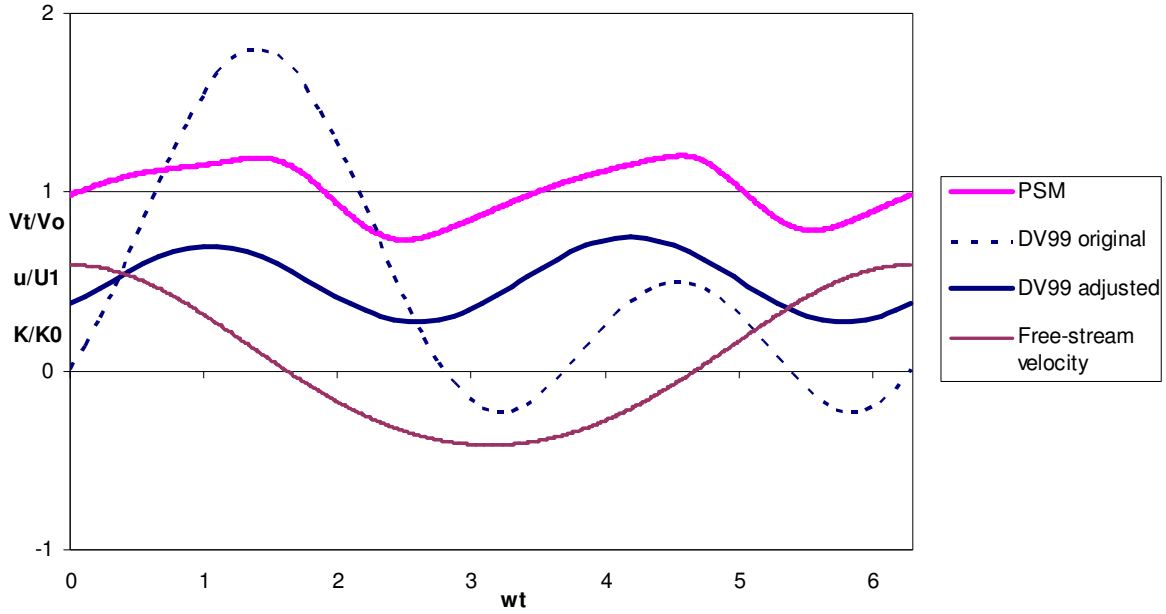

Figure 18: Adjusted eddy viscosity model for flat beds (wave 1)

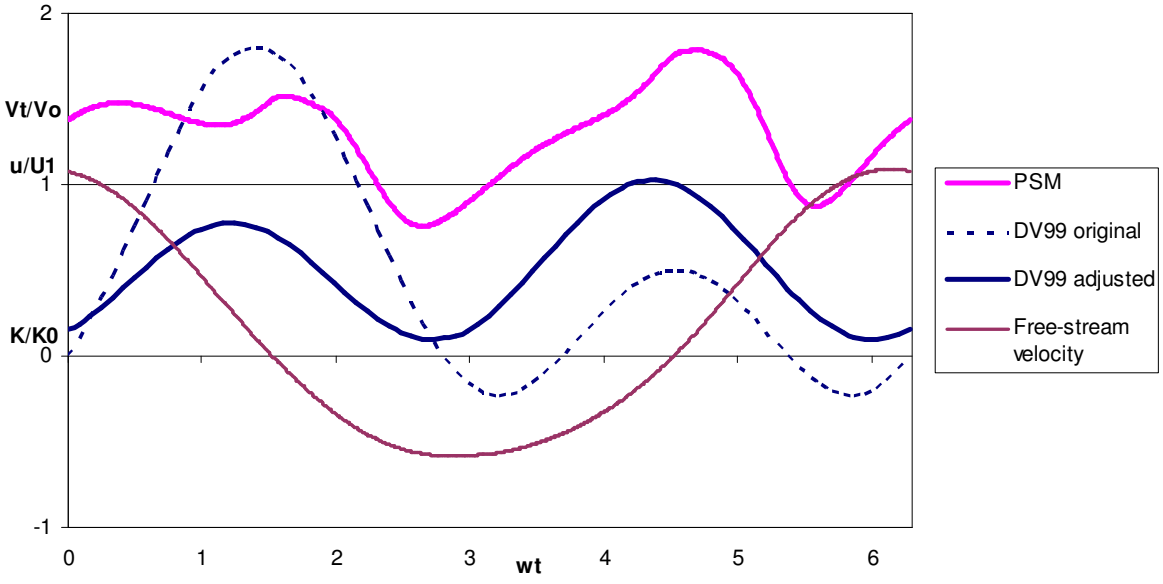

Figure 19: Adjusted eddy viscosity model for flat beds (wave 2)

Using the adjusted values of the parameters in the eddy viscosity model of Davies and Villaret [1999] the cross-shore streaming profiles for the (wave) conditions formulated in section 1.5 are calculated and are shown in the figures below. Here K_0 is calculated using equation (3.1.5) as for flat beds A_1/k_s is greater than 2.5 where k_s is assumed to be 2.5 times the mean grain size diameter D_{50} = 0.24 m.

Where the original model of Davies and Villaret [1999] above rough rippled beds (hereafter referred to as DV99$^{(a)}$) shows velocity profiles that grow from zero at the bed to an asymptotic negative or positive value (see section 3.1.2), the adjusted model for flat beds (hereafter referred to as DV99$^{(b)}$) gives streaming velocities that are positive for both waves regardless of the cross-shore water depths. This seems to be in agreement with the results found from the POINT SAND model as shown in section 3.1.3. This is further investigated in paragraph 3.2 where the streaming models are compared. Furthermore, for both waves the streaming velocities increase with decreasing water depths.

To understand the cross-shore behaviour of DV99$^{(a)}$ as illustrated in the figures below, the behaviour of the individual terms ($U^{(1)}$, $U^{(2)}$ and $U^{(3)}$) of this model is analyzed. The cross-shore behaviour of the different terms for the DV99$^{(b)}$ are shown in appendix F. As discussed in section 3.1.2, the shape of the different terms depends on the values of ϕ_1 and ϕ_2 while the magnitude of the velocities given by each term is determined by ε_1 and ε_2. From the figures in appendix F, it can be seen that the $U^{(1)}$ term gives the largest contribution to streaming velocities followed by $U^{(3)}$ and eventually by $U^{(2)}$. Therefore, it can be concluded that above flat beds the streaming velocities are mostly determined by the contribution of the wave Reynolds stress, where the contribution of the wave part of the mean turbulent Reynolds stress is significantly smaller. This is also observed in the cross-shore streaming profiles for wave 1 and wave 2 as shown in the figures below. From these figures it can be seen that the shape of the streaming profiles are greatly determined by the $U^{(1)}$ term: positive velocities near-bed as well as away from bed.

Shortly summarized, above flat beds the adjusted model of Davies and Villaret [1999] shows positive streaming velocities near-bed as well as further away from the bed. Furthermore, it can be concluded that above flat beds the streaming velocities are mostly determined by the contribution of the wave Reynolds stress, where the contribution of the wave part of the mean turbulent Reynolds stress is significantly smaller. The opposite is true for the streaming velocities above rough rippled beds as discussed in section 3.1.2. The reason for this is the strong, well-organized process of vortex shedding above rippled beds where above flat beds the momentum transfer is dominated by random turbulence.

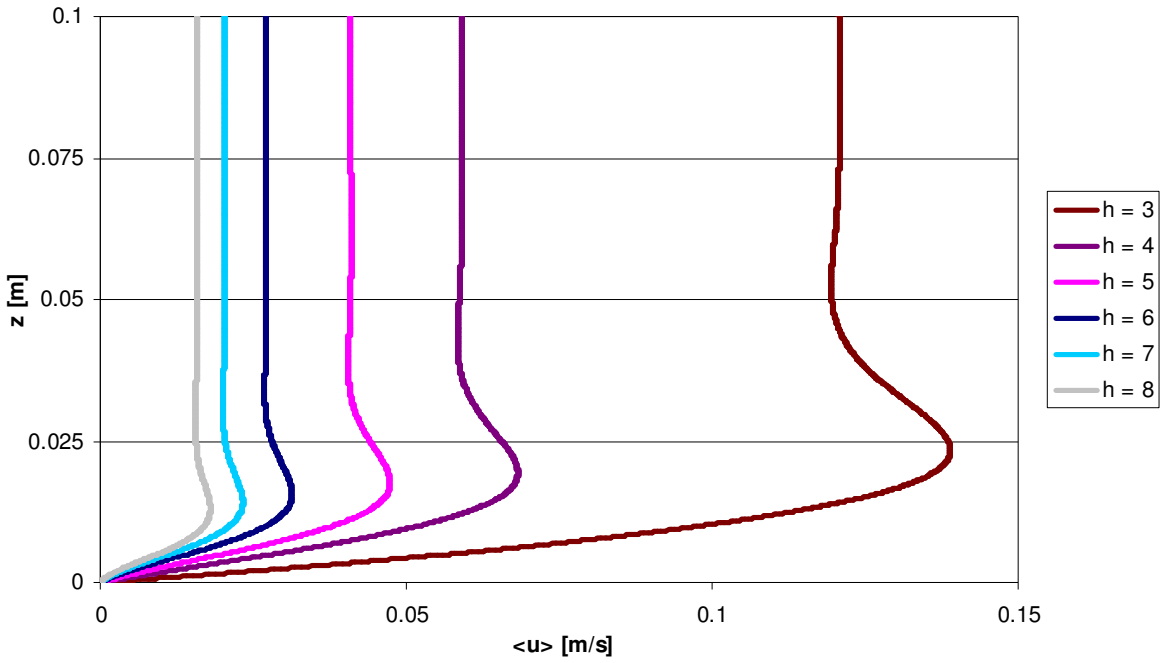

Figure 20: DV99 solution for flat beds (wave 1)

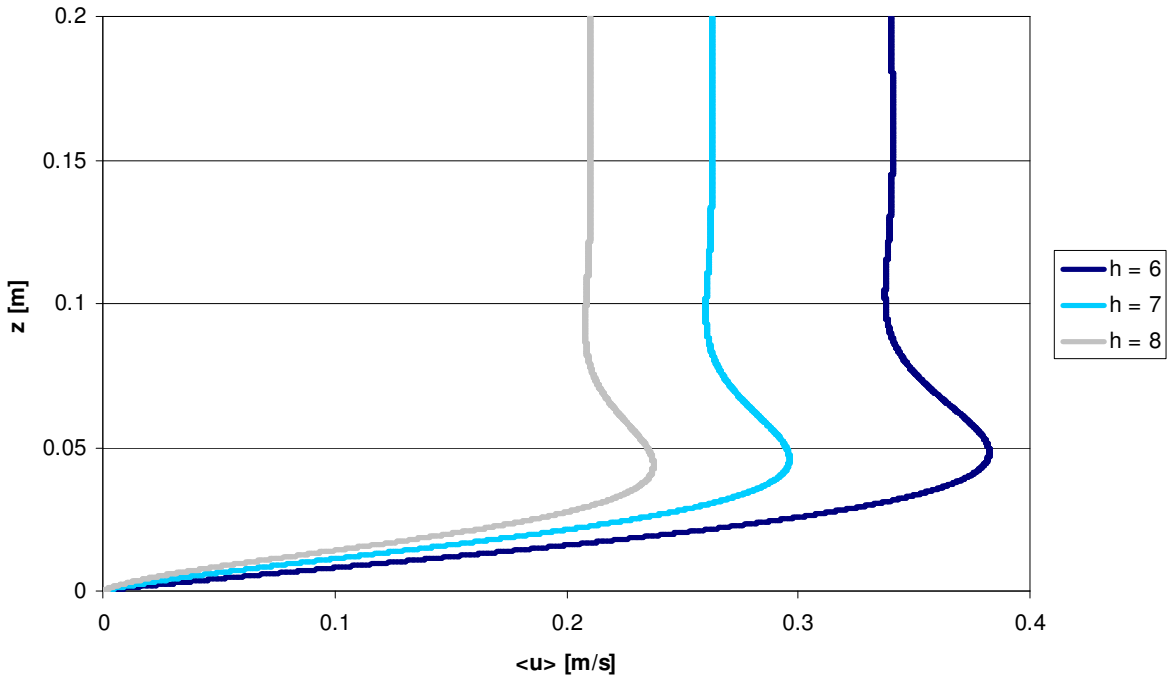

Figure 21: DV99 solution for flat beds (wave 2)

3.2 Comparison of the streaming models

In this paragraph the streaming models discussed in 3.1 are compared to examine how the streaming velocities are affected by different models that take account for different flow mechanisms (answer to central question 1). In order to examine the behaviour of these models under the characteristic (wave) conditions, the streaming velocities given by each model are plotted together in one figure for a certain water depth. Furthermore, a characteristic level z (edge of the boundary layer) is chosen to analyze the behaviour of these models. The observed behaviour is analyzed on the basis of the driving forces of streaming: the wave component of mean turbulent Reynolds stress and the wave Reynolds stress.

In order to make a good comparison of the behaviour of the streaming models discussed in paragraph 3.1, the streaming profiles given by each model are plotted in one figure for a certain water depth (h=3 to 8 meters, see the figures below). Here the streaming velocities as well as the vertical *z* are made dimensionless. The streaming velocities are divided by the near-bed horizontal velocity amplitude U_1, where the vertical *z* is divided by the Stokes length β. In this way the top of the boundary layer for each model is at level z/β=4.8 as will be shown later on. For the LH53 solution β is given by $(2\nu/\omega)^{1/2}$ where for the DV99 solution and the POINT SAND model, β is given by $(K_0/\omega)^{1/2}$. For the DV99 solution K_0 is the time-averaged eddy viscosity as discussed in section 3.1.2. For the PSM K_0 is the time- and depth-averaged (over the boundary layer thickness) eddy viscosity as discussed in section 3.1.4.

From the figures below it can be seen that above flat beds (LH53, DV99$^{(b)}$ and PSM) the dimensionless streaming velocities are positive at all levels z/β and for all water depths considered. Furthermore, these velocities increase with decreasing water depths. Above flat beds the largest velocities (near-bed as well as away from the bed) are given by the POINT SAND model followed by the adjusted Davies and Villaret solution and the LH53 solution. As the (wave) conditions are the same for all of these models it can be concluded that above flat beds the magnitude of the streaming velocities increases from a constant viscosity model (LH53) to a time-dependent viscosity model (DV99$^{(b)}$) and to a time- and depth-dependent eddy viscosity model (PSM). This can be explained by considering the positive contribution to streaming of the time variation in the eddy viscosity (see $U^{(3)}$ term in the solution of DV99, equation 3.1.11). The contribution of this term to streaming is zero in case of a constant viscosity (ε_2=0). However, this contribution increases with increasing time variation in the eddy viscosity. Therefore, the streaming velocities given by DV99$^{(b)}$ are higher than that of LH53. As the eddy viscosity in the PSM is time- and depth-dependent, there is not only a time variation in the eddy viscosity but also a depth variation. Apparently, also a depth variation in the eddy viscosity results into a positive contribution to streaming and therefore the streaming velocities given by the PSM are the largest.

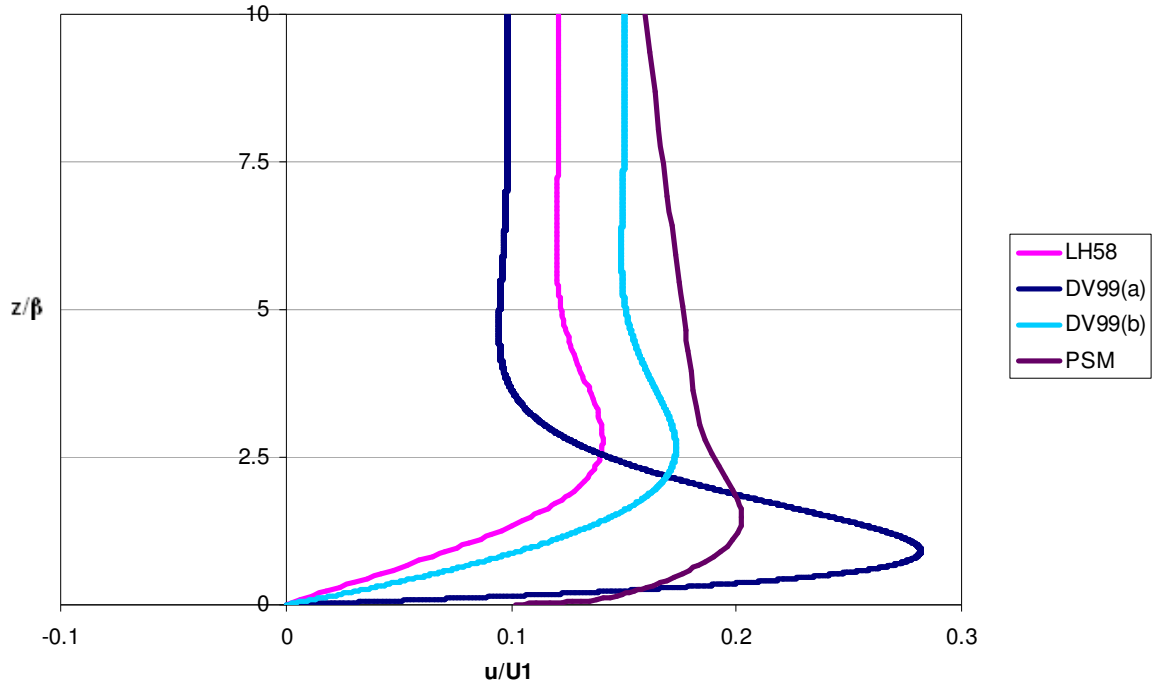

Figure 22: Streaming profiles for each model at h=3 m

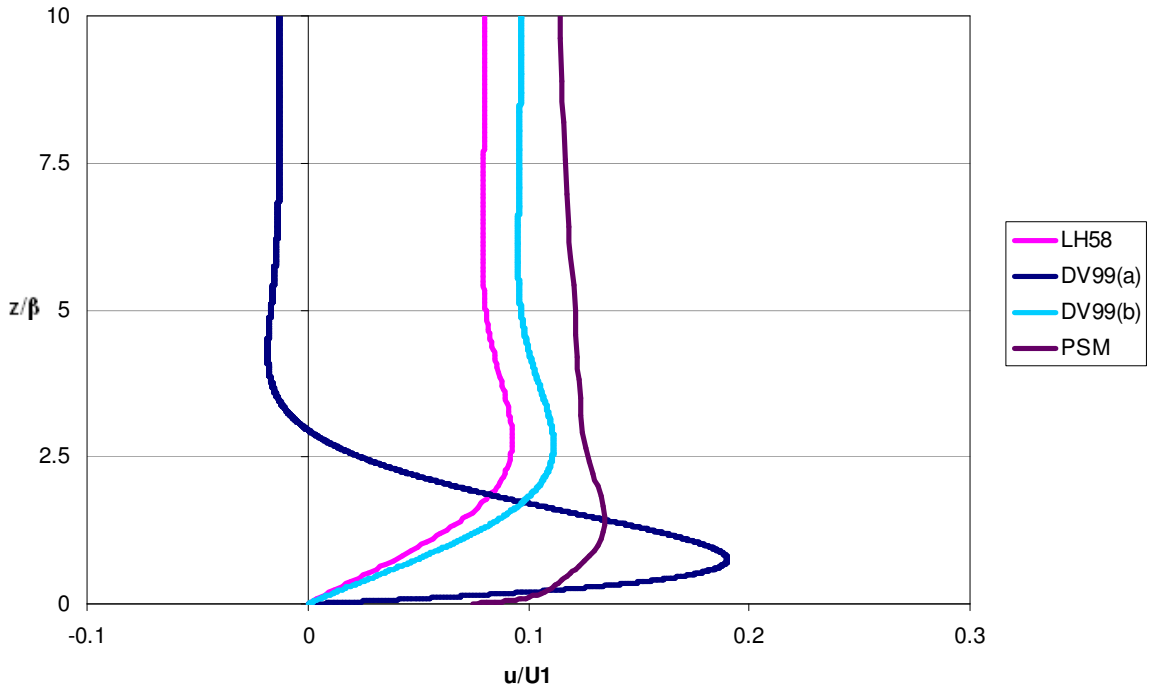

Figure 23: Streaming profiles for each model at h=4 m

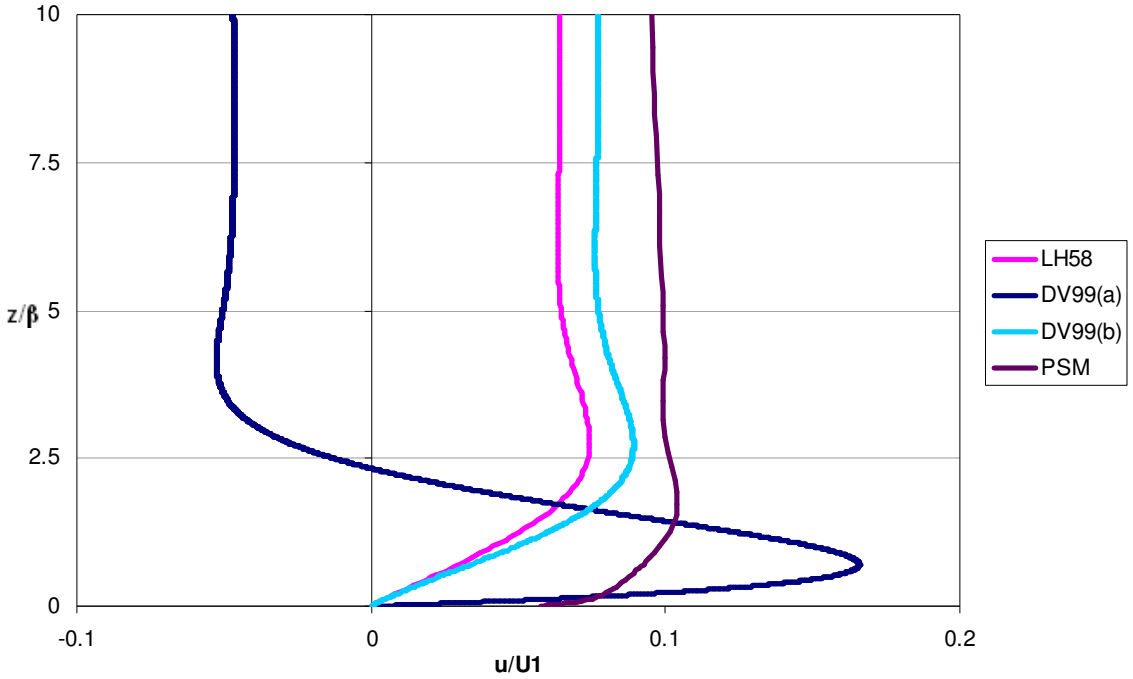

Figure 24: Streaming profiles for each model at h=5 m

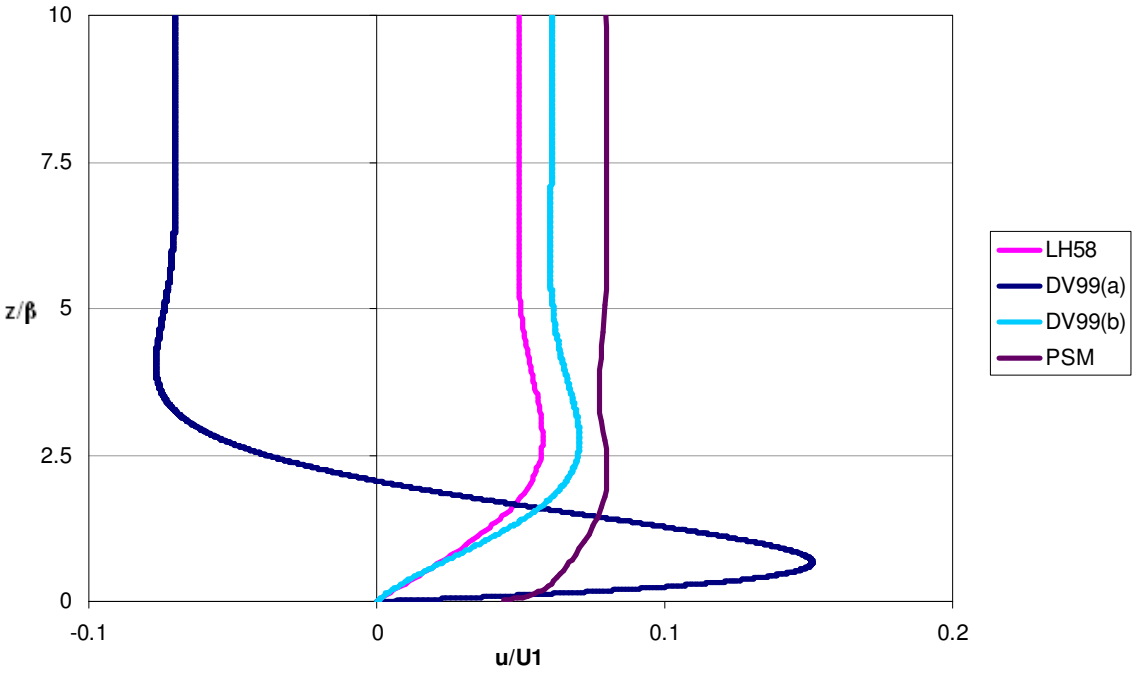

Figure 25: Streaming profiles for each model at h=6 m

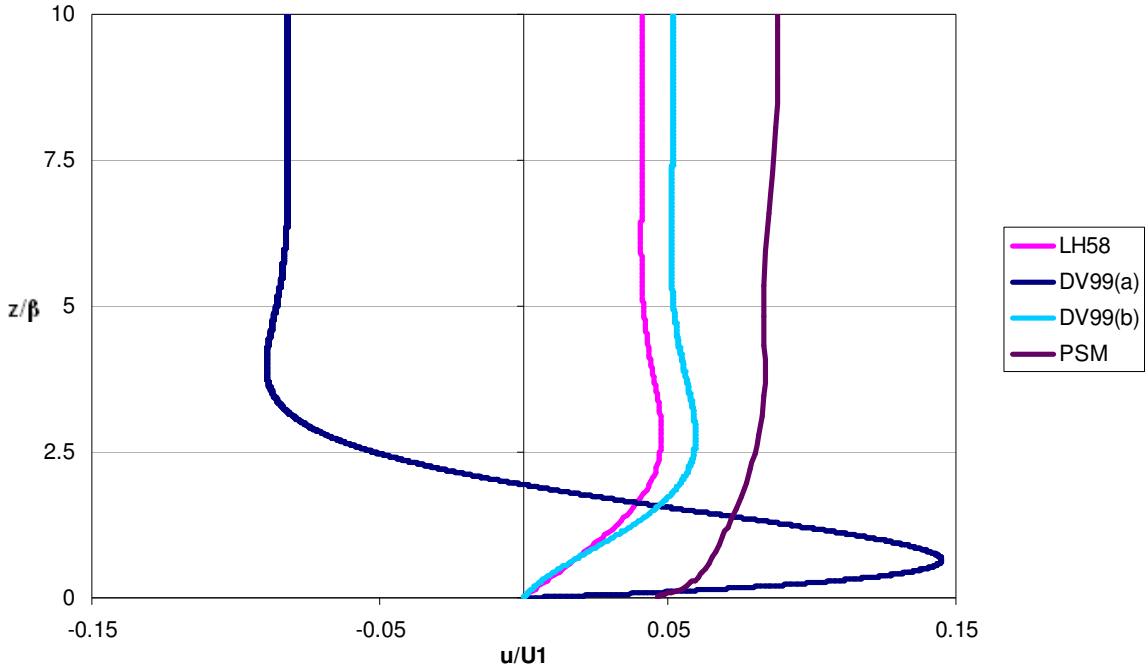

Figure 26: Streaming profiles for each model at h=7 m

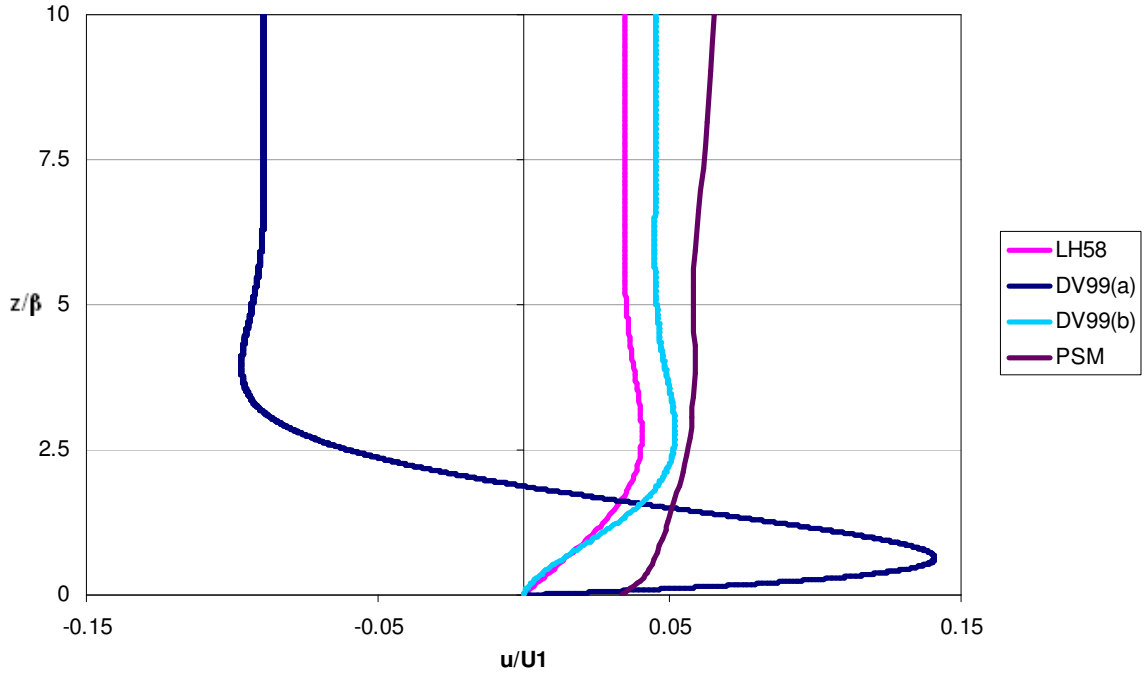

Figure 27: Streaming profiles for each model at h=8 m

For the LH53, DV99$^{(a)}$ and DV99$^{(b)}$ the dimensionless streaming velocities increase from zero at the bed towards an asymptotic value where the PSM shows velocities that do not tend to grow towards an asymptotic value. The reason for this is the inclusion of the mean pressure gradient in the POINT SAND model where this term is neglected in other streaming models as discussed before. The profiles of the PSM become less steep with decreasing water depths which shows the growing importance of the mean pressure gradient while approaching the coast (closed boundary).
When the results of the original and the adjusted model of Davies and Villaret [1999] are compared it can be seen that the shape of the streaming profiles of the adjusted model gives much better agreement to the streaming profiles given by the POINT SAND model. However, the magnitude of the velocities given by the DV99$^{(b)}$ are smaller than the PSM as well near-bed as at higher levels away from bed.

As mentioned before, above flat beds the dimensionless streaming velocities according to LH53, DV99$^{(b)}$ and PSM are positive at all levels z/β and for all water depths considered. Therefore, above flat beds and the considered (wave) conditions it can be concluded that for all levels z/β the positive contribution of the wave Reynolds stress term to streaming should be larger than the negative contribution of the wave component of mean turbulent Reynolds stress. This statement is justified by calculating the behaviour of both terms using the POINT SAND model and DV99$^{(b)}$ where for three levels z/β the magnitude of the wave component of mean turbulent Reynolds stress and the wave Reynolds stress are shown as a function of different water depths (Figure 28 and Figure 29). Here the level z/β=4.8 corresponds to the top of the boundary layer as discussed later on. From these figures it can be seen that for all water depths the magnitude of the wave Reynolds stress is larger than the wave component of mean turbulent Reynolds stress. Furthermore, approaching the coast the contribution of the wave Reynolds stress becomes much more important compared to the wave component of mean turbulent Reynolds stress. From the figures below it can be seen that the DV99$^{(b)}$ shows constant value of the wave component of mean turbulent Reynolds stress for all levels z/β which reflects the depth-independent eddy viscosity of the DV99 model. In contrast to this the PSM shows different values of the wave component of mean turbulent Reynolds stress for different levels z/β which reflects depth-dependent eddy viscosity in the PSM.

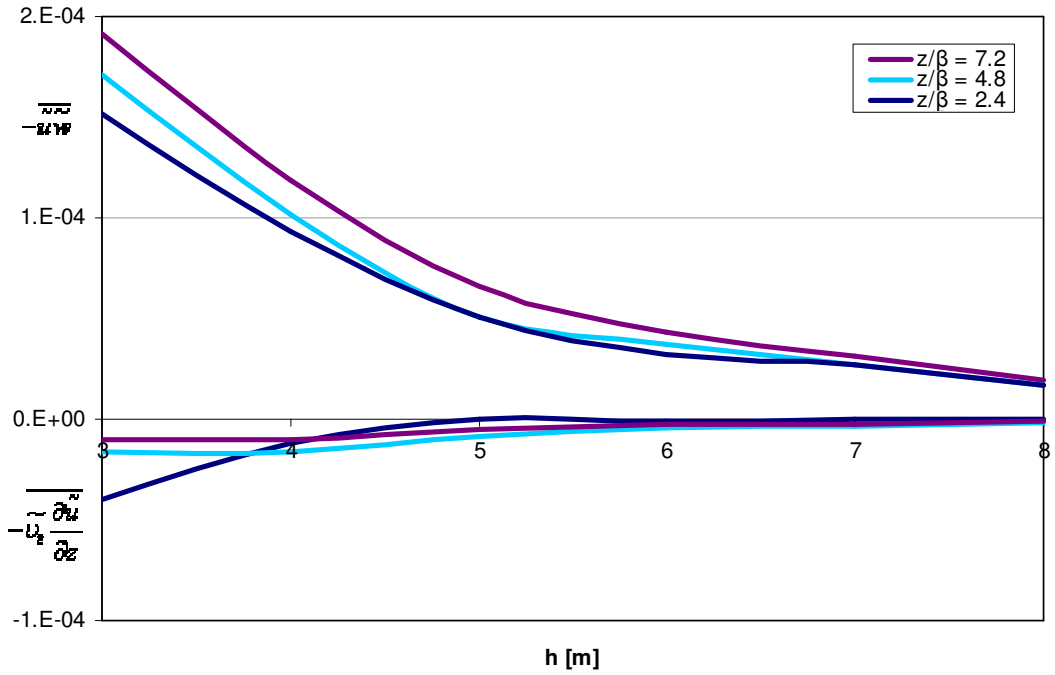

Figure 28: Cross-shore behaviour of the driving forces of streaming from PSM

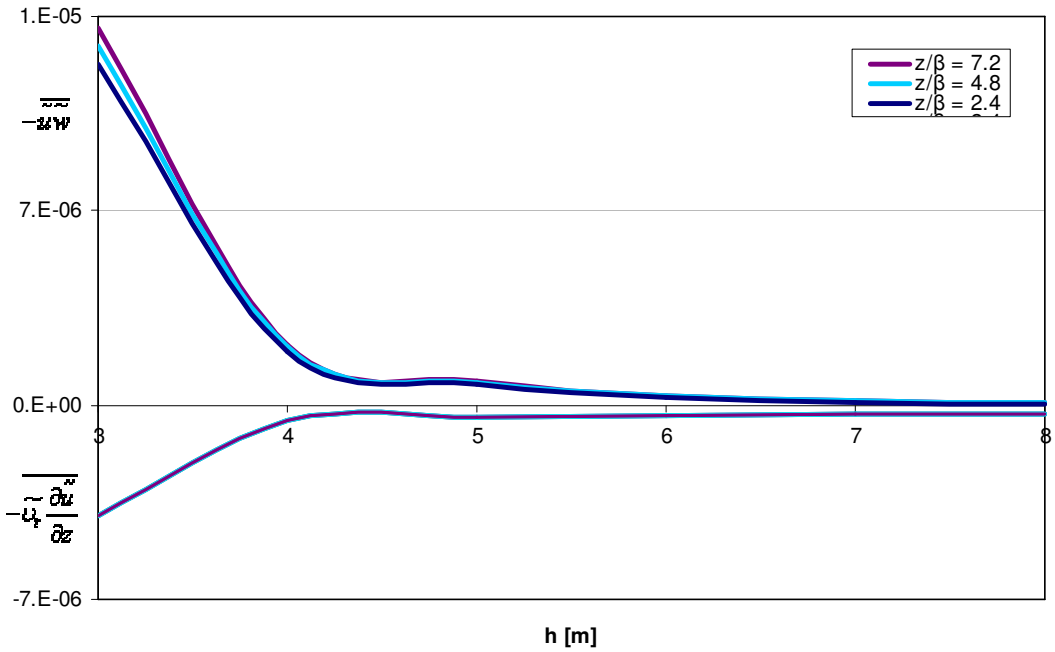

Figure 29: Cross-shore behaviour of the driving forces of streaming for DV99[-(b)]

In order to get insight in the differences between the magnitudes of the streaming velocities given by each model, the behaviour of these models is analyzed at the edge of the boundary layer. As mentioned before, the boundary layer thickness δ in this research is defined as twice the distance from the bed where the amplitude of the horizontal oscillating velocity has reached the maximum value. For LH53, the amplitude of the horizontal oscillating velocity is given by the first order solution in equation (2.2.14) where θ is zero. For the original and the adjusted model of DV99, the amplitude of the horizontal oscillating velocity is given by the second order solution of the boundary layer equations (see Svendsen, 2006, pp. 480). Using the given definition the top of the boundary layer is found to be at level z/β=4.8. The boundary layer thickness as a function of cross-shore water depths are shown in Appendix D. Here Figure 53 gives the boundary layer thickness for the PSM as determined in section 3.1.4 where Figure 54 and Figure 55 give the boundary layer thickness for the LH53 and DV99 solutions, respectively.

The streaming velocities at the edge of the boundary layer given by each model are illustrated in the figure below for different cross-shore water depths. It should be noticed that each water depth corresponds to certain characteristic wave condition (see Table 1) as formulated in section 1.5. The streaming velocities at the edge of the boundary layer z/β=4.8 are positive for the streaming models that represent flat bed situations (LH53, DV99$^{(b)}$ and PSM) and increase with decreasing water depths. Furthermore, at this level the streaming velocities given by the POINT SAND model are the largest followed by the adjusted Davies and Villaret solution and the LH53 solution. As shown in the previous figures, this behaviour is observed for all levels z/β. However, the magnitude of the streaming velocities at the edge of the boundary layer is not representative for the streaming velocities at all levels in the vertical. As can be seen from figures 22 to 27 the streaming velocities have a certain course: the streaming velocities increase from zero at the bed towards a certain maximum value and decreases again at higher levels further away from the bed.

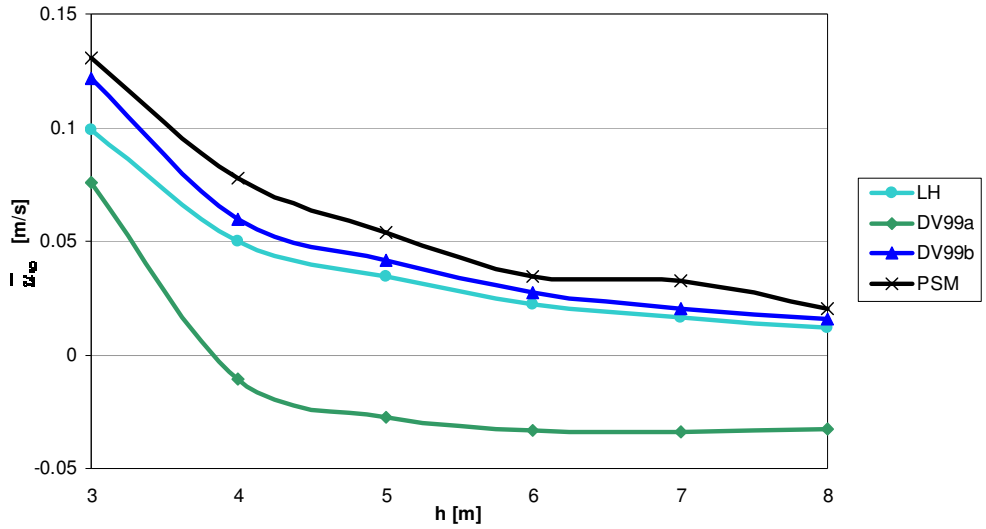

Figure 30: Streaming velocities $\bar{u}_\infty$ as a function of different water depths

Shortly summarized, above flat beds the streaming velocities given by LH53, DV99$^{(b)}$ and PSM are positive as well near-bed as away from the bed. Therefore, it can be concluded that above flat beds the positive contribution of the wave Reynolds stress term to streaming is more dominant than the negative contribution of the wave component of mean turbulent Reynolds stress. In contrast to this, above rough rippled beds, the streaming velocities are greatly determined by the wave component of the turbulent mean wave Reynolds stress where the contribution of the wave Reynolds stress is much smaller.
Above flat beds, the magnitude of the streaming velocities is the largest for the PSM followed by adjusted DV99$^{(b)}$ solution and the LH53 solution. As the (wave) conditions are the same in all of these models it can be concluded that above flat beds the magnitude of the streaming velocities increases from a constant viscosity model (LH53) to a time-dependent viscosity model (DV99$^{(b)}$) and to a time-and depth-dependent eddy viscosity model (PSM). Furthermore, the adjusted model of Davies and Villaret [1999] gives quite good agreement with the PSM and could therefore be used as a simple, analytical model to represent the numerical PSM. However, considering the edge of the boundary layer the magnitude of the velocities given by DV99$^{(b)}$ and the PSM differ about 30 percent in the worst case (for h=4 m). Finally, it is concluded that the edge of the boundary layer is not a representative level for the behaviour of streaming models at all levels in the vertical.

Summary of chapter 3

In this chapter an analysis is done on the cross-shore behaviour of streaming above flat beds as well as rippled beds. It is shown that above flat beds the streaming velocities are positive near-bed as well as further away from bed. In contrast to this, above rippled beds the streaming velocities are positive near-bed and negative further away from the bed. Furthermore, it is shown that above flat beds the positive contribution of the wave Reynolds stress term to streaming is more dominant than the negative contribution of the wave component of mean turbulent Reynolds stress. The opposite is true for rippled beds.
This chapter also shows that the streaming velocities have a certain course as a function of the vertical z and therefore the edge of the boundary layer is not a representative level for the behaviour of the streaming velocities at all levels in the vertical.

4 Analysis on bed shear stress models

In this chapter, firstly, two sediment transport models are discussed that take account for streaming. Here the focus is on the modelling of the bed shear stress as in both models the instantaneous transport rates are expressed in terms of the instantaneous bed shear stress rather than in terms of the instantaneous free stream velocity. Next, an assessment of both transport models is made by comparing these models with the calculated bed shear stresses from the POINT SAND model.

4.1 Bed shear stress models including streaming

In this paragraph the bed shear stress models of Nielsen and Callaghan [2003], and Van Rijn [2007] are discussed. These models take account for streaming in different ways. Nielsen and Callaghan [2003] add a constant, positive shear stress (wave Reynolds stress at the edge of the boundary layer) to the time-dependent bed shear stress where Van Rijn [2007] adds the steady streaming velocity (at the edge of the boundary layer) to the time-dependent bed shear stress.

4.1.1 Nielsen & Callaghan - model

The sediment transport model of Nielsen and Callaghan [2003] takes account for two near-bed sand transport mechanisms under real waves. Here the effects of boundary layer streaming and acceleration skewness, i.e., the front of the waves being steeper than the back (saw-tooth asymmetry), are incorporated. Like boundary layer streaming, waves with saw-tooth asymmetry may generate a net landward sediment transport because of the more abrupt acceleration under the steep front [Nielsen and Callaghan, 2003]. The instantaneous transport rates in the transport model of Nielsen and Callaghan [2003] are expressed in terms of the instantaneous bed shear stress rather than in terms of the instantaneous free stream velocity. Therefore the focus will be on the modelling of bed shear stress rather than on actual transport rates.
The modelling of the bed shear stress in the transport model of Nielsen and Callaghan [2003] is based on the work of Jonsson [1966] where the instantaneous bed shear stress was calculated according to equation (4.1.1) over flat beds in high energy, oscillatory flow. Here the subscript 2.5 on the grain roughness wave friction factor refers to the hydraulic roughness being 2.5 times the medium grain diameter d_{50} and the subscript ∞ means "above the bottom boundary layer".

$$\tau_b(t) = \frac{1}{2}\rho f_{2.5} \left|u_\infty(t)\right| u_\infty(t) \tag{4.1.1}$$

In order to account for the effects of streaming and acceleration skewness the bed shear stress is calculated according to the time domain filter method suggested by Nielsen [1992]. This method involves the usual grain roughness wave friction factor $f_{2.5}$ and a phase lead φ_τ of the bed shear stress compared to the free stream velocity.

Firstly, a linear filter incorporating the friction factor and the phase lead is applied to an arbitrary free stream velocity which gives the instantaneous grain roughness friction velocity u_* as shown in equation (4.1.2). Here A is the near-bed semi-excursion amplitude corresponding to the free stream velocity u_∞ and $f_{2.5}$ is the usual grain roughness friction factor.

$$u_*(t) = \sqrt{\frac{1}{2} f_{2.5}} \left[u_\infty(t)\cos(\varphi_\tau) + \frac{1}{\omega}\frac{du_\infty}{dt}\sin(\varphi_\tau) \right]$$
$$f_{2.5} = \exp\left[5.5\left(\frac{2.5 d_{50}}{A} \right)^{0.2} - 6.3 \right] \qquad (4.1.2)$$
$$A = \frac{\sqrt{2}}{\omega}\sqrt{\mathrm{var}\{u_\infty(t)\}}$$

Subsequently, a constant shear stress (the wave Reynolds stress at the edge of the boundary layer) is added to the time-dependent bed shear stress to account for the effects of streaming as shown in equation (4.1.3). The wave Reynolds stress at the edge of the boundary layer is given by (4.1.4) where f_e is the energy dissipation factor based on the flat bed data of Carstens et al., [1969]. The equation for wave Reynolds stress is based on the relationship between the streaming related bed shear stress and the energy dissipation (see Nielsen, 2006). Here $\theta_{2.5}$ is the instantaneous grain roughness Shields parameter given by (4.1.6).

$$\tau_b(t) = \rho |u_*| u_* - \rho\left(\widetilde{\widetilde{u}}\widetilde{w}\right)_\infty \qquad (4.1.3)$$

$$\left(\widetilde{\widetilde{u}}\widetilde{w}\right)_\infty = -\frac{2 f_e A^3 \omega^3}{3\pi c} \qquad (4.1.4)$$

$$f_e = \exp\left[5.5\left(\frac{170 d_{50}\sqrt{\theta_{2.5} - 0.05}}{A} \right)^{0.2} - 6.3 \right] \qquad (4.1.5)$$

$$\theta_{2.5} = \frac{f_{2.5}\rho A^2 \omega^2}{2\rho(s-1) g d_{50}} \qquad (4.1.6)$$

As can be seen from the equations above, different grain roughness factors are used to calculate the instantaneous friction velocity u_* and the wave Reynolds stress. Where $f_{2.5}$ is used to calculate u_*, f_e is used to calculate the wave Reynolds stress. Here $f_{2.5}$ is calculated using a hydraulic roughness of $2.5d_{50}$ where f_e is calculated using a hydraulic roughness of $170 d_{50}\sqrt{\theta_{2.5} - 0.05}$ which is considerably larger than $2.5d_{50}$ [Nielsen and Callaghan, 2003]. Nielsen and Callaghan [2003] use this way of calculation to get better agreement with experimental data but they also conclude that it is more logical to base the calculations of wave Reynolds stress and instantaneous friction velocity on same friction factors.

The parameters and quantities used in the bed shear stress model of Nielsen and Callaghan [2003] are discussed here. As usual, ω is the angular frequency, c is the wave celerity, ρ is the fluid density, s is the specific gravity of the sediment and g is the acceleration of gravity.

The sediment transport model of Nielsen and Callaghan [2003] is validated by Nielsen [2006] using several data sets. Based on the experimental data of Watanabe and Sato [2004], Nielsen [2006] has found an optimal phase angle φ_τ of 51 degrees**.** Using this phase angle Nielsen [2006] found good agreement with measured sediment transport rates of Ribberink et al., [2000] that have strong influence from boundary layer streaming. Furthermore, good agreement was found with large body of U-tube data simulating sine waves with superimposed currents and second order Stokes waves, all of which have zero acceleration skewness [Nielsen, 2006] as is the case in this research.

Nielsen and Callaghan [2003] thus take account for streaming by considering the presence of the wave Reynolds stress but not the wave part of the mean turbulent Reynolds stress. This concept could work well above flat beds as the wave Reynolds stress is more dominant than the wave part of the mean turbulent Reynolds stress as shown in chapter 3 for the considered (wave) conditions. The way the bed shear stress model of Nielsen and Callaghan [2003] takes account for streaming is assessed in paragraph 4.2 where this model is illustrated with and without the inclusion of streaming.

4.1.2 Van Rijn - model

The sediment transport model of Van Rijn [2007] is a general bed-load transport model that can be used for both oscillatory flows and real waves. The focus here will also be on the modelling of the bed shear stress rather than on actual transport rates.

The modelling of the bed shear stress in the transport model of Van Rijn [2007] is based on the previous work of Van Rijn [1984a, 1993]. In order account for the effects of boundary layer streaming, the streaming velocity at the edge of the boundary layer $u_{\infty,c}$ (current related) is added to an arbitrary free stream velocity $u_{\infty,w}$ (wave related) as shown in equation (4.1.7).

$$\tau_b(t) = \frac{1}{2}\rho f_{cw}^{'} \left|\left(u_{\infty,c} + u_{\infty,w}\right)\right| \left(u_{\infty,c} + u_{\infty,w}\right) \tag{4.1.7}$$

The streaming velocity at the edge of the boundary layer is calculated according to the work of Davies and Villaret [1997, 1999] and Longuet-Higgins [1953]. The streaming velocity as a function of relative roughness is shown in equation (4.1.8). For flat beds (relative roughness larger than 100) the streaming velocity is given by the first condition in (4.1.8) which is in line with the results of Longuet-Higgins. The other two conditions are applied in case of smaller relative roughness coefficients e.g. rippled beds.

$$\begin{aligned} u_{\infty,c} &= \frac{3}{4c}U_w^2 \qquad for \qquad A_w/k_s \geq 100 \\ u_{\infty,c} &= -\frac{1}{8c}U_w^2 \qquad for \qquad A_w/k_s = 10 \\ u_{\infty,c} &= -\frac{U_w^2}{c} \qquad for \qquad A_w/k_s \leq 1 \end{aligned} \tag{4.1.8}$$

From equation (4.1.8) it can be seen that Van Rijn [2007] takes account for streaming in the bed shear stress model by adding a positive streaming velocity (at the edge of the boundary layer) in case of flat beds but a negative streaming velocity in case of rippled beds. As discussed in chapter 3, the edge of the boundary layer is quite debatable and the streaming velocities at the edge of the boundary layer are not necessarily representative for the behaviour of streaming in the water columns as a whole. Furthermore, above rippled beds the streaming velocity at the edge of the boundary layer is not negative at all levels *z* as shown in previous chapter (see section 3.2, Figure 30: DV99[(a)]). In paragraph 4.2 the bed shear stress model of Van Rijn [2007] is assessed by illustrating its behaviour with and without the inclusion of streaming.

The equations used to determine the bed shear stress of Van Rijn [2007] are shown below. The parameters and quantities used in the bed shear stress model of Van Rijn [2007] are explained here. As usual, ρ is the fluid density, g is the acceleration of gravity, H is the wave height, T is the wave period, h is the water depth, f'_{cw} is the grain friction coefficient due to currents (f'_c) and waves (f'_w), α is a coefficient related to relative strength of waves and currents while β is a coefficient related to the vertical structure of the velocity profile. The wave related near-bed semi-excursion is given by A_w where U_w is the near-bed peak orbital velocity, the depth-averaged current (steady part) velocity is denoted by u_c, the equivalent bed roughness k_s is assumed to be $2.5d_{50}$, the boundary layer thickness is given by δ where the wave related boundary layer thickness is given by δ_w. Finally, $k_{s,c}$ is the current-related bed roughness determined by equation (4.1.12) where f_{cs} is a factor that expresses the effect of a gradually decreasing ripple roughness and equals to 1 for sheet flow conditions (ripples are washed out).

$$f'_{cw} = \alpha\beta f'_c + (1-\alpha) f'_w$$
$$f'_c = \frac{8g}{\left[18\log\left(12h/k_s\right)\right]^2}, \qquad f'_w = \exp\left[-6 + 5.2\left(A_w/k_s\right)^{-0.19}\right] \tag{4.1.9}$$

$$\alpha = \frac{u_c}{u_c + U_w}, \quad \beta = 0.25\left[\frac{-1+\ln\left(30h/k_{s,c}\right)}{\ln\left(30\delta/k_{s,c}\right)}\right]^2 \tag{4.1.10}$$

$$A_w = \frac{H}{2\sinh\left(kh\right)}, \quad U_w = \frac{\pi H}{T\sinh\left(2kh\right)} \tag{4.1.11}$$

$$k_{s,c} = 20 f_{cs} d_{50}$$
$$\delta = \max\left(3\delta_w, k_{s,c}\right), \quad \delta_w = 0.072 A_w \left(\frac{A_w}{k_s}\right)^{-0.25} \tag{4.1.12}$$

4.2 Assessment of the bed shear stress models

As discussed in the previous sections the bed shear stress models of Nielsen and Callaghan [2003], and Van Rijn [2007] take account for streaming in different ways. The way in which these models take account for streaming is assessed in this paragraph. Here, the bed shear stress models are illustrated with and without the inclusion of streaming together with the bed shear stresses calculated with the POINT SAND model.

In order to assess the inclusion of streaming in the models of Nielsen and Callaghan [2003], and Van Rijn [2007] the bed shear stresses are compared to the bed shear stresses calculated with the POINT SAND model. Here, four quantities are considered: the wave-averaged bed shear stress, the maximum on- and offshore-directed bed shear stresses, and the ratio of the maximum on- and offshore-directed bed shear stresses that is very important considering sediment transport. In the following figures these quantities are shown for different cross-shore water depths (h=3 to 8 meters). It should be noticed that each water depth corresponds to certain characteristic wave condition (see Table 1) as formulated in section 1.5. Furthermore, for both models the free stream velocity $u_\infty(t)$ corresponding to a certain water depth is obtained from the POINT SAND model. In order to make sure that the flow is not influenced by the bed the free stream velocity is obtained at level z = 20 centimetres. This level z is quite large compared to the boundary layer thickness (see Appendix D, Figure 53).

In the figure below, the wave-averaged bed shear stress is shown for the model of Nielsen and Callaghan [2003], and Van Rijn [2007] with and without taking streaming into account. From this figure, it can be seen that the wave-averaged bed shear stresses increase with decreasing water depths. The reason for this is the increasing near-bed horizontal velocities with decreasing water depths. The magnitude of the wave-averaged bed shear stresses according to the models of Nielsen and Callaghan [2003], and Van Rijn [2007] are the same when streaming is not taken into account. The reason for this is the fact that both models are based on the quadratic friction law and that same (wave) inputs are used in both models. Furthermore, the grain roughness friction coefficient used in both models is of same order of magnitude when streaming is not taken into account (see equations (4.1.2) and (4.1.9) for $f_{2.5}$ and f_w', respectively). However, when streaming is taken into account the model of Nielsen and Callaghan [2003] shows quite good agreement for all water depths (except for h=4m) with the wave-averaged bed shear stresses from the PSM. In contrast to this the model of Van Rijn [2007] barely changes. The reason for this is that Van Rijn [2007] takes account for streaming by adding the streaming velocities which are much smaller than the free stream velocities $u_\infty(t)$. As a result the wave-averaged bed shear stresses remain unchanged. In contrast to this, Nielsen and Callaghan [2003] take account for streaming by adding the wave Reynolds stress to $\rho u_* u_*$ that are of same order of magnitude. As a result the wave-averaged bed shear stresses change significantly in the good direction.

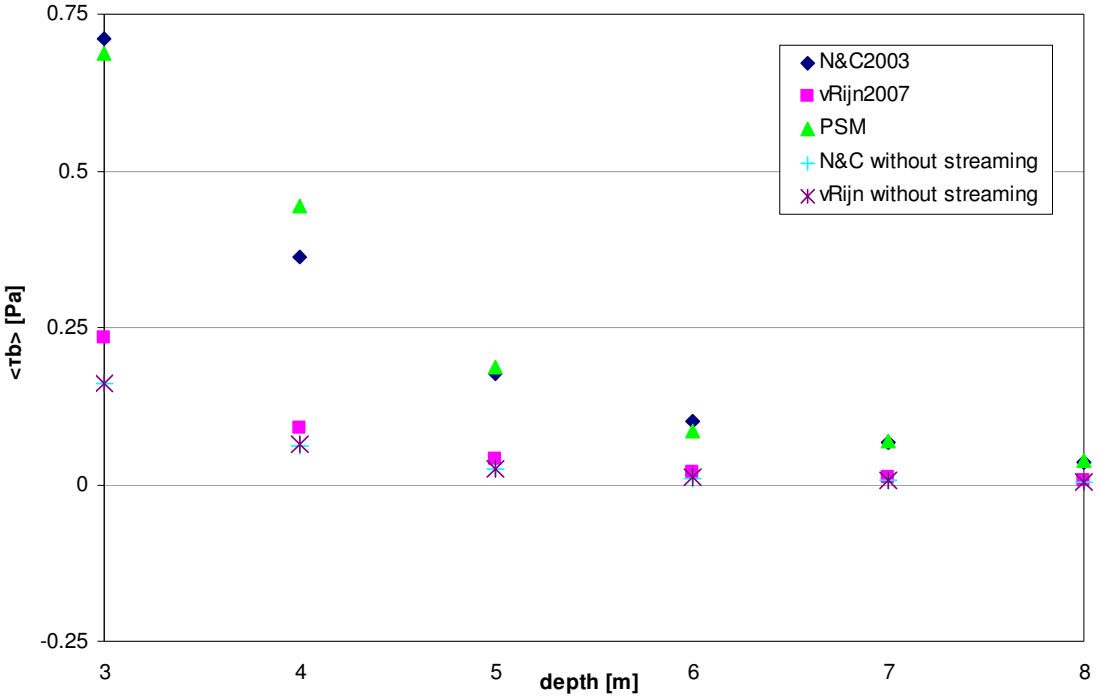

Figure 31: Wave-averaged bed shear stress for different models, with and without streaming

Subsequently, the maximum on- and offshore-directed bed shear stresses, and the ratio of these quantities are shown in Figure 32, Figure 33 and Figure 34, respectively. Considering these figures it can be seen that the models of Nielsen and Callaghan [2003], and Van Rijn [2007] show different values when streaming is not taken into account in contrast to the wave-averaged bed shear stresses as shown in Figure 31. For both maximum on- and offshore-directed bed shear stresses the model of Van Rijn [2007] shows larger values than that of Nielsen and Callaghan [2003]. This is caused by the value of grain roughness friction coefficient: for all water depths the value of f_w' calculated by Van Rijn [2007] is (slightly) larger than the value of $f_{2.5}$ calculated by Nielsen and Callaghan [2003].
Furthermore, when streaming is taken into account the model of Van Rijn [2007] barely changes considering the maximum on- and offshore-directed bed shear stresses, and the ratio of these quantities (Figure 34). In contrast to this the model of Nielsen and Callaghan [2003] shows good agreement with the results of the PSM. The reason for this improvement is the relative large value of f_e that is used to calculate the wave Reynolds stress compared to the value of f_c' that is used by Van Rijn [2007] to take account for streaming.
Another remarkable aspect is the relative large deviation in the maximum offshore-directed bed shear stress compared to the maximum onshore-directed bed shear stress when streaming is taken into account. As the streaming velocities are positive above flat beds (see chapter 3), the effect of taking streaming into account will be larger on the offshore-directed bed shear stresses than on the onshore-directed bed shear stresses.

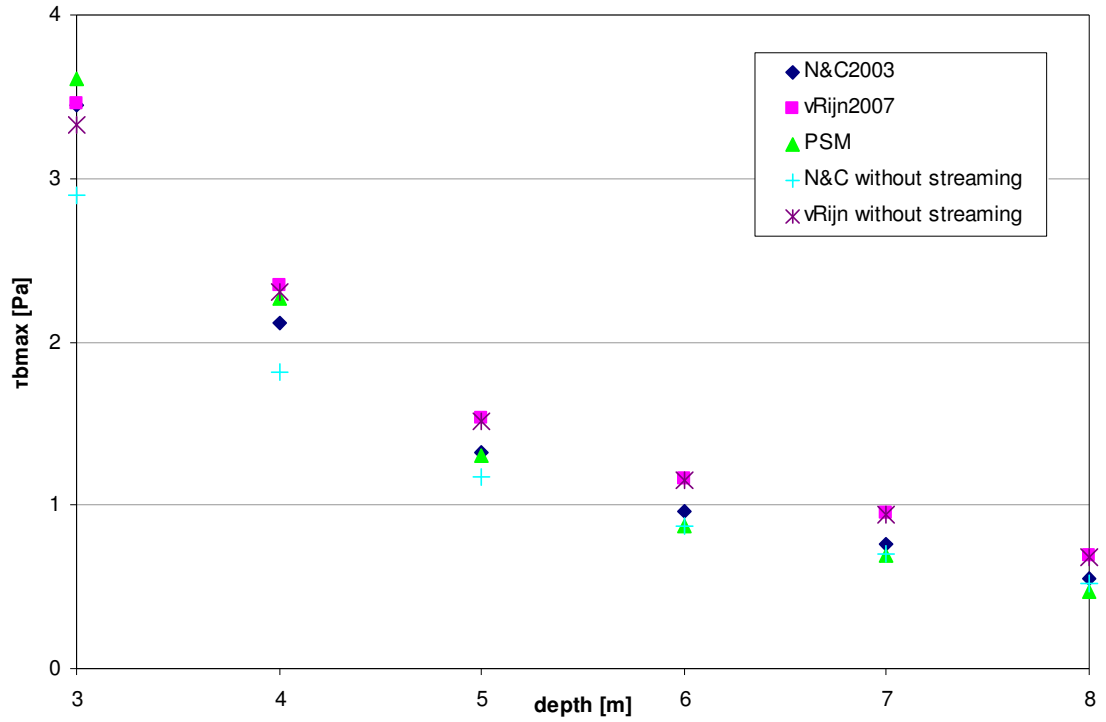

Figure 32: Maximum onshore-directed bed shear stress for different models, with and without streaming

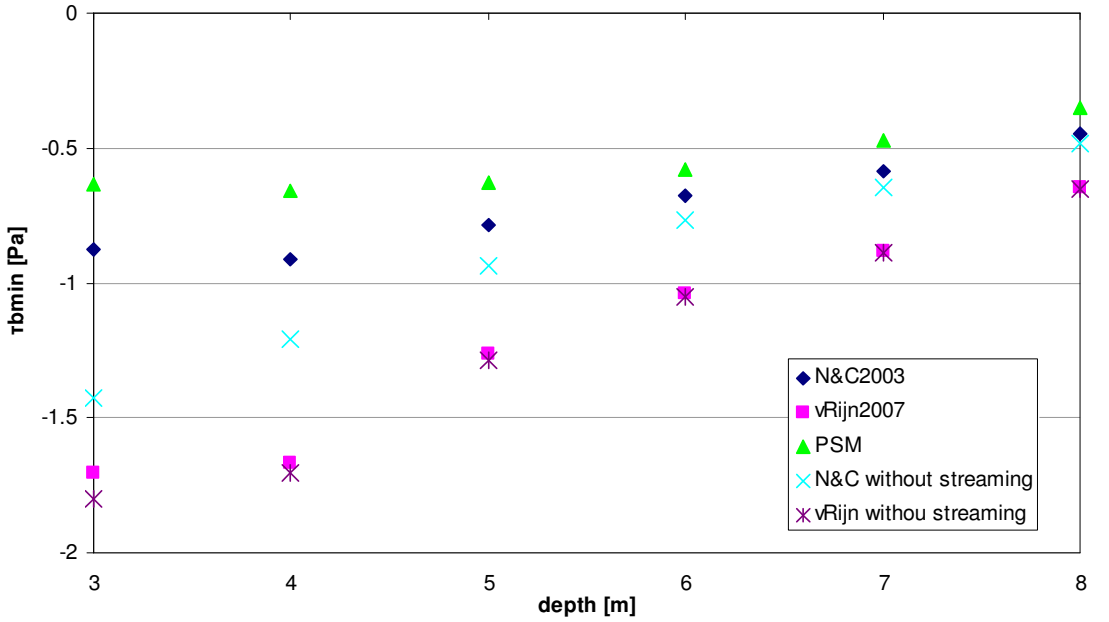

Figure 33: Maximum offshore-directed bed shear stress for different models, with and without streaming

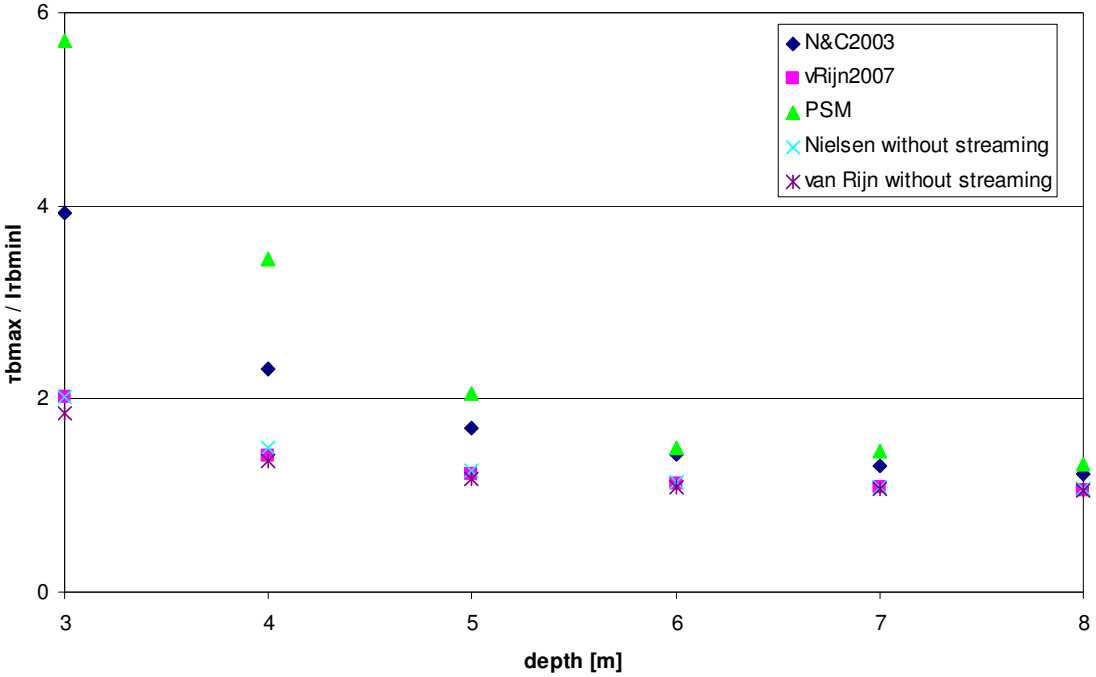

Figure 34: Ratio of the maximum on- and offshore-directed bed shear stresses, with and without streaming

From the figures shown in this section it can be concluded that the bed shear stress model of Nielsen and Callaghan [2003] shows better agreement with the PSM compared to the bed shear stress model of Van Rijn [2007]. Therefore, it can be concluded that the concept of Nielsen and Callaghan [2003] works better than that of Van Rijn [2007]. As discussed before Van Rijn [2007] takes account for streaming in the bed shear stress model by adding a positive streaming velocity (at the edge of the boundary layer) where Nielsen and Callaghan [2003] add the wave Reynolds stress at the edge of the boundary layer to take account for streaming. The edge of the boundary layer is quite debatable and the streaming velocities at the edge of the boundary layer are not necessarily representative for the behaviour of streaming profiles as the streaming velocities could be positive as well as negative (see streaming profiles in chapter 3). In contrast to this the wave Reynolds stress is always negative and its value on the edge of the boundary layer is quite comparable to other levels *z* as shown in Figure 28 and Figure 29 (in these figures the wave Reynolds stress is positive as $-\widetilde{\widetilde{uw}}$ is shown). In the next chapter the model of Nielsen and Callaghan [2003] is (possibly) improved by considering the wave Reynolds stress term in this model.

Summary of chapter 4

In this chapter two analytical bed shear stress models are discussed that are based on the quadratic friction law of Jonsson [1966]. These models take account for streaming in different ways. When streaming is taken into account, the model of Nielsen and Callaghan [2003] shows good agreement with the result of the POINT SAND model. In contrast to this the model of Van Rijn [2007] barely changes. The reason for this is the fact that Van Rijn [2007] takes account for streaming by adding the streaming velocities which are much smaller than the free stream velocities. As a result the calculated bed shear stresses remain practically unchanged. In contrast to this, Nielsen and Callaghan [2003] take account for streaming by adding the wave Reynolds stress which is calculated using a much larger grain friction coefficient than $f_{2.5}$. As a result the wave Reynolds stress is of same order of magnitude as the time-dependent bed shear stress. Therefore, adding the wave Reynolds stress to the time-dependent bed shear stress leads to significantly different values of the bed shear stresses.

Another reason for the difference in the performance of both models is the fact that the edge of the boundary layer is quite debatable and the streaming velocities at the edge of the boundary layer are not necessarily representative for the behaviour of streaming profiles as the streaming velocities could be positive as well as. In contrast to this the wave Reynolds stress is always negative and its value on the edge of the boundary layer is quite comparable to other levels in the vertical. In other words, the concept used by Nielsen and Callaghan [2003] works better than the concept used by Van Rijn [2007].

5 Adjusted bed shear stress model

In this chapter the bed shear stress model of Nielsen and Callaghan [2003] is (possibly) improved by considering the wave Reynolds stress in this model. This is done by comparing the wave Reynolds stress given by Nielsen and Callaghan [2003] to that of the POINT SAND model. Subsequently, the wave Reynolds stress from the PSM is used as input for the bed shear stress model of Nielsen and Callaghan [2003] and the results are compared to the bed shear stresses from the PSM.

5.1 Inclusion of wave Reynolds stress

In this section the wave Reynolds stress given by Nielsen and Callaghan [2003] is compared to that of the POINT SAND model. Nielsen and Callaghan [2003] give the following equation for the wave Reynolds stress, at the edge of the boundary layer, as discussed in chapter 4. As can be seen from this equation, the importance of the wave Reynolds stress increases with decreasing water depths: approaching the coast the wave celerity c decreases while the near-bed semi-excursion amplitude A and the energy dissipation factor f_e , given in equation (4.1.5), increase.

$$\left(\overline{\tilde{u}\tilde{w}}\right)_{\infty} = -\frac{2 f_e A^3 \omega^3}{3\pi c} \tag{5.1.1}$$

At the edge of the boundary layer (z/β=4.8), the wave Reynolds stress from the PSM is already calculated in paragraph 3.2 (see Figure 28). In the figure below the wave Reynolds stress is shown for the model of Nielsen and Callaghan [2003] and the PSM.

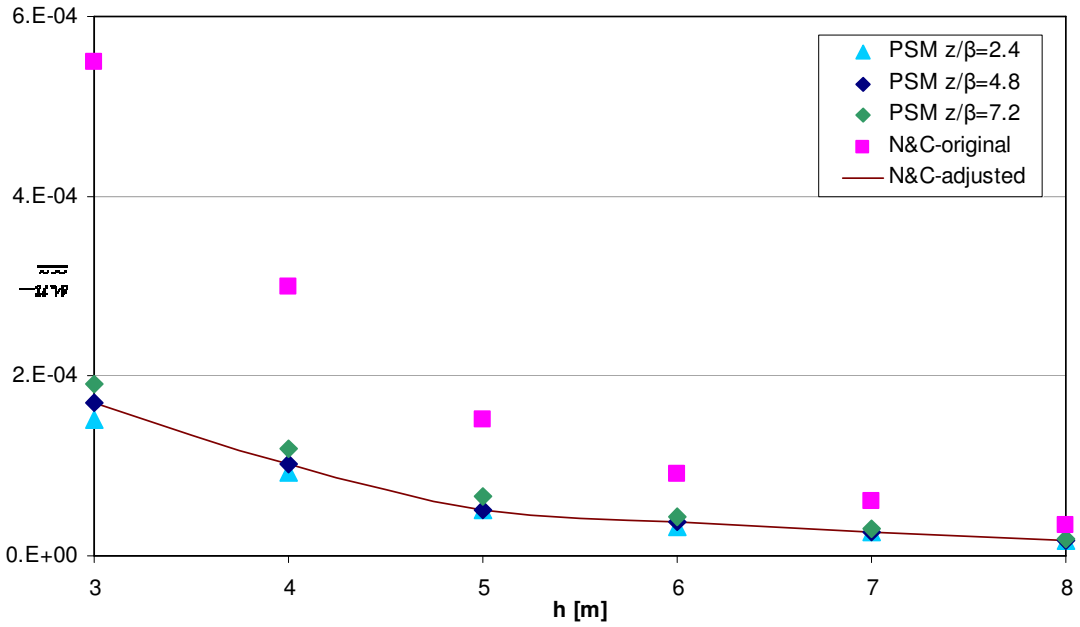

Figure 35: Wave Reynolds stress for N&C2003 and PSM

From this figure it can be seen that the wave Reynolds stress according to the model of Nielsen and Callaghan [2003] shows an overestimation compared to that of the PSM. This can be explained by the fact that Nielsen and Callaghan [2003] use a much larger grain roughness friction coefficient (f_e) to calculate the wave Reynolds stress than $2.5d_{50}$ which is used in the PSM. The degree of this overestimation increases with decreasing water depths and can run up to three times the value of wave Reynolds stress given by PSM. However, the course of the wave Reynolds stress is the same for both models. In order to get better agreement between the bed shear stress model of Nielsen and Callaghan [2003], and the PSM, the wave Reynolds stress at the edge of the boundary layer given by the PSM should be used as input in the model of Nielsen and Callaghan [2003] instead of equation (5.1.1). The following equation represents the wave Reynolds stress at the edge of the boundary layer given by the POINT SAND model (see Figure 35, N&C-adjusted). Here the factor 2/3 in equation (5.1.1) is replaced by 1/5.

$$\left(\widetilde{\widetilde{uw}}\right)_{\infty} = -\frac{f_e A^3 \omega^3}{5\pi c} \tag{5.1.2}$$

Another way to adjust equation (5.1.1) is to consider the value of the grain roughness friction coefficient f_e. As mentioned before f_e is much larger than $2.5d_{50}$ which is used in the POINT SAND model. Therefore, to get better agreement between the wave Reynolds stress given by Nielsen and Callaghan [2003], and wave Reynolds stress from the PSM, $f_{2.5}$ could be used instead of f_e. However, in this research the adjustment of the wave Reynolds stress given by Nielsen and Callaghan [2003] is limited to equation (5.1.2).

5.2 Assessment of the adjusted model

In this section the wave Reynolds stress from the POINT SAND model as shown in equation (5.1.2) is used as input for the bed shear stress model of Nielsen and Callaghan [2003]. The calculated bed shear stresses are then compared to the bed shear stresses from the PSM.

The wave-averaged, the maximum on- and offshore-directed bed shear stresses, and the ratio between maximum on- and offshore-directed bed shear stresses are shown in the figures below. For the adjusted model of Nielsen and Callaghan [2003], the wave Reynolds stress at the edge of the boundary is given by (5.1.2). The bed shear stresses are also shown for the original model of Nielsen and Callaghan [2003] together with the results of the PSM. Considering these figures it can be seen that using the wave Reynolds stress from the PSM as input for the model of Nielsen and Callaghan [2003] leads to worse agreement with the results of the PSM. This is caused by the much smaller wave Reynolds stress given by the PSM compared to the wave Reynolds stress given by Nielsen and Callaghan [2003]. As discussed before, the reason for this is the smaller grain roughness friction coefficient used by the PSM compared to the grain friction coefficient used by Nielsen and Callaghan [2003]. Especially for water depths smaller than 6 meters, the results are significantly worse. However, for more offshore water depths the results of the adjusted model remain practically unchanged. This is explained by the decreasing difference between the wave Reynolds stress from the PSM and the wave Reynolds stress given by Nielsen and Callaghan [2003] with increasing water depths as shown in Figure 35.

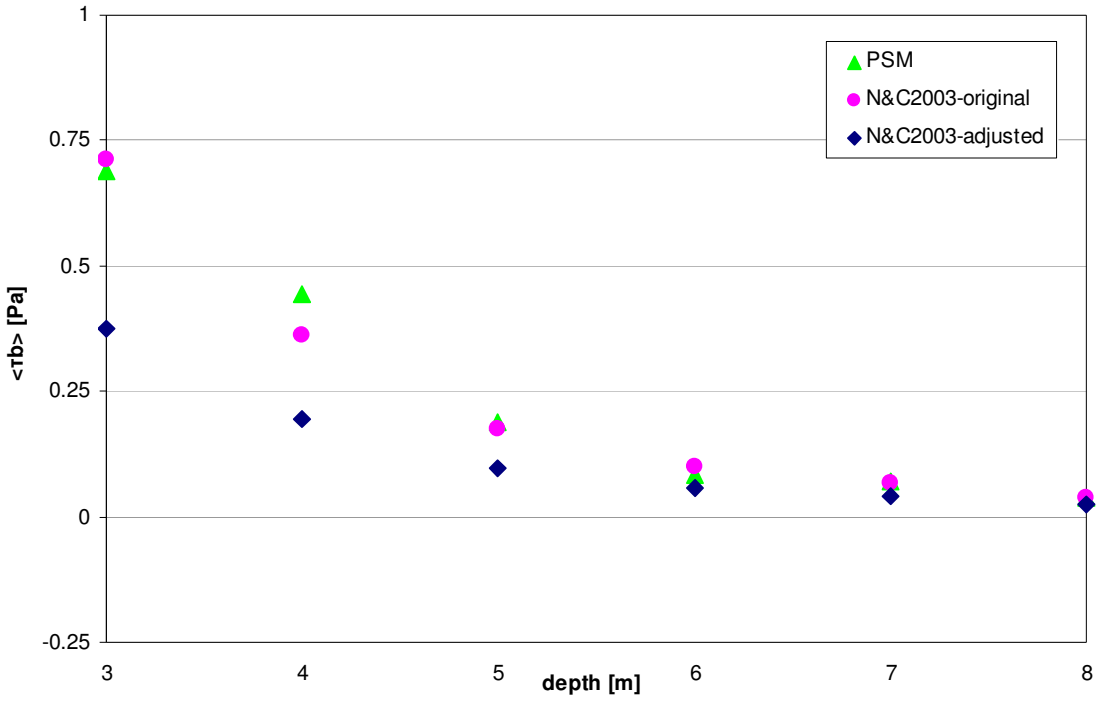

Figure 36: Wave-averaged bed shear stress for different models

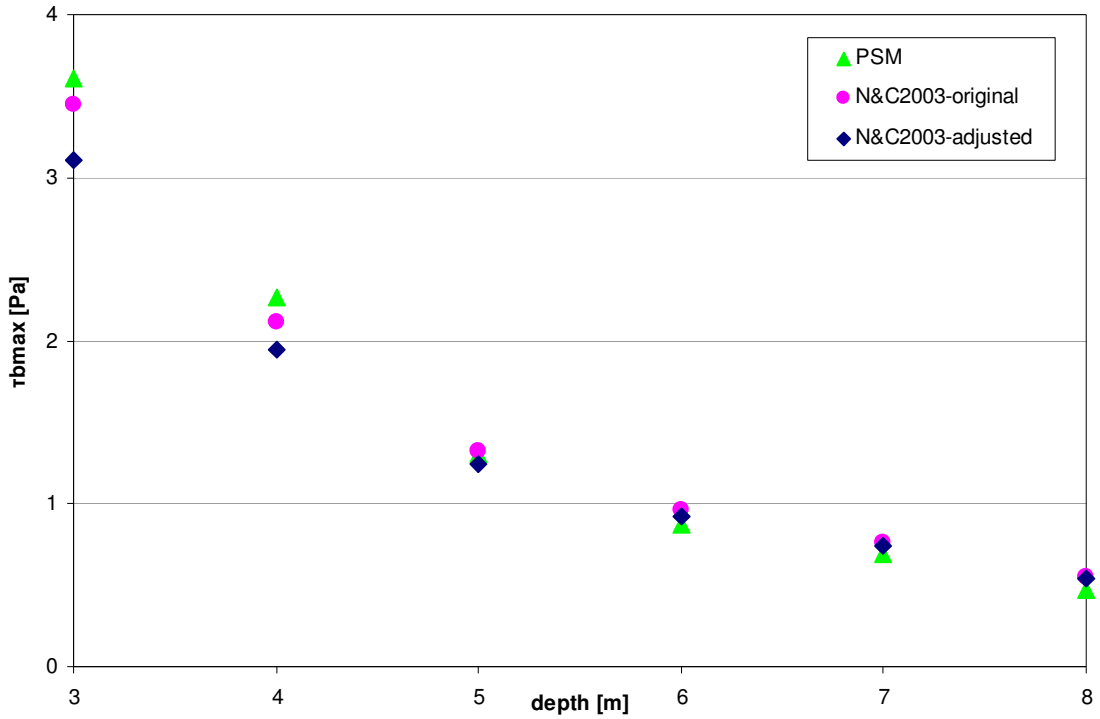

Figure 37: Maximum onshore-directed bed shear stress for different models

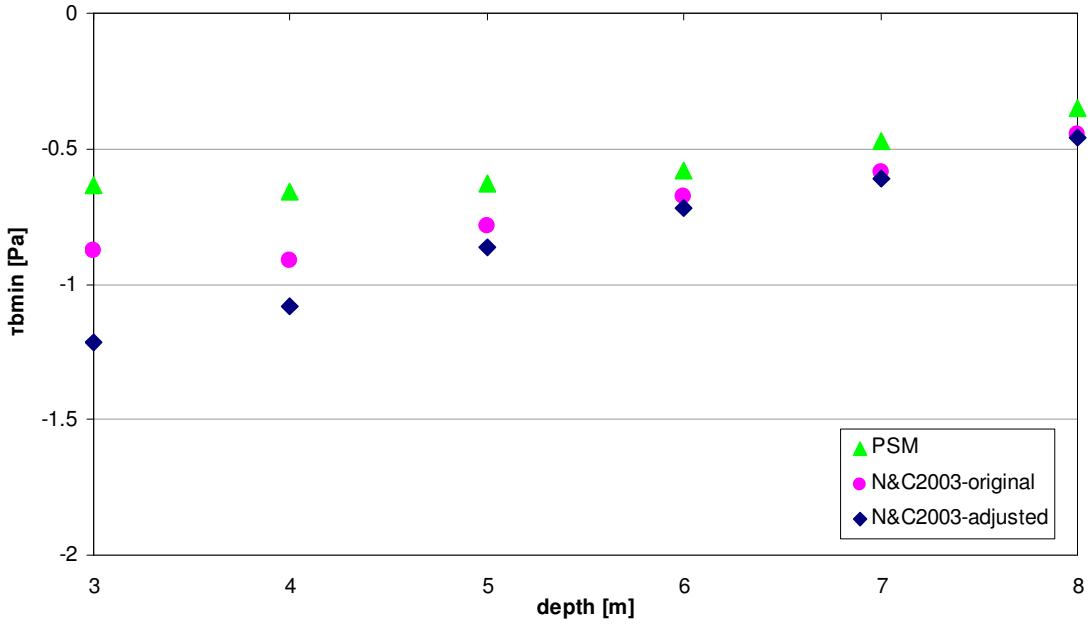

Figure 38: Maximum offshore-directed bed shear stress for different models

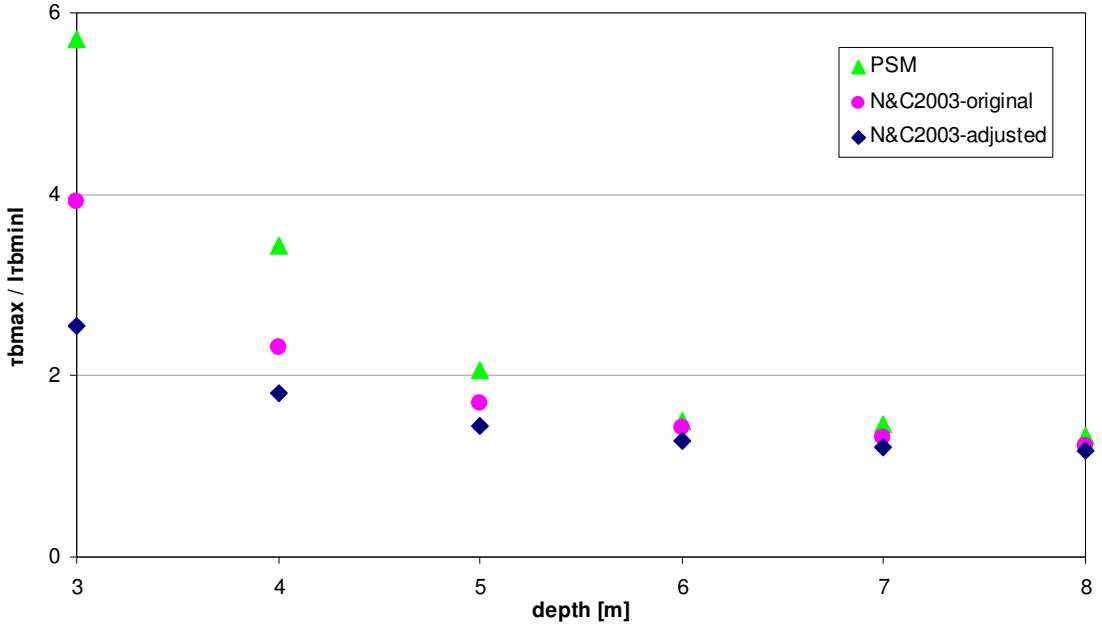

Figure 39: Ratio of the maximum on- and offshore-directed bed shear stresses, with and without streaming

The results as shown in the figures above for the adjusted model of Nielsen and Callaghan [2003] are in contrast to what might be expected as the wave Reynolds stress is better modelled with the PSM compared to the analytical approximation given by Nielsen and Callaghan [2003]. Considering the bed shear stress model of Nielsen and Callaghan [2003] the results do not only depend on the modelling of the wave Reynolds stress but also on the modelling of the instantaneous grain roughness friction velocity u_* and the grain roughness friction factor $f_{2.5}$ (see equation 4.1.3). As discussed in section 4.1.1 the instantaneous grain roughness friction velocity u_* depends on the value of the phase lead φ_τ of the bed shear stress compared to the free stream velocity. Based on the experimental data of Watanabe and Sato [2004], Nielsen and Callaghan [2006] suggest an optimum phase lead of 51˚. However, Nielsen and Callaghan [2006] also conclude that this value is much smaller for flat and immobile beds as is the case in this research. Therefore, a value of 11˚ is used for the phase lead (after Nielsen, 1992) to calculate the instantaneous grain roughness friction velocity and subsequently the new bed shear stresses where the wave Reynolds stress is given by equation (5.1.2). This results in the following figures for the wave-averaged, the maximum on- and offshore-directed bed shear stresses, and the ratio between maximum on- and offshore-directed bed shear stresses.

Considering the wave-averaged bed shear stresses (Figure 40) and the maximum onshore-directed bed shear stresses (Figure 41) it can be seen that the results of the adjusted model and the original model of Nielsen and Callaghan [2003] do not differ significantly (except for h=3). However, for the maximum offshore-directed bed shear stresses (Figure 42) the adjusted model with a phase lead of 11˚ results in better agreement with the PSM. The reason for this is that a smaller phase lead φ_τ results in smaller u_* and subsequently to smaller bed shear stresses from equation (4.1.3).
Furthermore, the ratio between the maximum onshore- and offshore-directed bed shear stresses is significantly better for the adjusted model. The reason for this is that the maximum onshore-directed bed shear stress remains practically unchanged while the maximum offshore-directed bed shear stresses decrease. As a result an increase is seen in the ratio between these quantities which shows better agreement with the PSM than the original model of Nielsen and Callaghan [2003].
Therefore, it can be concluded that adjusting only the wave Reynolds stress in the model of Nielsen and Callaghan [2003] is not sufficient to represent the physical situation as simulated by the POINT SAND model. The instantaneous grain roughness friction velocity u_* should also be adjusted using a suitable phase lead φ_τ for the bed shear stress.

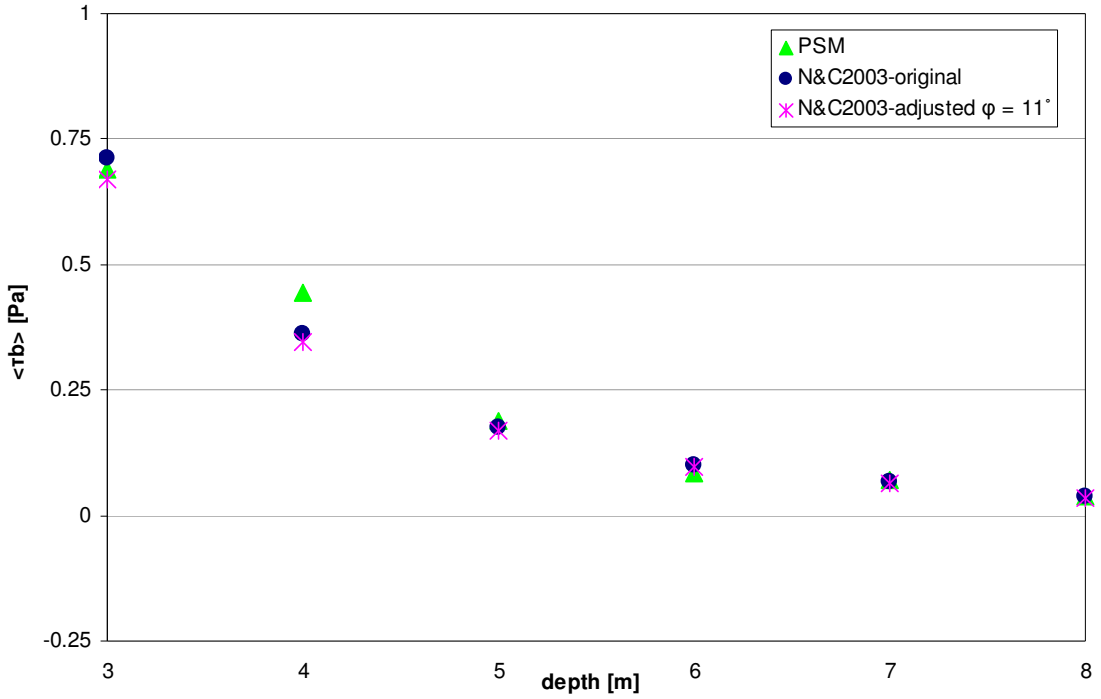

Figure 40: Wave-averaged bed shear stress for different models

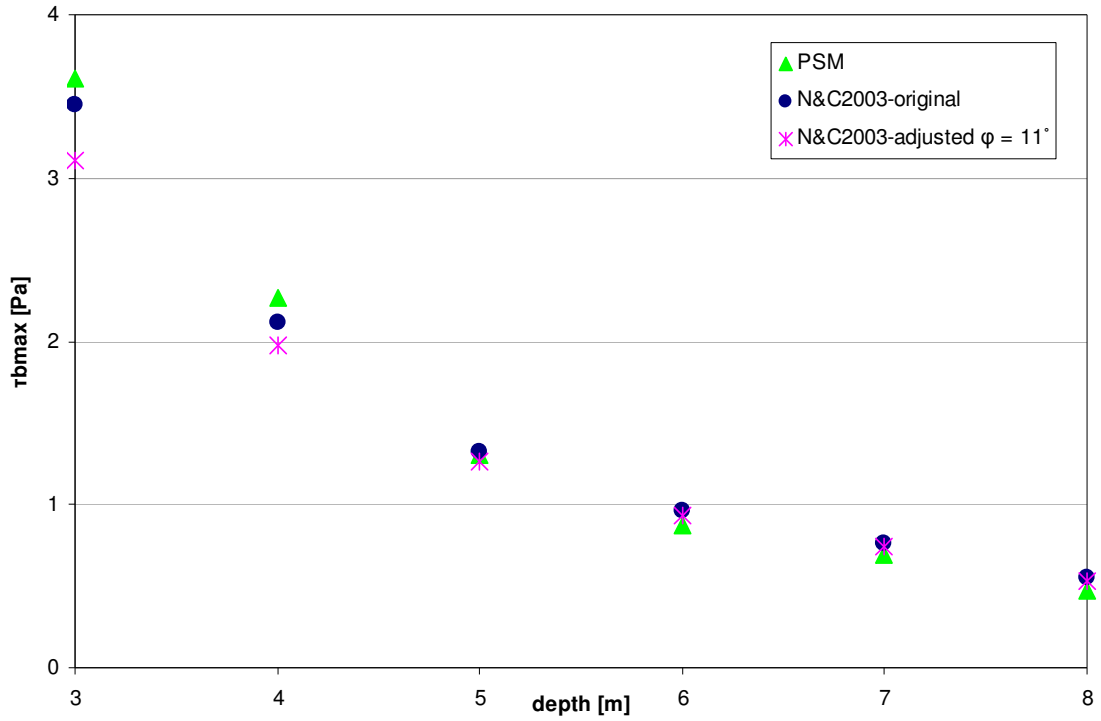

Figure 41: Maximum onshore-directed bed shear stress for different models

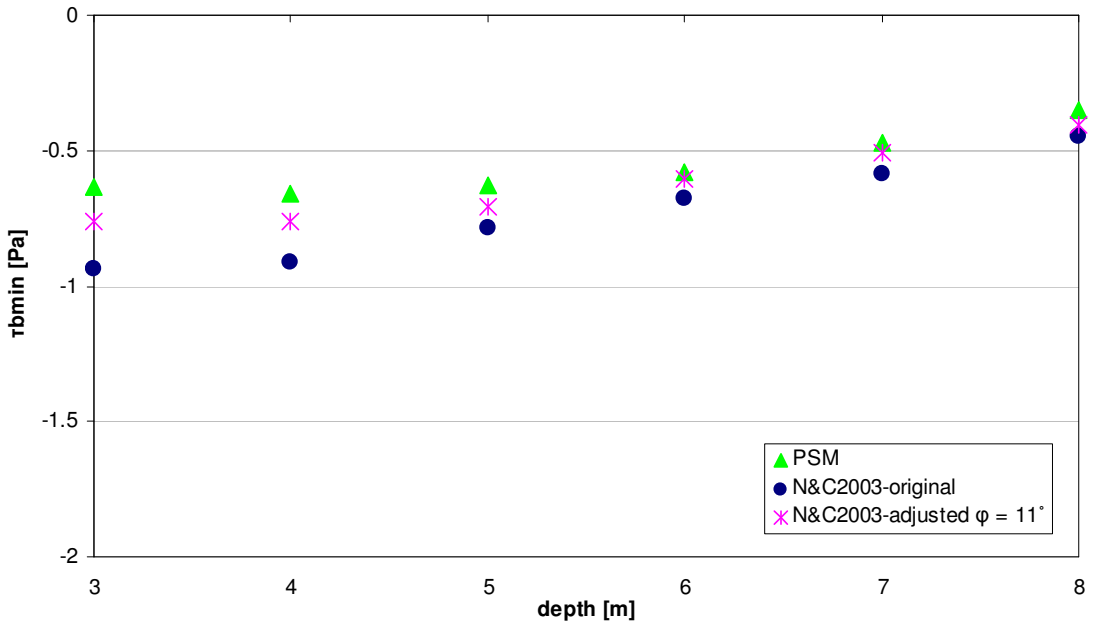

Figure 42: Maximum offshore-directed bed shear stress for different models

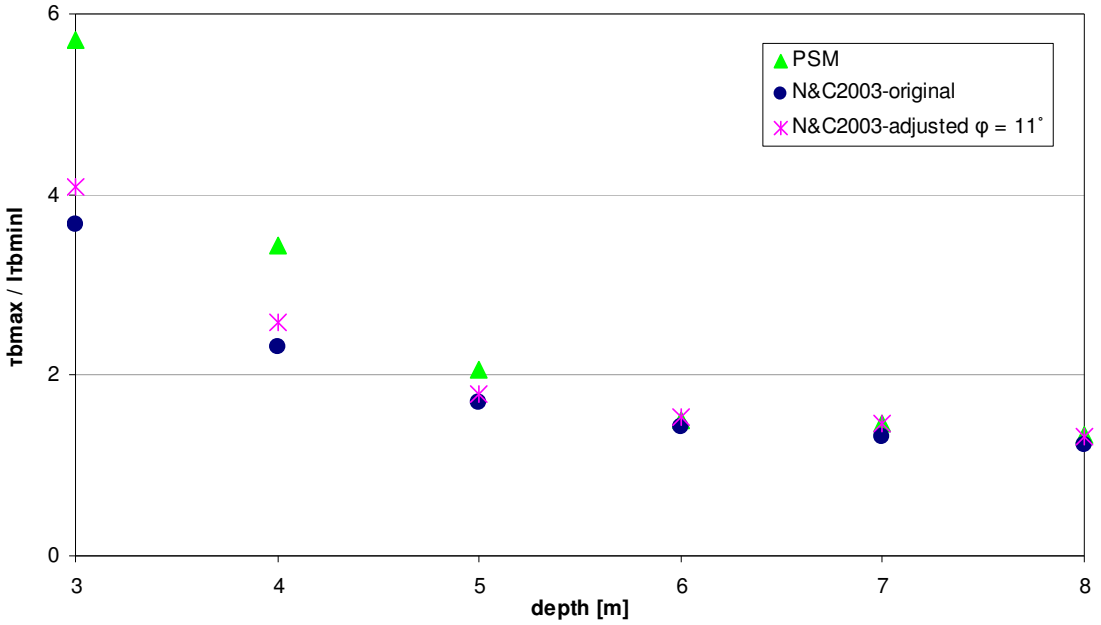

Figure 43: Ratio of the maximum on- and offshore-directed bed shear stresses, with and without streaming

Summary of chapter 5

In this chapter the bed shear stress model of Nielsen and Callaghan [2003] is adjusted to represent the physical situation as is simulated with the PONIT SAND model. This is done by considering the wave Reynolds stress and the instantaneous grain roughness friction velocity in this model. It is shown that the wave Reynolds stress given by Nielsen and Callaghan [2003] overestimates the wave Reynolds stress calculated from the PSM. Furthermore, the phase lead of 51˚ that is used to calculate the instantaneous grain roughness coefficient is much larger than should be the case for flat and immobile beds. Using a phase lead of 11˚ and the adjusted wave Reynolds stress new bed shear stresses are calculated that generally show better agreement with the POINT SAND model.

6 Discussion

In this research the POINT SAND model by Uittenbogaard [1999] is used as reference for the assessment of other analytical models. The PSM is able to simulate different situations: the presence of only an oscillatory horizontal flow in a tunnel and, the presence of both horizontal and vertical orbital velocities in free-surface wave channel. However, the validity of this model for individual wave processes is not shown yet. Therefore, it is highly recommended to examine whether the PSM is valid for tunnel situations where streaming is a result of asymmetry in the turbulence intensity. This could be done by comparing the results of the PSM to the laboratory data sets of Ribberink and Al Salem [1995]. Furthermore, the convergence of the PSM should be investigated in more detail. As discussed the results of the PSM are strongly affected by the model's run time, choice of grid size and time steps. Other parameters should be identified that affect the convergence of this model and their effect should be analysed.

Another point of discussion is the effect of a closed boundary (pressure gradient) on the streaming velocities. In this research the effect of this driving force is not considered as different studies suggest that the effect of a closed boundary on the streaming velocities is negligible. However, it is shown that the streaming velocities from the POINT SAND model are affected by the presence of a closed boundary, especially at higher levels in the water column. Therefore, it is recommended to investigate the exact effect of a closed boundary on the streaming velocities. The POINT SAND model could be used to get insight in this.

The choice of the boundary layer thickness is quite arbitrary in literature as several definitions are used. In order to get good representation of the behaviour of the streaming models, the boundary layer thickness in this research is defined as twice the distance from the bed where the amplitude of the horizontal oscillating velocity has reached the maximum value. Furthermore, the streaming velocities at the edge of the boundary layer are not necessarily representative for the behaviour of streaming profiles as the streaming velocities could be positive as well as negative considering the water column. Therefore, streaming velocities should not be analyzed at one level z but streaming profiles should be considered.

Finally, when the analytical bed shear stress models of Nielsen and Callaghan [2003], and Van Rijn [2007] are compared to the POINT SAND model it should be noticed that the physical representation of these models are not the same. As discussed before, the analytical bed shear stress models of Nielsen and Callaghan [2003], and Van Rijn [2007] are based on tunnel experiments where the bed shear stresses from the POINT SAND model are based on simulations of the free-surface wave channels.

7 Conclusion

The overall objective of this research is to get insight in the underlying mechanisms of Eulerian streaming and to include its effects in bed shear stress modelling that is determinative for sediment transport. In this research three hydrodynamic models are discussed that take account for real wave processes such as the effects of boundary layer streaming: the models of Longuet-Higgins [1953], Davies and Villaret [1999], and the POINT SAND model of Uittenbogaard [1999]. These models are used, together with basic flow equations derived for the wave boundary layer, to get insight in the mechanisms that affect streaming. In order to do this the streaming models are compared under representative wave conditions where the Davies and Villaret [1999] solution is adjusted to represent flat bed situations. The conclusions drawn in this section are related to the following central questions of this research:

1) How is the Eulerian streaming affected by different flow mechanisms?
2) How well do the existing analytical bed shear stress models take account for streaming? And in what way can the analytical model(s) be improved?

The following conclusions are drawn with respect to the first central question:

- This study has shown that the driving forces for streaming are the wave Reynolds stress that originates from the existence of vertical velocities and the wave component of mean turbulent Reynolds stress that is associated with wave asymmetry. Above flat beds the wave Reynolds stress has a positive contribution to streaming where the wave component of mean wave Reynolds stress has a negative contribution to streaming.
- Furthermore, the streaming velocities are affected by several wave parameters such as wave height H, wave length L, wave period T and wave asymmetry R. Considering the analytical models of Longuet-Higgins [1953], and Davies and Villaret [1999] it is shown that above flat beds the streaming velocities increase with increasing wave height and wave period. In contrast to this, an increase in the wave lengths and wave asymmetry results in a decrease of the streaming velocities.
- It is also shown that the streaming velocities, above flat beds, are positive as well near-bed as away from the bed. This is the result of the dominant, positive contribution to streaming of the wave Reynolds stress compared to the negative contribution of the wave component of mean turbulent Reynolds stress.
- Another insight that is provided by this study is that above flat beds, a time variation as well as a depth variation in the eddy viscosity results into a positive contribution to the streaming velocities. This explains the fact that above flat beds the PSM (time- and depth-dependent eddy viscosity) gives the largest streaming velocities followed by DV99 (time-dependent eddy viscosity) and LH53 (constant viscosity).

The following conclusions are drawn with respect to the second central question:

- This study has shown that the bed shear stress model of Nielsen and Callaghan [2003] takes quite good account for streaming as good agreement is found with the result of the POINT SAND model. In contrast to this the model of Van Rijn [2007] shows poor agreement with the POINT SAND model. The reason for this is the fact that Van Rijn [2007] takes account for streaming by adding the streaming velocities which are much smaller than the free stream velocities. As a result the calculated bed shear stresses remain practically unchanged. In contrast to this, Nielsen and Callaghan [2003] take account for streaming by adding the wave Reynolds stress which is calculated using a much larger grain friction coefficient. As a result the wave Reynolds stress is of same order of magnitude as the time-dependent bed shear stress. Therefore, adding the wave Reynolds stress to the time-dependent bed shear stress leads to significantly different values of the bed shear stresses. Another reason for the difference in the performance of both models is the fact that the edge of the boundary layer is quite debatable and the streaming velocities at the edge of the boundary layer are not necessarily representative for the behaviour of streaming profiles as the streaming velocities could be positive as well as negative. In contrast to this the wave Reynolds stress is always negative and its value on the edge of the boundary layer is quite comparable to other levels in the vertical. In other words, the concept used by Nielsen and Callaghan [2003] works better than the concept used by Van Rijn [2007].
- Furthermore, the model of Nielsen and Callaghan [2003] is adjusted to represent the physical situation as is simulated with the PONIT SAND model. This is done by considering the wave Reynolds stress and the instantaneous grain roughness friction velocity in this model. It is shown that the wave Reynolds stress given by Nielsen and Callaghan [2003] overestimates the wave Reynolds stress calculated from the PSM. Furthermore, the phase lead of 51˚ that is used to calculate the instantaneous grain roughness coefficient is much larger than should be the case for flat and immobile beds. Using a phase lead of 11˚ and the adjusted wave Reynolds stress new bed shear stresses are calculated that show better agreement with the POINT SAND model than the original model of Nielsen and Callaghan [2003].

References

Bosboom, J., Klopman, G. (2000). *Intra-wave sediment transport modelling.* Proc. International Conference on Coastal Engineering, Vol. 3, pages 2453-2466.

Davies, A. G., Villaret, C. (1999). *Eulerian drift induced by progressive waves above rippled and rough beds.* Journal of Geophysical research, Vol. 104, NO. C1, pages 1465-1488.

Davies, A. G., Li, Z. (1997). *Modelling sediment transport beneath regular symmetrical and asymmetrical waves above a plane bed.* Continental Shelf Research, 17(5), pages 555-582.

Dohmen-Janssen, C. M., Hanes, D. H. (2002). *Sheet flow dynamics under monochromatic nonbreaking waves.* Journal of Geophysical Research, Vol. 107, NO. C10, 3149.

Hulscher, S. J. M. H., Ribberink, J. S., Knaapen, M.A.F. (2002). *Marine dynamics*. College book, University Twente, Enschede, The Netherlands.

Jonsson, I.G. (1966). *Wave boundary layers and friction factors*. Proc. 10th Int. Conf. on Coast. Eng., pp. 127–148.

Klopman, G. (1994). *Vertical structure of the flow due to waves and currents: Laser- Doppler flow measurements for waves following or opposing a current.* Delft Hydraulics, progress report, H 840.30, part II.

Longuet-Higgins, M. S. (1953). *Mass transport in water waves.* Trans.R.Soc.London Ser. A245, pp. 535-581.

Longuet-Higgins, M. S. (1958). *The mechanics of the boundary-layer near the bottom in a progressive wave.* National Institute of Oceanography, pages 184-193.

Marin, F. (2003). *Eddy viscosity and Eulerian drift over rippled beds in waves.* Coastal Engineering 50, pp. 139-159.

Mathisen, P. P., Madsen, O. S. (1996). *Waves and currents over a fixed rippled bed.* Bottom roughness experienced by waves in the presence and absence of currents. Journal of Geophysical research, 101(C7), 16533-16542, 1996a.

Mathisen, P. P., Madsen, O. S. (1996). *Waves and currents over a fixed rippled bed.* Bottom and apparent roughness experienced by currents in the presence of waves. Journal of Geophysical research, 101(C7), 16543-16550, 1996b.

Mei, C. C. (2003). *The applied dynamics of ocean surface waves*. Advanced series on ocean engineering, Vol 1. World Scientific, Singapore.

Myrhaug, D., Slaattelid, O. H. (1989). *Combined wave and current boundary layer model for fixed, rough seabeds.* Ocean Engineering, Vol 16, pp. 119-142.

Nielsen, P. (1992). *Coastal bottom boundary layers and sediment transport.* Advanced series on ocean engineering, Vol 4. World Scientific, Singapore.

Nielsen, P., You, Z-J. (1996). *Eulerian mean velocities under non-breaking waves on horizontal bottoms.* Proc. 25th Int. Conf. Coast. Eng., pp. 4066-4078, ASCE, Orlando.

Nielsen, P., Callaghan, D. P. (2003). *Shear stress and sediment transport calculations for sheet flow under waves.* Coastal Engineering 47, pp. 347-354.

Nielsen, P. (2006). *Sheet flow sediment transport under waves with acceleration skewness and boundary layer streaming.* Coastal Engineering 53, pp. 749-758.

O'Donoghue, T., Ribberink, J. S. (2007). *Laboratory experiments and the development of wave-driven sand transport models*. PUBLS. INST. GEOPHYS. POL. ACAD. SC., E-7 (401).

Reniers, A. J. H. M., Thornton, E. B., Stanton, T. P. and Roelvink, J.A. (2004). *Vertical flow structure during Sandy Duck: observations and modelling*. Coastal Engineering 51, pp. 237-260, Elsevier.

Ribberink, J. S., Al Salem, A. A. (1995). *Sheet flow and suspension of sand in oscillatory boundary layers.* Coastal Engineering, 25, pp. 205-225.

Ribberink, J.S., Dohmen-Janssen, C.M., Hanes, D.M., McLean, S.R., Vincent, C. (2000). *Near-bed sand transport mechanisms under waves*. Proc. 27th Int. Conf. Coastal Eng., Sydney, A S C E, New York, pp. 3263–3276.

Rienecker, M.M., Fenton, J.D., (1981). *A Fourier approximation method for steady water waves.* Journal of Fluid Mechanics, vol. 104, pp. 119-137.

Svendsen, I. A. (2006). *Introduction to nearshore hydrodynamics.* Advanced series on ocean engineering, Vol 24. World Scientific, Singapore.

Trowbridge, J., Madsen, O. S. (1984). *Turbulent wave boundary layers, 2, Second-order theory and mass transport.* Journal of geophysical research, 89(C5), pp. 7999-8007.

Uittenbogaard, R. E. (1999). *Overview of the POINT SAND MODEL.* Delft Hydraulics, Z2899.10.

Uittenbogaard, R. E. (2000). *1DV Simulation of wave current interaction.* Proc. 27th International Conference on Coastal Engineering, Sydney.

Uittenbogaard, R. E., Klopman, G. (2001). *Numerical simulation of wave-current driven sediment transport.* Coastal dynamics, pp. 568-577.

van Doorn, T. (1981). *Experimental investigation of near-bottom velocities in water waves without and with a current.* TOW report M 1423 part 1, Delft Hydraulics Laboratory.

Van Rijn, L. C. (1984a). *Sediment transport. Part I: Bed load transport.* Journal of hydraulic engineering, 110 (10), pp. 1431-1456.

Van Rijn, L. C. (1993). *Principles of sediment transport in rivers, estuaries, and coastal seas.* Aqua publications, Blokzijl, The Netherlands.

Van Rijn, L. C. (2007). *Unified view of sediment transport by currents and waves. I: Initiation of motion, bed roughness, and bed load transport.* Journal of hydraulic engineering, Vol. 133, No. 6, pp. 649-667.

Watanabe, J. F. A., Soto, S. (2004). *A sheet flow transport rate formula asymmetric forward leaning waves and currents.* Proc. 29th ICCE, Lisbon, World Scientific, pp. 1703-1714.

Appendices

Appendix A – Wave averaged equations

To derive the wave-averaged equations Reynolds decompositions is used which considers flow that contains a periodic flow component $\tilde{u}$ as well as the familiar steady $\overline{u}$ and turbulent components u'. Here also the pressure term is assumed to contain a periodic component as well as a steady and turbulent component. The first step in this method is to insert the different flow components and pressure components into the continuity and momentum equations. Next, these equations are phase- (~) and time-averaged (¯). This is done by using the definitions of phase- and time-averaging given by [Nielsen, 1992] as listed below.

Definitions by [Nielsen, 1992]:

$$\begin{gathered} \overline{\tilde{x}} = \overline{\tilde{x}'} = \tilde{\tilde{x}}' = 0 \\ \overline{\overline{x}\tilde{y}} = \overline{\overline{x}\tilde{y}'} = \overline{\tilde{x}\tilde{y}'} = \tilde{\overline{x}\tilde{y}'} = \tilde{\tilde{x}\tilde{y}'} = 0 \\ \tilde{\tilde{x}\tilde{y}} = \tilde{x}\tilde{y} - \overline{\tilde{x}\tilde{y}} \end{gathered} \tag{A.1}$$

Here the line (¯) denotes the time average of a quantity given by (A.2) where the tilde (~) denotes the periodic component given by (A.3) that is defined as the phase average over several (N) wave periods minus the time average.

$$\overline{u}(t) = \frac{1}{T}\int_{-T/2}^{T/2} u(t)dt, \quad \text{for t } \in [0,T) \tag{A.2}$$

$$\tilde{u}(z,t) = \frac{1}{N}\sum_{j=1}^{N} u(z,t+jT) - \overline{u}(z) \tag{A.3}$$

Given the definitions above, the first step is to insert the different flow components $(u,w) = (\overline{u} + \tilde{u} + u', \overline{w} + \tilde{w} + w')$ *and pressure components* $P = \overline{P} + \tilde{P} + P'$ *into the continuity and momentum equations. Here only derivations are shown for the momentum equation in the x-direction.*

Continuity equations

$$\begin{gathered} \frac{\partial(\overline{u} + \tilde{u} + u')}{\partial x} + \frac{\partial(\overline{w} + \tilde{w} + w')}{\partial z} = 0 \\ \frac{\partial \overline{u}}{\partial x} + \frac{\partial \tilde{u}}{\partial x} + \frac{\partial u'}{\partial x} + \frac{\partial \overline{w}}{\partial z} + \frac{\partial \tilde{w}}{\partial z} + \frac{\partial w'}{\partial z} = 0 \end{gathered} \tag{A.4}$$

Momentum equation

$$x-direction$$

$$\begin{aligned}&\frac{\partial\left(\overline{u}+\tilde{u}+u'\right)}{\partial t}+\frac{\partial\left(\overline{u}+\tilde{u}+u'\right)^2}{\partial x}+\frac{\partial\left(\overline{u}+\tilde{u}+u'\right)\left(\overline{w}+\tilde{w}+w'\right)}{\partial z}\\&=-\frac{1}{\rho}\frac{\partial\left(\overline{P}+\tilde{P}+P'\right)}{\partial x}+\nu\left(\frac{\partial^2\left(\overline{u}+\tilde{u}+u'\right)}{\partial x^2}+\frac{\partial^2\left(\overline{u}+\tilde{u}+u'\right)}{\partial z^2}\right)\end{aligned} \tag{A.5}$$

*Next, **phase averaging** (~) is applied on the continuity (A.4) and momentum (A.5) equations:*

Continuity equation

$$\begin{aligned}&\widetilde{\frac{\partial\overline{u}}{\partial x}}+\widetilde{\frac{\partial\tilde{u}}{\partial x}}+\widetilde{\frac{\partial u'}{\partial x}}+\widetilde{\frac{\partial\overline{w}}{\partial z}}+\widetilde{\frac{\partial\tilde{w}}{\partial z}}+\widetilde{\frac{\partial w'}{\partial z}}=0\\&\frac{\partial\overline{u}}{\partial x}+\frac{\partial\tilde{u}}{\partial x}+\frac{\partial\overline{w}}{\partial z}+\frac{\partial\tilde{w}}{\partial z}=0\end{aligned} \tag{A.6}$$

Momentum equation

$$x-direction:$$

$$\begin{aligned}&\frac{\partial\widetilde{\left(\overline{u}+\tilde{u}+u'\right)}}{\partial t}+\frac{\partial\widetilde{\left(\overline{u}+\tilde{u}+u'\right)^2}}{\partial x}+\frac{\partial\widetilde{\left(\overline{u}+\tilde{u}+u'\right)\left(\overline{w}+\tilde{w}+w'\right)}}{\partial z}\\&=-\frac{1}{\rho}\frac{\partial\widetilde{\left(\overline{P}+\tilde{P}+P'\right)}}{\partial x}+\nu\left(\frac{\partial^2\widetilde{\left(\overline{u}+\tilde{u}+u'\right)}}{\partial x^2}+\frac{\partial^2\widetilde{\left(\overline{u}+\tilde{u}+u'\right)}}{\partial z^2}\right)\rightarrow\end{aligned} \tag{A.7}$$

$$\begin{aligned}&\frac{\partial\overline{u}}{\partial t}+\frac{\partial\tilde{u}}{\partial t}+\frac{\partial\overline{u}^2}{\partial x}+2\frac{\partial\overline{u}\tilde{u}}{\partial x}+\frac{\partial\tilde{u}^2}{\partial x}+\frac{\partial\widetilde{u'^2}}{\partial x}+\frac{\partial\overline{u}\overline{w}}{\partial z}+\frac{\partial\overline{u}\tilde{w}}{\partial z}+\frac{\partial\tilde{u}\overline{w}}{\partial z}+\frac{\partial\tilde{u}\tilde{w}}{\partial z}+\frac{\partial\widetilde{u'w'}}{\partial z}\\&=-\frac{1}{\rho}\left(\frac{\partial\overline{P}}{\partial x}+\frac{\partial\tilde{P}}{\partial x}\right)+\nu\left(\frac{\partial^2\overline{u}}{\partial x^2}+\frac{\partial^2\tilde{u}}{\partial x^2}+\frac{\partial^2\overline{u}}{\partial z^2}+\frac{\partial^2\tilde{u}}{\partial z^2}\right)\end{aligned}$$

*Finally, **time-averaging** (¯) the continuity (A.6) and momentum (A.7) equations give:*

Continuity equation

$$\begin{aligned}&\overline{\frac{\partial \overline{u}}{\partial x}}+\overline{\frac{\partial \tilde{u}}{\partial x}}+\overline{\frac{\partial \overline{w}}{\partial z}}+\overline{\frac{\partial \tilde{w}}{\partial z}}=0\\&\frac{\partial \overline{u}}{\partial x}+\frac{\partial \overline{w}}{\partial z}=0\end{aligned} \tag{A.8}$$

Momentum equation

$$x-direction:$$

$$\begin{aligned}&\overline{\frac{\partial \overline{u}}{\partial t}}+\overline{\frac{\partial \tilde{u}}{\partial t}}+\overline{\frac{\partial \overline{u}^2}{\partial x}}+2\overline{\frac{\partial \overline{u}\tilde{u}}{\partial x}}+\overline{\frac{\partial \tilde{u}^2}{\partial x}}+\overline{\frac{\partial \widetilde{u'^2}}{\partial x}}+\overline{\frac{\partial \overline{u}\overline{w}}{\partial z}}+\overline{\frac{\partial \overline{u}\tilde{w}}{\partial z}}+\overline{\frac{\partial \tilde{u}\overline{w}}{\partial z}}+\overline{\frac{\partial \tilde{u}\tilde{w}}{\partial z}}+\overline{\frac{\partial \widetilde{u'w'}}{\partial z}}\\&=-\frac{1}{\rho}\left(\overline{\frac{\partial \overline{P}}{\partial x}}+\overline{\frac{\partial \tilde{P}}{\partial x}}\right)+\nu\left(\overline{\frac{\partial^2 \overline{u}}{\partial x^2}}+\overline{\frac{\partial^2 \tilde{u}}{\partial x^2}}+\overline{\frac{\partial^2 \overline{u}}{\partial z^2}}+\overline{\frac{\partial^2 \tilde{u}}{\partial z^2}}\right)\rightarrow\end{aligned} \tag{A.9}$$

$$\frac{\partial \overline{u}^2}{\partial x}+\frac{\partial \overline{\tilde{u}^2}}{\partial x}+\frac{\partial \overline{u'^2}}{\partial x}+\frac{\partial \overline{uw}}{\partial z}+\frac{\partial \overline{\tilde{u}\tilde{w}}}{\partial z}+\frac{\partial \overline{u'w'}}{\partial z}=-\frac{1}{\rho}\frac{\partial \overline{P}}{\partial x}+\nu\left(\frac{\partial^2 \overline{u}}{\partial x^2}+\frac{\partial^2 \overline{u}}{\partial z^2}\right)$$

The same steps are taken for the momentum equation in the z-direction which results into:

$$z-direction:$$

$$\frac{\partial \overline{w}^2}{\partial z}+\frac{\partial \overline{\tilde{w}^2}}{\partial z}+\frac{\partial \overline{w'^2}}{\partial z}+\frac{\partial \overline{wu}}{\partial x}+\frac{\partial \overline{\tilde{w}\tilde{u}}}{\partial x}+\frac{\partial \overline{w'u'}}{\partial x}=-g-\frac{1}{\rho}\frac{\partial \overline{P}}{\partial z}+\nu\left(\frac{\partial^2 \overline{w}}{\partial x^2}+\frac{\partial^2 \overline{w}}{\partial z^2}\right) \tag{A.10}$$

Appendix B – Components of DV99$^{(a)}$

Here the contributions of different components to the DV99$^{(a)}$ streaming solution, above rough rippled beds, is presented. The streaming profiles are made for different cross-shore depths for wave 1 and 2.

The cross-shore behaviour of term $U^{(1)}$ for wave 1 and 2 is shown in Figure 44 and Figure 45, respectively. This term reflects the LH53-solution that arises from the wave Reynolds stress and is therefore positive at all water depths. Approaching the coast, the streaming velocities increase as discussed in section 3.1.1.
The cross-shore behaviour of term $U^{(2)}$ for wave 1 and 2 is shown in Figure 46 and Figure 47, respectively. Approaching the coast, the shape of this term is more pronounced as the near-bed jet is increased while the negative outer flow away from bed is further decreased. As mentioned before $U^{(2)}$ reflects the contribution to the streaming velocity associated with asymmetry in the turbulent intensity and thus the contribution of the wave part of the mean turbulent Reynolds stress term. Therefore, above rough rippled beds this term increases the near-bed streaming velocities but reduces the outer flow at higher levels from the bed while approaching the coast.
The cross-shore behaviour of term $U^{(3)}$ for wave 1 and 2 is shown in Figure 48 and Figure 49, respectively. As mentioned before this term reflects the contribution to streaming associated with time variation in the eddy viscosity. Both figures show positive contributions for all cross-shore water depths.

When the magnitude of the individual components are considered, it can be seen that the $U^{(2)}$ term gives the largest contribution to streaming velocities followed by $U^{(3)}$ and eventually by $U^{(1)}$. Therefore, it can be concluded that above rough rippled beds the streaming velocities are mostly determined by the contribution of the wave part of the mean turbulent Reynolds stress, where the contribution of the wave Reynolds stress is significantly smaller.

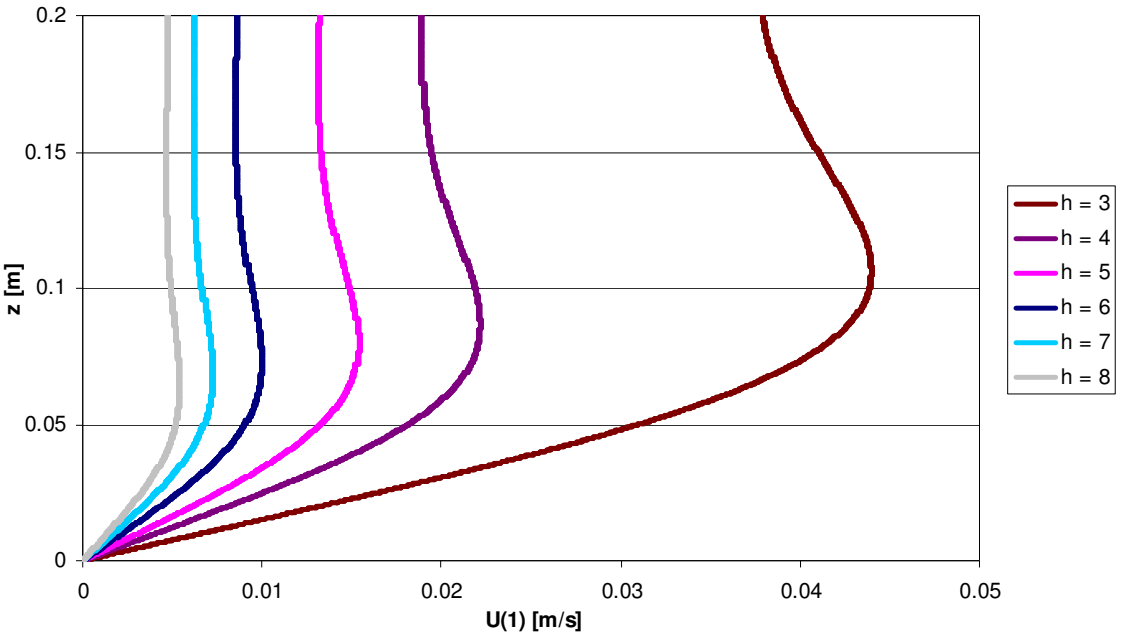

Figure 44: $U^{(1)}$ contribution to streaming, for wave 1

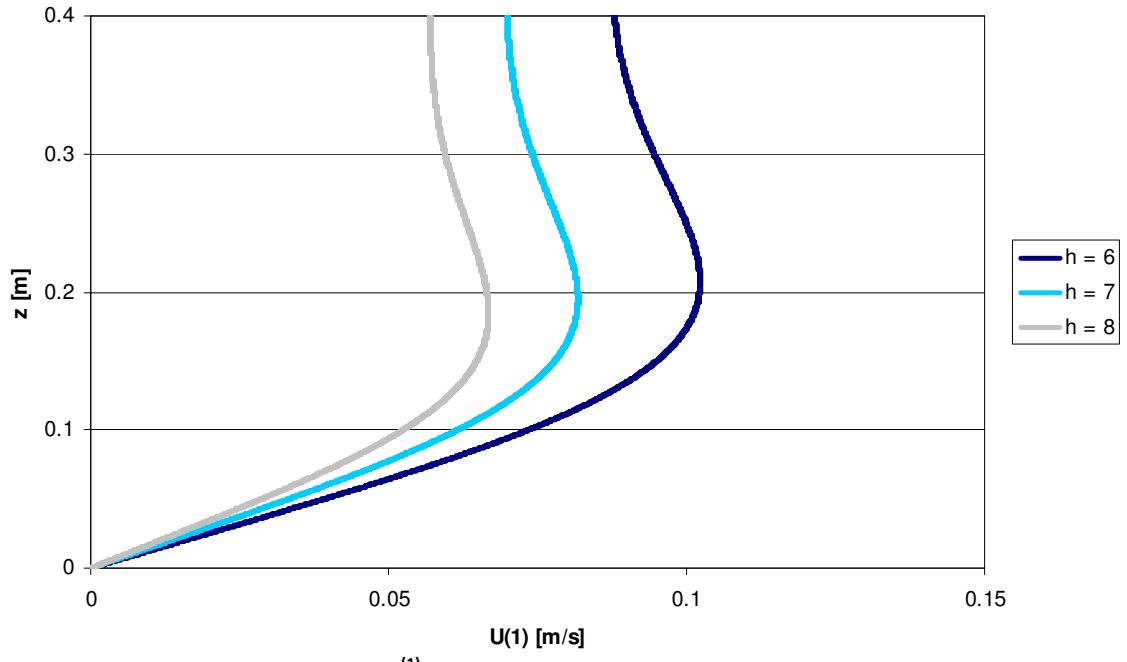

Figure 45: $U^{(1)}$ contribution to streaming, for wave 2

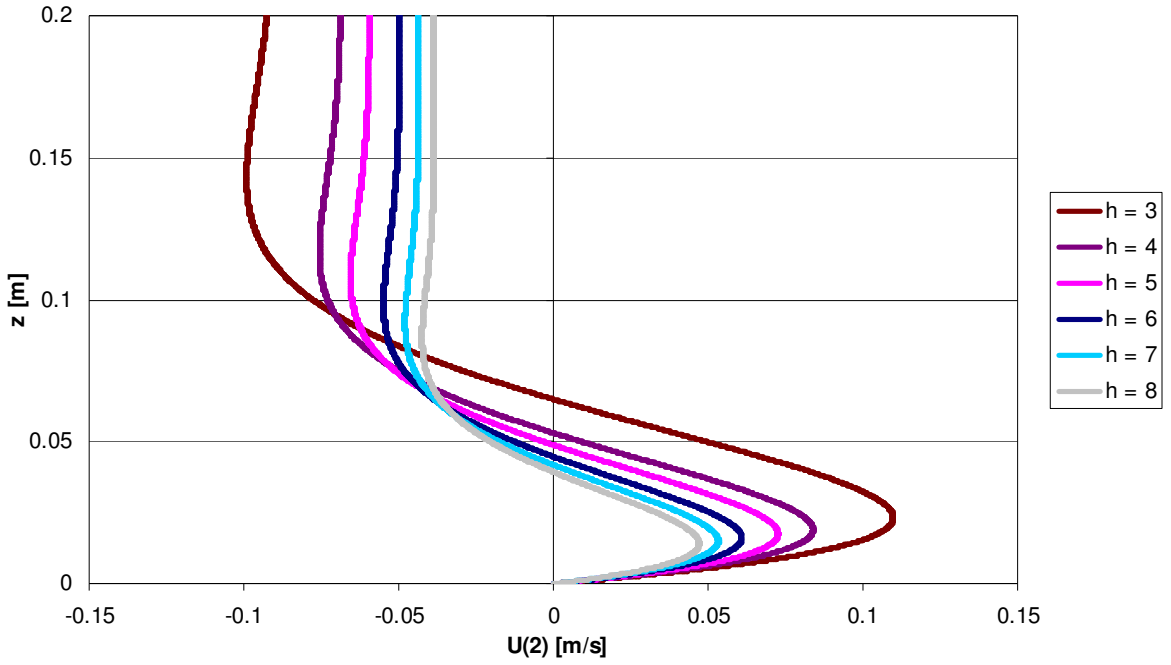

Figure 46: $U^{(2)}$ contribution to streaming, for wave 1

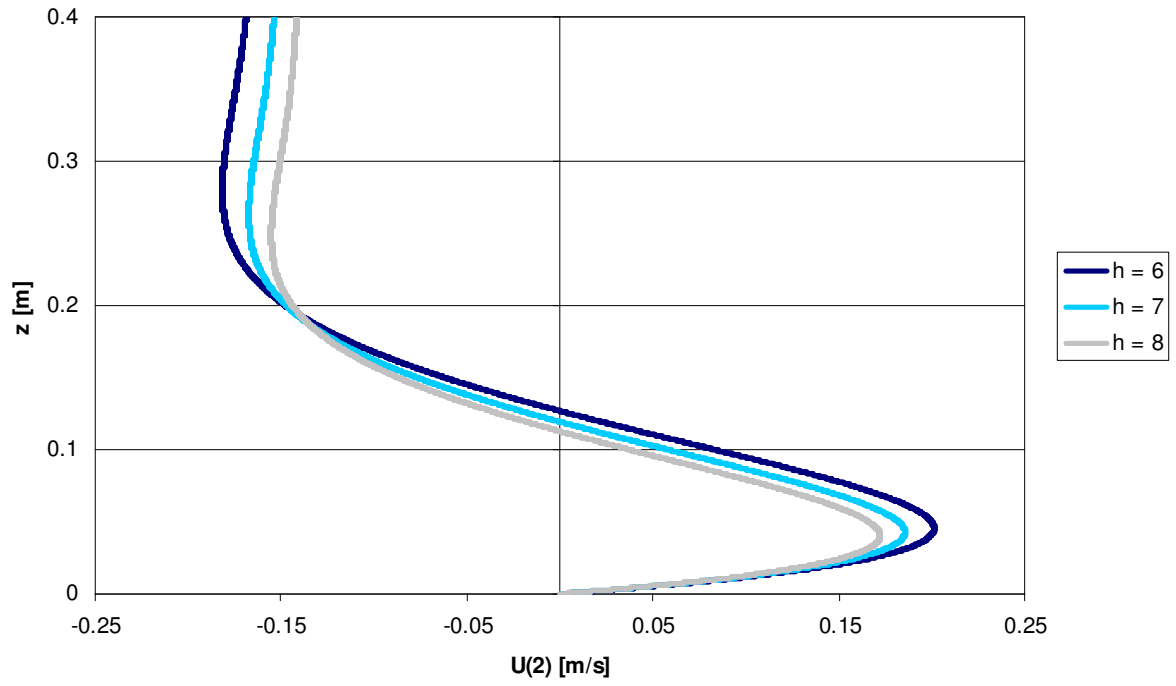

Figure 47: $U^{(2)}$ contribution to streaming, for wave 2

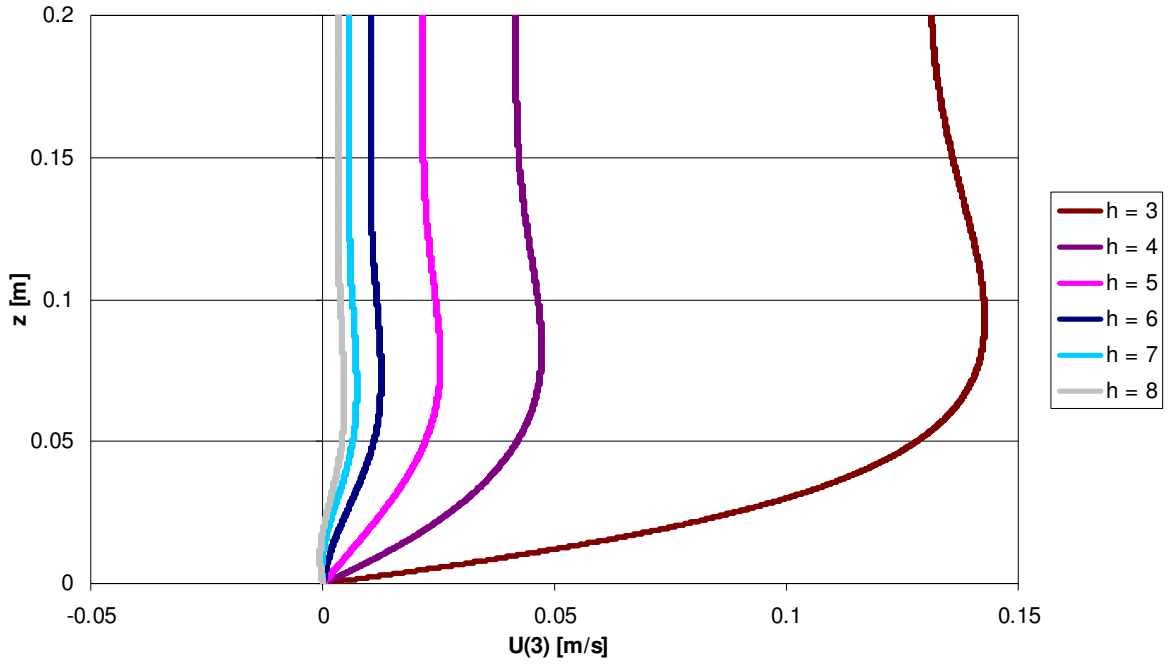

Figure 48: $U^{(3)}$ contribution to streaming, for wave 1

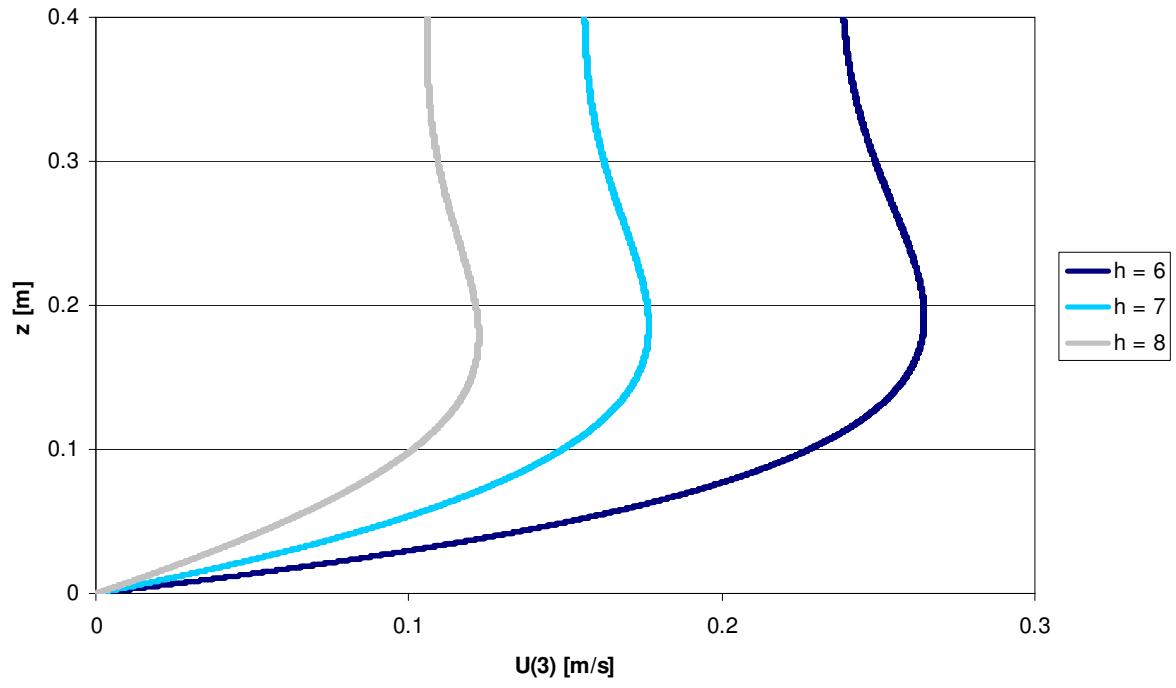

Figure 49: $U^{(3)}$ contribution to streaming, for wave 2

Appendix C – Sensitivity analysis on PSM

Here a sensitivity analysis is performed where the stability of the POINT SAND model is examined. Furthermore, an example of an input file of the PSM is shown.
The effect of different model run time (Figure 50), grid size (Figure 51) and time steps (Figure 52) on the time-averaged horizontal velocity is considered. Considering Figure 50, it can be seen that the time-averaged velocity is stable for almost all grid size for a run time of about 2300 seconds. However, considering Figure 51 and Figure 52 it can be concluded that a grid size of h/200 (water depth divided by 200) and time steps of T/600 (wave period divided by 600) give the most stable results for the time-averaged velocity.

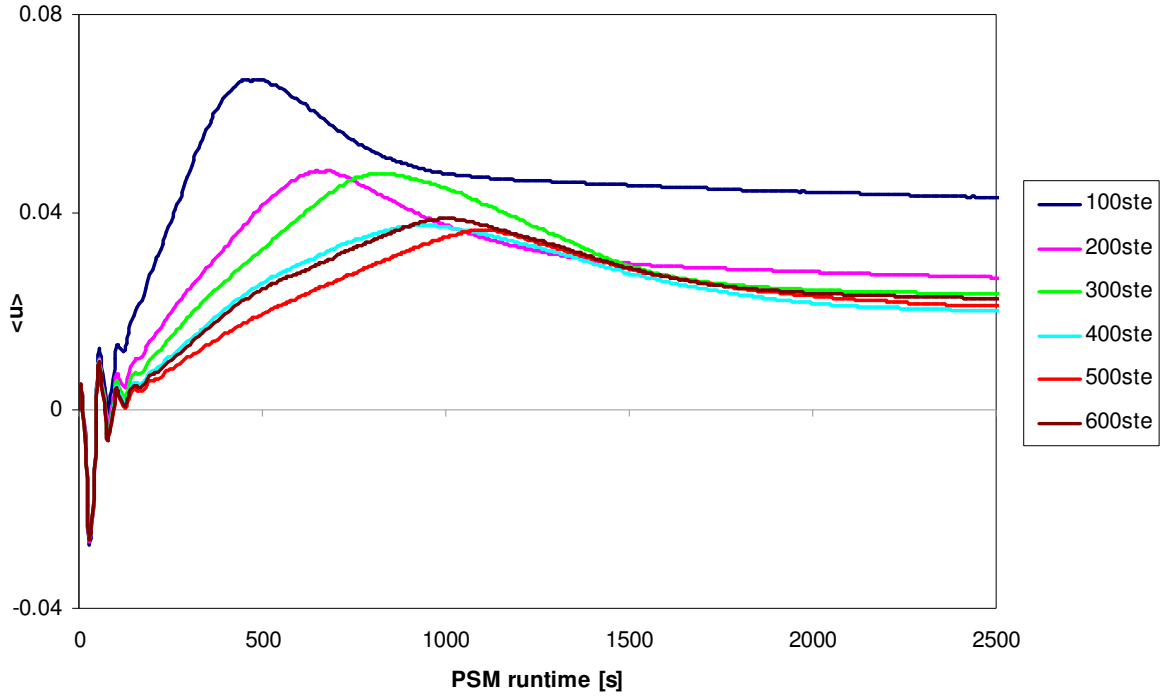

Figure 50: Time-averaged velocity for different grid sizes as a function of model run time

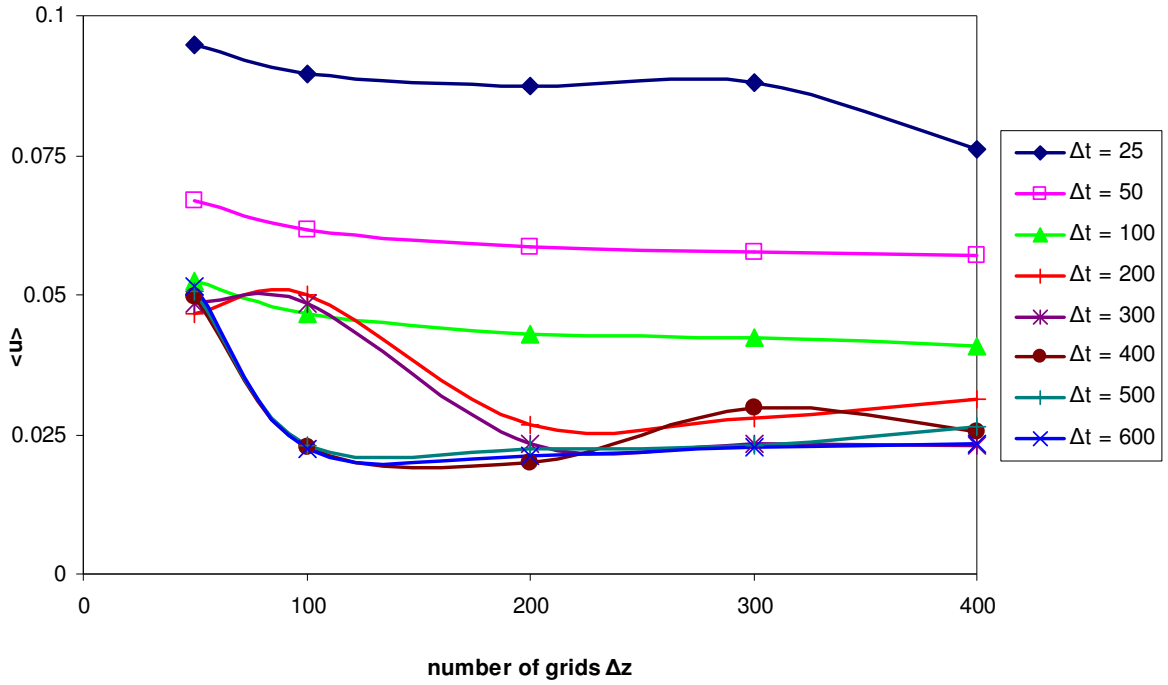

Figure 51: Time-averaged velocity for different time steps as function of grid sizes

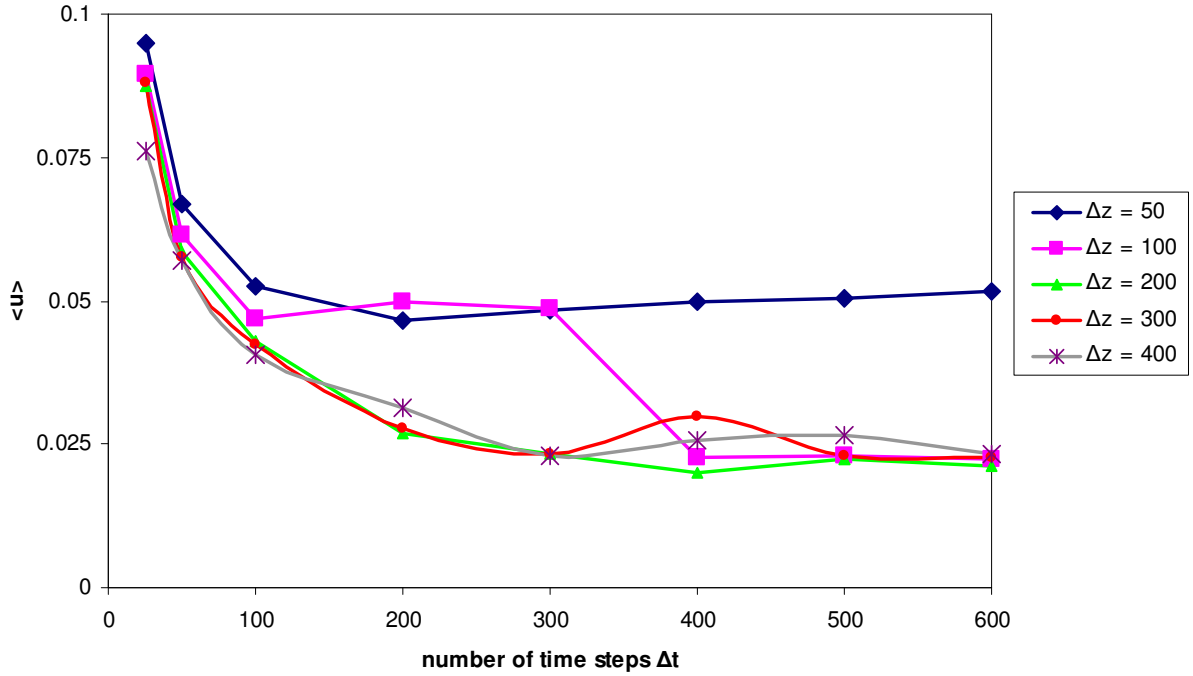

Figure 52: Time-averaged velocity for different grid sizes as function of time steps

Example of an input file of the POINT SAND model: wave 1 and water depth h=3 m

In the first part of this input file the general parameter settings are shown under which the water depth. Next, the time management of the model simulations are shown. Here the model run time together with number of time steps are given. Furthermore, the turbulence and wave settings are shown together with the 'layer input' where the grid size can be entered. Here it can be seen that an exponential course of the grid size is chosen. The other settings are related to sediment characteristics. Here only the D_{50} is of concern.

```
*****General                input********
1dv                                     DIMENS: choose 1DV or DPM
0.0                                     FCORIO: Coriolis parameter
0.0                                     DP    : depth
3.00                                    ZETA  : water-level (or)
                                        FILTSZ: file time series ZETA (or)
                                        FILFOZ: file fourier comp. ZETA (or)
0.0                                     UMEAN : West-to-East depth-averaged velocity (or)
0.0                                     VMEAN : South-to-North depth-averaged velocity (or)
                                        FILTSU: file time series (U,V)-MEAN (or)
                                        FILFOU: file fourier comp.(U,V)-MEAN
-1.0                                    REFLVL: velocity reference level [m] above bed if ZREF<0 then depthaveraged is taken
zrefs.s01                               FILREF: file with z-levels for output per time step.
********Time             management*****
sec                                     TUNIT : time unit (SEC/MIN)
1.425                                   TIMEST: time step (in TUNIT)
1600                                     NUMTIM: number of timestep simulation
150                                      NUMWAV: number of timestep orbital motion per TIMEST
1.                                      REDTIM: reduction factor in time of current&wind forcing
0  5.7  2280.0                          TIMEWR: STRT-INC-STOP time frame writing output (TUNIT)
1.0                                     TETA  : par. theta-method(rec. theta =1)
********Turbulence & Waves settings*****
kep                                     MODEL : choice between LAM ; KEP ; K-L   , alg
1e-6                                    VISCOU: kinematic viscosity [m^2/s]
Z0                                      ROUMET: roughness meth. MANN/CHEZ/Z0
2.00e-05                                ROUCOF: roughness height (ROUMET)
1                                       IRO   : IRO=0: hydr.smooth, IRO=1: hydr.rough
                                        FLTWIN: file time series (directional) wind and surface waves (or)
0.                                      DIRWI : direction from which the wind blows
0.                                      WIND  : wind speed, 10 m above free surface
wavspc.s01                              FILSPC: file with directional spectrum of surface waves (or) wavspc.mp1
********Layer       Input*********
expo2                                   LAYDIS: choose USDEF, EQUID, POWER or EXPON OR expo2
200                                      KMAX  : number of layers
1.e-2                                   DZtop : >1 for POWER power in layer distribution; DZBED for EXPON
0.1e-3                                  dzbed
********Constituent Input*********
1000.0                                  RHOM  : reference density
0                                       LMAX  : number of constituents
0                                       LSAL  : index nr for salinity
0                                       LTEM  : index nr for temperature
0.0                                     SALEQS: eq. of state salinity (always input)
15.0                                    TEMEQS: eq. of state temperarture (always input)
********Sediment    Input*********
1                                       LSED     : number of sediment
SED1UP                                  SEDADV   : vertical advection scheme for sediment: SEDCEN, SED1UP
********First    fraction*********
SAND                                    SEDTYP(L): type of sediment
0.7                                     SIGSED(L): prandtl schmidt number
2650                                    RHOSOL(L): density sediment
0.24e-3                                 SEDDIA(L): D_50 [m] of sand
NOFLUX                                  EROTYP(L): PICKUP or BEDCON for type of bed condition , or SERIES     conft.mp1
                                        FILTCN   : file time series bed concentration
********Initial   profile*********
step                                    SEDDIS   : "step" or "linear"
0.0                                     SEDTOP(L): sediment concentration above step
0.0                                     SEDBED(L): sediment concentration below step
1                                       KSTEP    : k-value of sediment step position
********End         Input*********
```

Appendix D – Boundary layer thickness

In this appendix the boundary layer thickness δ for the different models is shown. The boundary layer thickness is defined as twice the distance from the bed where the amplitude of the horizontal oscillating velocity has reached its maximum value. Here Figure 53 shows the boundary layer thickness for the PSM where Figure 54 and Figure 55 show the boundary layer thickness for the LH53 and DV99 solutions, respectively.

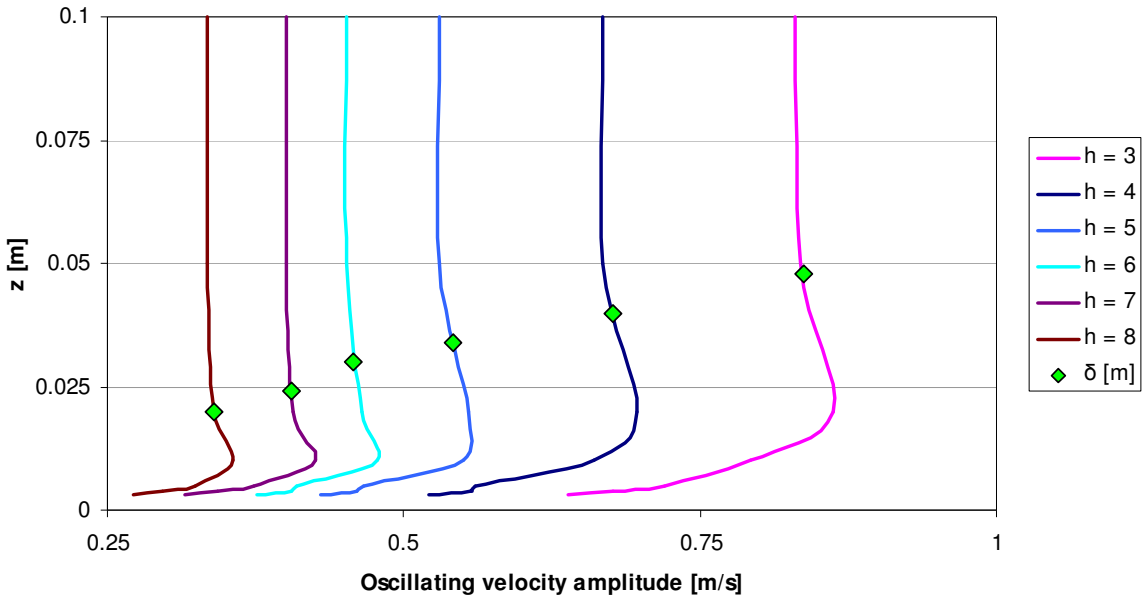

Figure 53: Boundary layer thickness as a function of water depth for the PSM

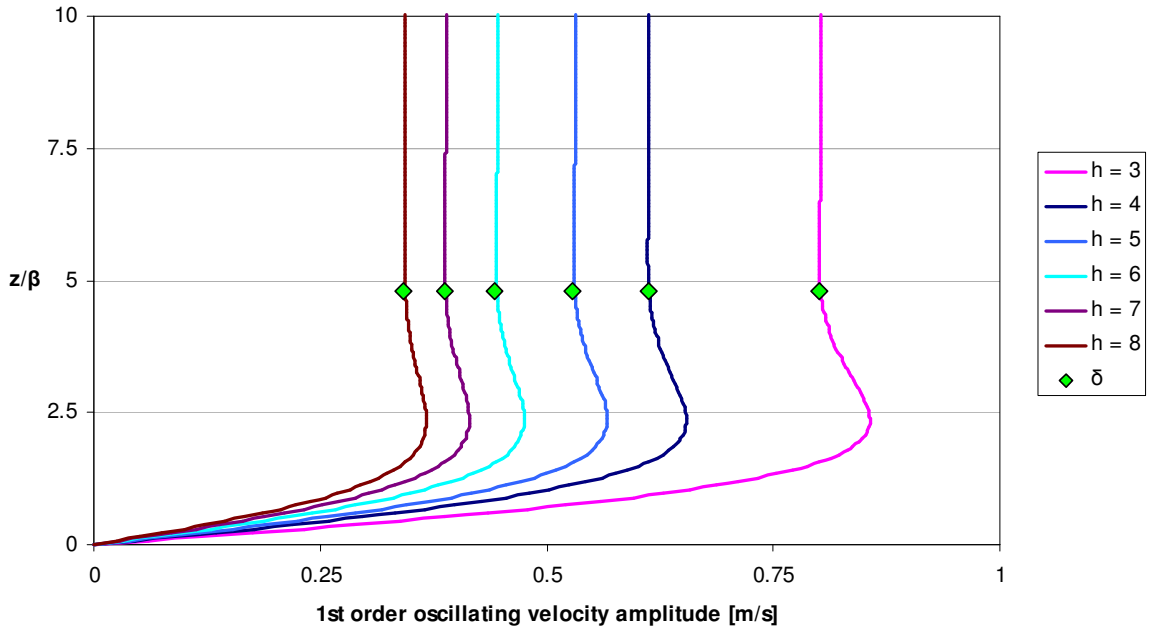

Figure 54: Boundary layer thickness as a function of water depth for LH53

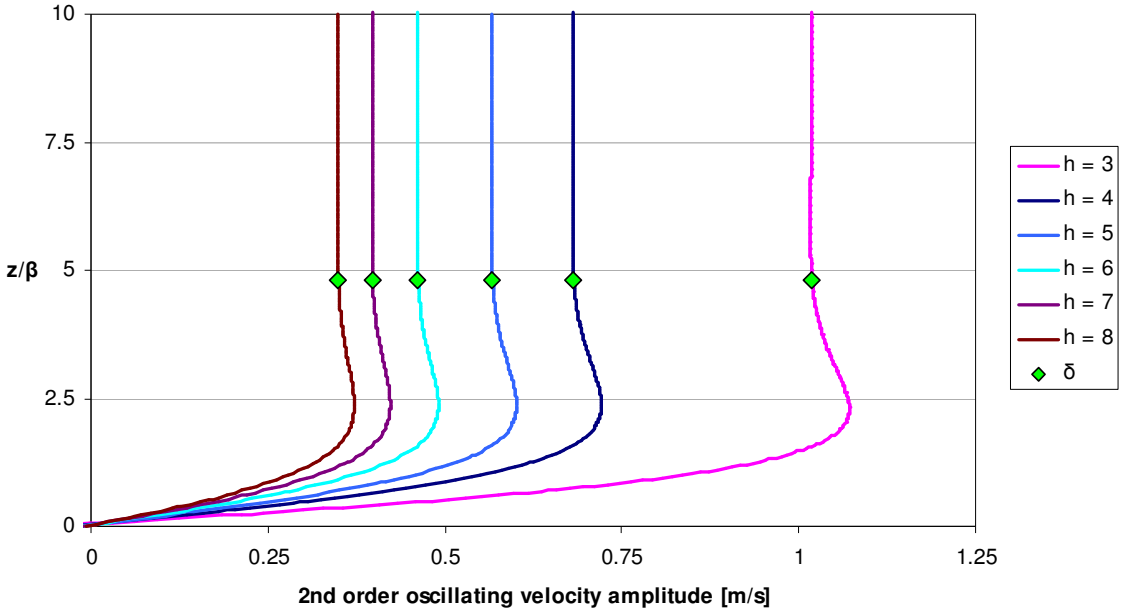

Figure 55: Boundary layer thickness as a function of water depth for DV99(a) and DV99(b)

Appendix E – Eddy viscosity profiles from PSM

In this appendix Figure 56 and Figure 57 show the depth-averaged (over the boundary layer thickness) eddy viscosity profiles for both waves obtained from the POINT SAND model.

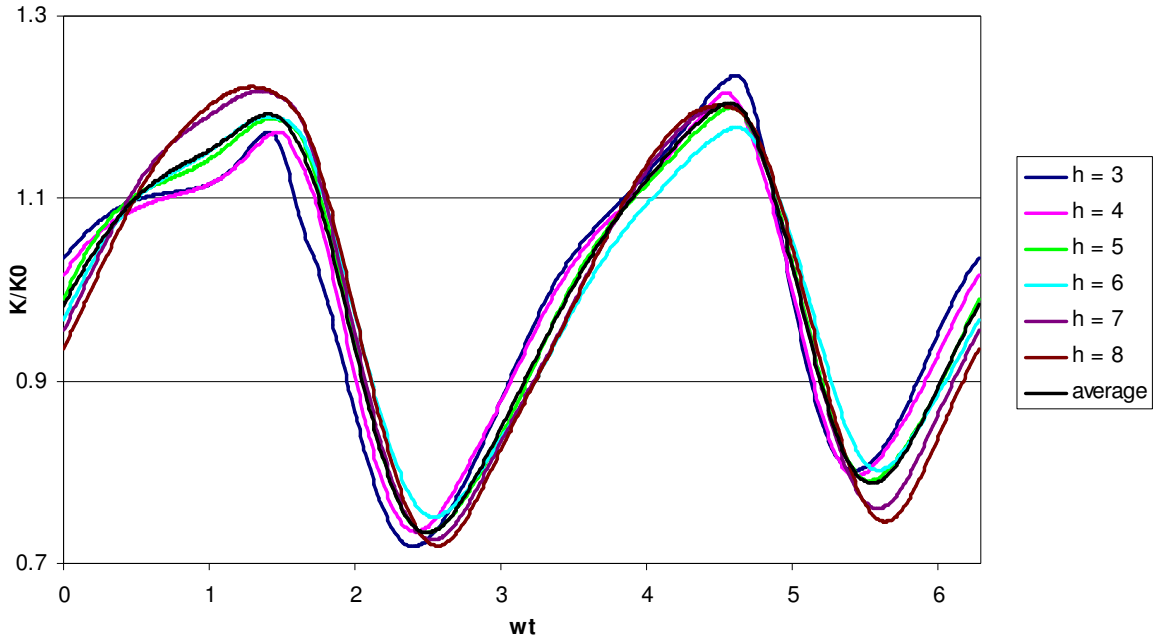

Figure 56: Eddy viscosity profiles, depth-averaged over the boundary layer (wave 1)

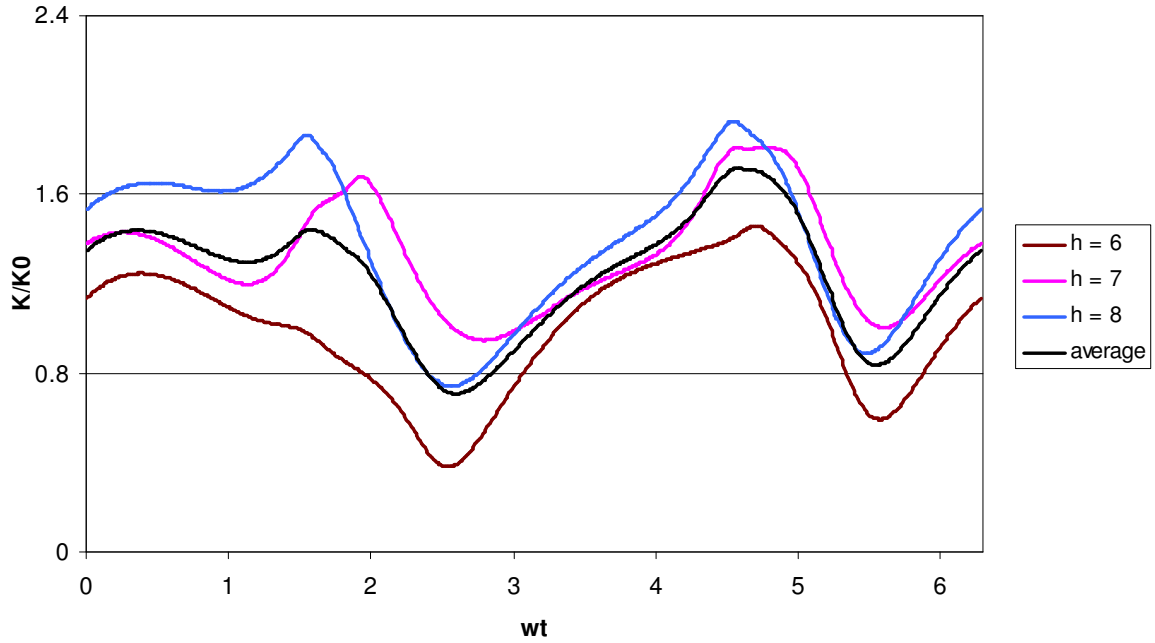

Figure 57: Eddy viscosity profiles, depth-averaged over the boundary layer (wave 2)

Appendix F – Components of DV99$^{(b)}$

In this appendix the contributions of different components to the DV99$^{(b)}$ streaming solution are shown. Furthermore, the behaviour of the individual terms of DV99$^{(b)}$ are compared to that of DV99$^{(a)}$.

Figure 58 and Figure 59 show the cross-shore behaviour of term $U^{(1)}$ for wave 1 and 2, respectively. Compared to the $U^{(1)}$ term of DV99$^{(a)}$, the $U^{(1)}$ term of DV99$^{(b)}$ shows greater streaming velocities at same cross-shore water depths. The reason for this is a smaller value of ε_2 for DV99$^{(b)}$ than for DV99$^{(a)}$. This reflects the smaller time variation in the eddy viscosity profile of DV99$^{(b)}$ compared to DV99$^{(a)}$. Therefore, the contribution of the wave Reynolds stress is greater above flat beds than above rippled beds.
The cross-shore behaviour of the $U^{(2)}$ term for wave 1 and 2 is shown in Figure 60 and Figure 61, respectively. Where the $U^{(2)}$ term of DV99$^{(a)}$ is positive near-bed and negative away from the bed, the $U^{(2)}$ term of DV99$^{(b)}$ is negative near-bed and positive away from the bed for both waves. This is in agreement with the statement made in section 2.2 that the effect of the asymmetry in the turbulent intensity (wave part of mean turbulent Reynolds stress) above flat beds is to reduce the near-bed streaming. Furthermore, for wave 2 (Figure 61) the shape of the $U^{(2)}$ term is more pronounced compared to wave 1 (Figure 60) which is a result of the larger value of ε_1 for wave 2.
Finally, the cross-shore behaviour of the $U^{(3)}$ term for wave 1 and 2 is shown in Figure 62 and Figure 63, respectively. Compared to the $U^{(3)}$ term of DV99$^{(a)}$, the $U^{(3)}$ term of DV99$^{(b)}$ shows much smaller streaming velocities at same cross-shore water depths. The reason for this is a smaller value of ε_2 for DV99$^{(b)}$ than for DV99$^{(a)}$ as mentioned before. The value of ε_2 is also larger for wave 2 than for wave 1 and therefore the $U^{(3)}$ term of wave 2 shows larger velocities than wave 1.
When the magnitude of the individual components are considered, it can be seen that the $U^{(1)}$ term gives the largest contribution to streaming velocities followed by $U^{(3)}$ and eventually by $U^{(2)}$. Therefore, it can be concluded that above flat beds the streaming velocities are mostly determined by the contribution of the wave Reynolds stress, where the contribution of the wave part of the mean turbulent Reynolds stress is significantly smaller. The opposite is true for the streaming velocities above rough rippled beds as discussed in appendix B. The reason for this is the strong, well-organized process of vortex shedding above rippled beds where above flat beds the momentum transfer is dominated by random turbulence.

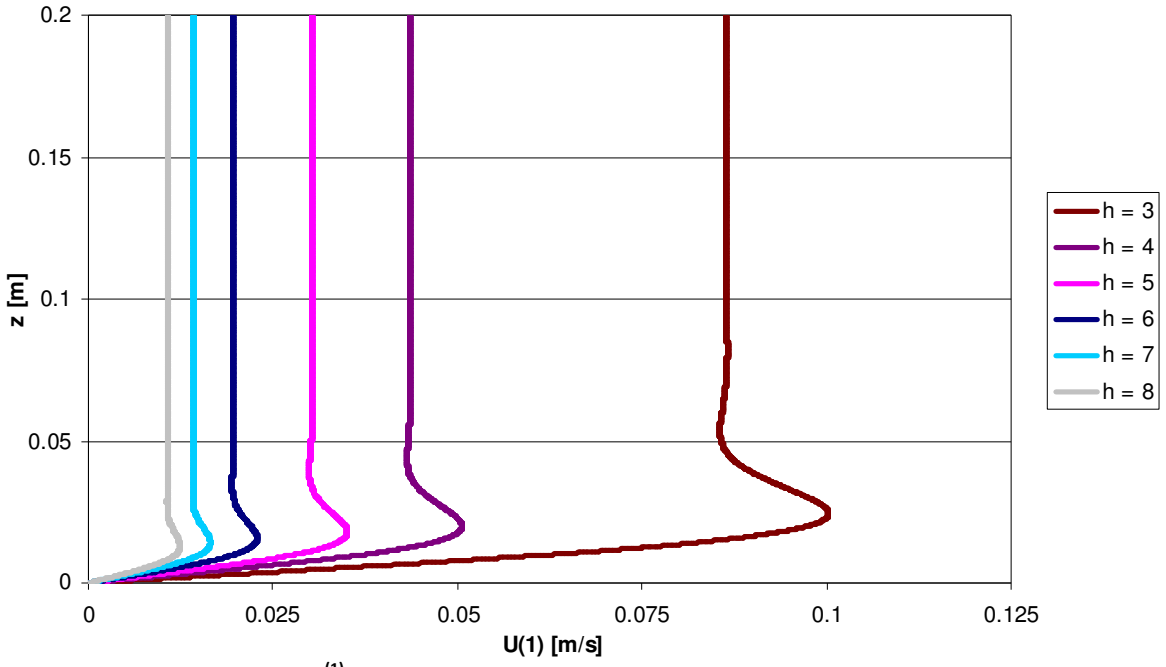

Figure 58: $U^{(1)}$ contribution to streaming, wave occurrence 50 % (wave 1)

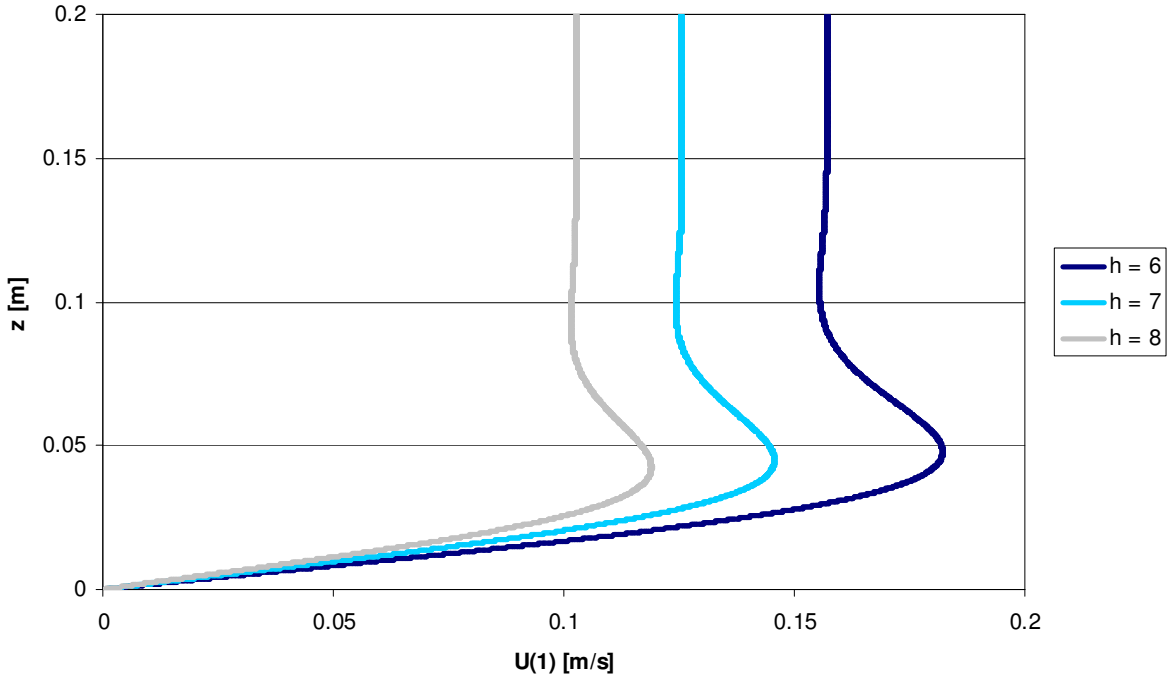

Figure 59: $U^{(1)}$ contribution to streaming, wave occurrence 2.5 % (wave 2)

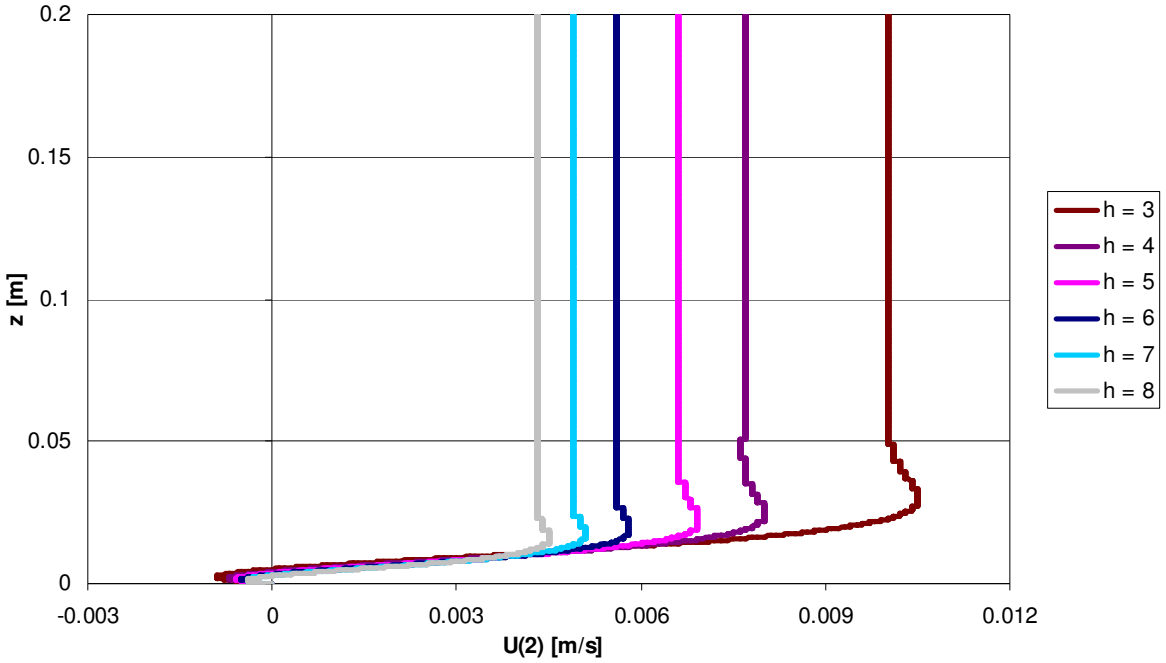

Figure 60: $U^{(2)}$ contribution to streaming, wave occurrence 50 % (wave 1)

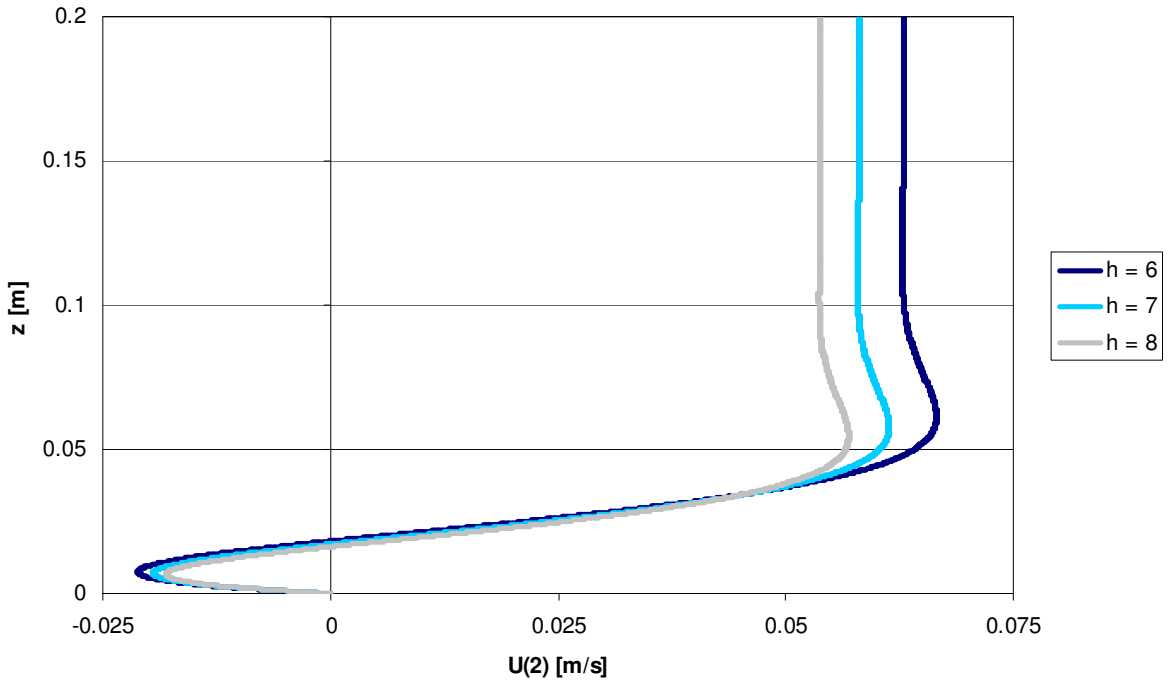

Figure 61: $U^{(2)}$ contribution to streaming, wave occurrence 2.5 % (wave 2)

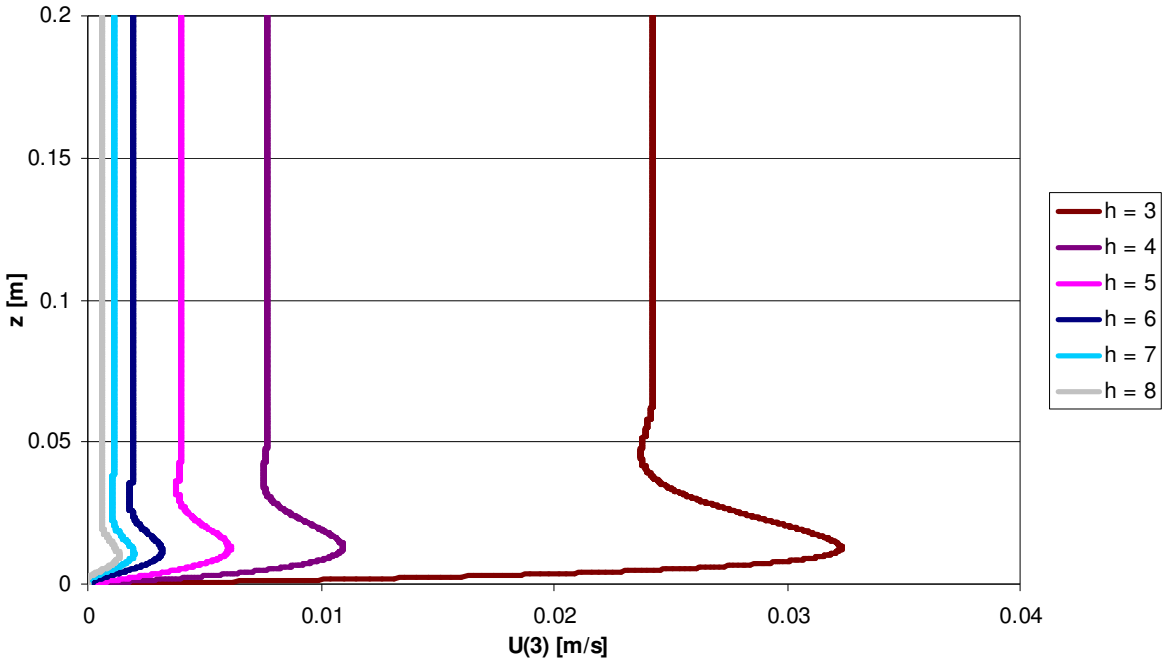

Figure 62: $U^{(3)}$ contribution to streaming, wave occurrence 50 % (wave 1)

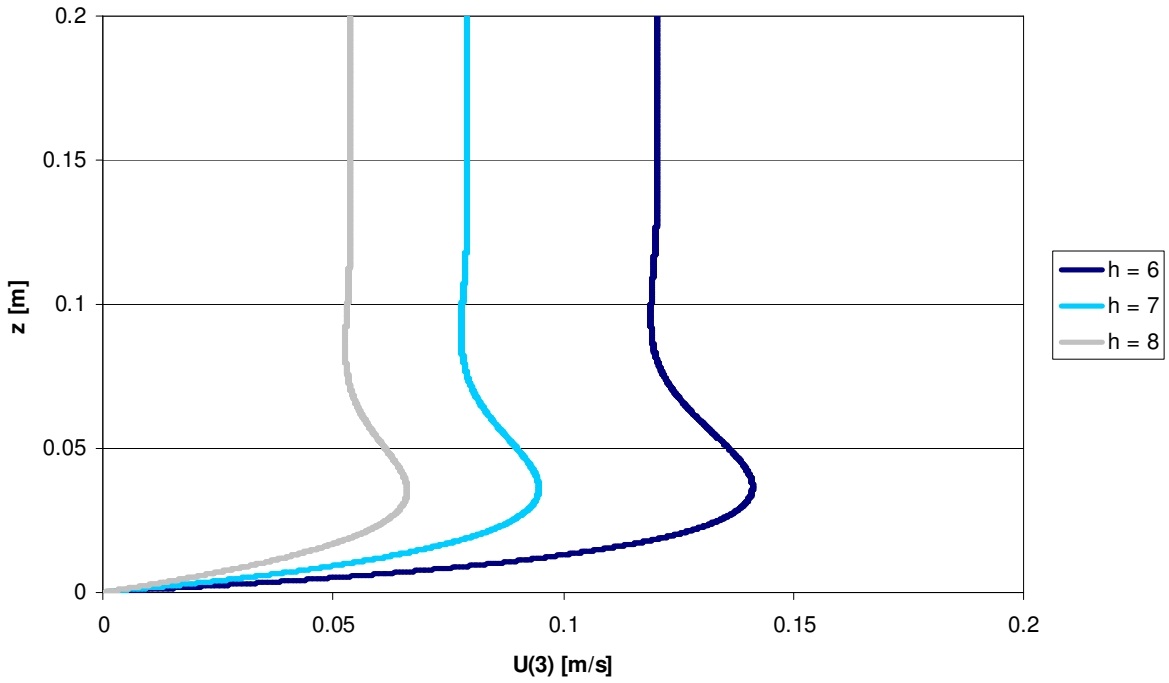

Figure 63: U(3) contribution to streaming, wave occurrence 2.5 % (wave 2)